

กระบวนการวิจัยขั้นของซุคภาพและเทคนิคการประมาณค่าภาพสำหรับการสร้างคืนภาพความละเอียดสูงยิ่ง



นายวรพจน์ พัฒนวิจิตร

สถาบันวิทยบริการ

จุฬาลงกรณ์มหาวิทยาลัย

วิทยานิพนธ์นี้เป็นส่วนหนึ่งของการศึกษาตามหลักสูตรปริญญาวิศวกรรมศาสตรดุษฎีบัณฑิต

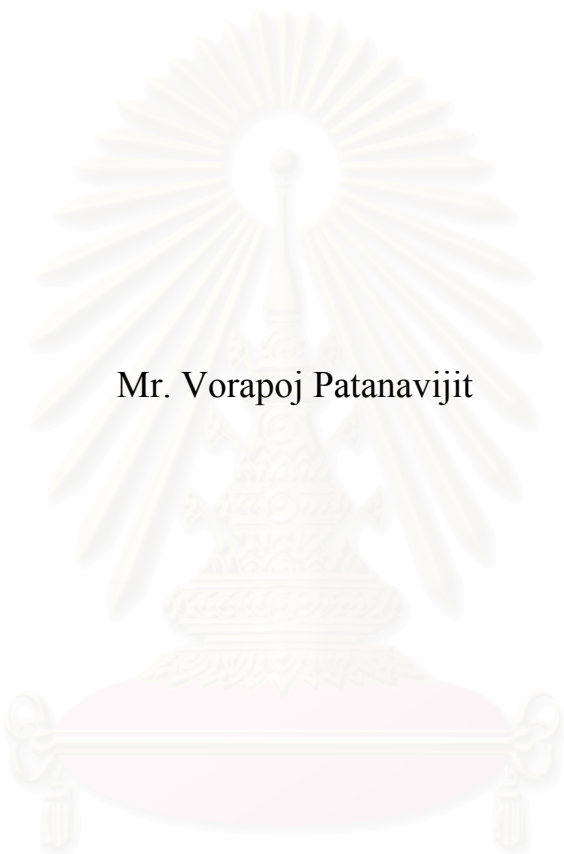
สาขาวิชาวิศวกรรมไฟฟ้า ภาควิชาวิศวกรรมไฟฟ้า

คณะวิศวกรรมศาสตร์ จุฬาลงกรณ์มหาวิทยาลัย

ปีการศึกษา 2550

ลิขสิทธิ์ของจุฬาลงกรณ์มหาวิทยาลัย

IMAGE SEQUENCE REGISTRATION AND IMAGE ESTIMATION
TECHNIQUES FOR SUPER-RESOLUTION RECONSTRUCTION



Mr. Vorapoj Patanavijit


สถาบันวิทยบริการ

จุฬาลงกรณ์มหาวิทยาลัย


A Dissertation Submitted in Partial Fulfillment of the Requirements
for the Degree of Doctor of Philosophy Program in Electrical Engineering
Department of Electrical Engineering
Faculty of Engineering
Chulalongkorn University
Academic Year 2007
Copyright of Chulalongkorn University

Thesis Title IMAGE SEQUENCE REGISTRATION AND
IMAGE ESTIMATION TECHNIQUES FOR
SUPER-RESOLUTION RECONSTRUCTION
By Mr. Vorapoj Patanavijit
Field of Study Electrical Engineering
Thesis Advisor Associate Professor Somchai Jitapunkul, Dr. Ing.


Accepted by the Faculty of Engineering, Chulalongkorn University
in Partial Fulfillment of the Requirements for the Doctoral Degree



..... Dean of the Faculty of Engineering
(Professor Direk Lavansiri, Ph.D.)


THESIS COMMITTEE


..... Chairman
(Assistant Professor Chedsada Chinrungrueng, Ph.D.)


..... Thesis Advisor
(Associate Professor Somchai Jitapunkul, Dr. Ing.)


..... Member
(Suebskul Phiphobmongkol, Ph.D.)


..... Member
(Saowaluck Kaewkamnerd, Ph.D.)


..... Member
(Widhyakorn Asdornwised, Ph.D.)

วรพจน์ พัฒนวิจิตร : กระบวนการรีจิสเตรชันของชุดภาพและเทคนิคการประมาณค่าภาพสำหรับการสร้าง
คืนภาพความละเอียดสูงยิ่ง. (IMAGE SEQUENCE REGISTRATION AND IMAGE ESTIMATION
TECHNIQUES FOR SUPER-RESOLUTION RECONSTRUCTION) อ. ที่ปรึกษา : รศ. ดร.สมชาย
จิตะพันธ์กุล, 157 หน้า.

วิทยานิพนธ์เล่มนี้มีวัตถุประสงค์ของงานวิจัยเพื่อนำเสนอกระบวนการรีจิสเตรชันของชุดภาพที่มีความ
แม่นยำสูงและเทคนิคการประมาณค่าภาพที่มีความทนทานต่อสัญญาณรบกวนสำหรับการสร้างคืนภาพความละเอียด
สูงยิ่ง กระบวนการรีจิสเตรชันของชุดภาพที่นำเสนอจะคำนวณหาความสัมพันธ์แบบ Affine ระหว่างบล็อกของภาพ
ปัจจุบันและภาพอ้างอิงซึ่งจะทำให้สามารถนำไปประยุกต์ใช้กับชุดภาพจริงที่มีลักษณะการเคลื่อนไหวอย่างซับซ้อน
ดังนั้นจึงสามารถนำไปประยุกต์ใช้กับการสร้างคืนภาพความละเอียดสูงยิ่งที่มีการใช้งานอยู่ในปัจจุบันได้ และ
นอกจากนี้แล้วยังสามารถนำไปประยุกต์ใช้งานกับการประมาณการเคลื่อนไหวได้ วิทยานิพนธ์เล่มนี้ยังนำเสนอ
อัลกอริทึมสำหรับการคำนวณความเร็วสูงของกระบวนการรีจิสเตรชันของชุดภาพดังกล่าวโดยจะลดความซับซ้อนใน
การคำนวณเพื่อทำให้กระบวนการรีจิสเตรชันของชุดภาพที่นำเสนอสามารถนำไปประยุกต์ใช้งานได้จริง วิทยานิพนธ์
เล่มนี้จะมุ่งเน้นการสร้างคืนภาพความละเอียดสูงยิ่งโดยวิธีการประมาณแบบ Regularized ML เนื่องจากวิธีนี้มี
ประสิทธิภาพสูงและมีความซับซ้อนต่ำโดยวิทยานิพนธ์เล่มนี้จะศึกษาประสิทธิภาพของตัวประมาณค่า (Norm
Estimator) อย่างเช่น L1 และ L2 ที่มีผลกระทบต่อการสร้างคืนภาพความละเอียดสูงยิ่ง วิทยานิพนธ์เล่มนี้จะนำเสนอ
ตัวประมาณค่าที่มีความทนทานต่อสัญญาณรบกวน (Huber, Lorentzian and Tukey's Biweight norm) เพื่อนำไป
ประยุกต์ใช้งานในการสร้างคืนภาพความละเอียดสูงยิ่ง

วิทยานิพนธ์เล่มนี้จะเสนอการทดลองจำนวน 5 การทดลองเพื่อประเมินผลเปรียบเทียบประสิทธิภาพ
กระบวนการรีจิสเตรชันของชุดภาพและเทคนิคการประมาณค่าภาพสำหรับการสร้างคืนภาพความละเอียดสูงยิ่ง โดย
จะปรับเปลี่ยนสัญญาณรบกวนประเภทต่างๆ, ตัวประมาณค่าแบบต่างๆ (L1, L2 Huber, Lorentzian and Tukey's
Biweight norm) และกระบวนการรีจิสเตรชันของชุดภาพทั้งที่นำเสนอและที่ใช้กัน โดยทั่วไป

จากผลการทดลองแสดงให้เห็นว่ากระบวนการรีจิสเตรชันของชุดภาพที่นำเสนอมีความแม่นยำสูงกว่า
กระบวนการรีจิสเตรชันของชุดภาพที่ใช้ในปัจจุบันอย่างมากดังนั้นการสร้างคืนภาพความละเอียดสูงยิ่งที่ใช้
กระบวนการรีจิสเตรชันของชุดภาพที่นำเสนอจะสามารถใช้กับชุดภาพมาตรฐานอย่างเช่นชุดภาพ Foreman และ
Susie ได้อย่างมีประสิทธิภาพ การสร้างคืนภาพความละเอียดสูงยิ่งที่ใช้เทคนิคการประมาณค่าภาพที่นำเสนอสามารถ
ประยุกต์ใช้กับสัญญาณรบกวนแบบต่างๆ อย่างเช่น Noiseless, AWGN, Poisson and Salt&Pepper และ Speckle
ได้อย่างมีประสิทธิภาพ

ภาควิชาวิศวกรรมไฟฟ้า
สาขาวิชาวิศวกรรมไฟฟ้า
ปีการศึกษา 2550

ลายมือชื่อนิสิต.....
ลายมือชื่ออาจารย์ที่ปรึกษา.....

4671823521 : MAJOR ELECTRICAL ENGINEERING

KEY WORD: SUPER-RESOLUTION RECONSTRUCTION (SRR) / IMAGE REGISTRATION / MOTION ESTIMATION / ML/MAP ESTIMATION / REGULARIZED FUNCTION

VORAPOJ PATANA VIJIT : (IMAGE SEQUENCE REGISTRATION AND IMAGE ESTIMATION TECHNIQUES FOR SUPER-RESOLUTION RECONSTRUCTION) THESIS ADVISOR : ASSOC. PROF. SOMCHAI JITAPUNKUL, Dr. Ing., 157 pp.

This dissertation proposes two novel algorithms: the highly accurate sub-pixel image registration and the robust norm for SRR algorithm. The proposed registration assumes the affine motion as the relationship between blocked images (the current frame and the reference frame). It is applicable to not only the standard sequences but also real sequences with complex motion. Therefore, it can be implemented in the previous SRR algorithms. Moreover, it can be implemented in motion estimation algorithm. To realize the implementation of the proposed sub-pixel image registration, the fast algorithm is designed to reduce the computational load for the proposed sub-pixel registration. This dissertation considers the use of a regularized maximum likelihood estimator in the image estimation process due to its high performance and low complexity. This dissertation also studies the effect of norm estimation in SRR algorithm. The L1 or L2 norms with different regularized functions are interested in this work. The novel robust norms (Huber norm, Lorentzian norm and Tukey's Biweigh norm) are proposed into the model of the SRR framework using the proposed registration.

To evaluate the effectiveness of the proposed image registration and the robust norm for SRR algorithm, various noise model and image sequences used in SRR algorithm have been investigated. Five experiments have been carried out to demonstrate the performance of the proposed methods: 1) Experimental on fast affine block-based registration, 2) Experimental on the SRR algorithm using fast affine block-based registration, 3) Experimental on robust estimation technique for SRR, 4) Experimental on the SRR algorithm using robust estimation technique with classical registration and 5) Experimental on robust estimation technique using affine block-based registration for SRR. Experimental results show than the affine block-based registration algorithm clearly gives a higher accuracy than the classical algorithm both objectively and subjectively. By using this proposed registration algorithm, the super-resolution algorithm can be applied on the general sequence such as Foreman and Susie sequence. Moreover, the proposed robust SRR can be effectively applied on the images that are corrupted by various noise models. Experimental results clearly demonstrated that the proposed robust algorithm is applicable on the several noise models such as Noiseless, AWGN, Poisson Noise and Salt&Pepper Noise and Speckle Noise and the proposed algorithm can obviously improve the result both subjectively and objectively.

Department.....Electrical Engineering.....Student's signature.....
Field of study.....Electrical Engineering.....Advisor's signature.....
Academic year....2007.....

ACKNOWLEDGEMENTS

This work contained in this dissertation represents the accumulation of four and half years of work made possible only by the collective support of family, friends, colleagues and mentors.

First and foremost, I would like to express my deep gratitude to advisor Assoc. Dr. Somchai Jitapunkul, my role model of an exceptional scientist and teacher. It was a great privilege and honor to work and study under his guidance. I would like to thank him for his support, friendship, empathy and great vision. My thanks also to the members of my dissertation defense committees, Asst. Dr. Chedsada Chinrungrueng, Dr. Suebskul Phiphobmongkol, Dr. Saowaluck Kaewkamnerd, and Dr. Widhyakorn Asdornwised for reviews and invaluable comments.

I would like to thanks to Assumption University for financial scholarship support and research equipments and to all colleagues at Assumption University, Dr. Sudhiporn Patumtaewapibal, Asst. Prof. Dr. Kittaphan Techakittiroj, Asst. Prof. Dr. Thiraphong Charoenkhunwiwat and Dr. Weerakhan Tantiphaiboont.

I would also like to express my sincere gratitude to Dr. Supatana Auethavekiat for their very helpful comments on various aspects of my work and comprehensive reviews on my dissertation document.

Many thanks to my all colleagues at DSPRL (Digital Signal Processing Research Laboratory) for academic documentary help, technical/theory information and programming/data information.

Finally, my life has been constantly fulfilled by love and support of my family. I am extremely grateful to my parents, Wonlop Patanavijit and Panida Patanavijit, for their love, caring and sacrifices, my father and mother for educating and preparing me for my future life since I was a kid, and my wonderful brother, Thanadej Patanavijit, for his incredible generosity. This work is dedicated to them. My only regret is that it is far too modest to do them justice.

Table of Contents

	Page
Abstract in Thai	iv
Abstract in English	v
Acknowledgements	vi
Table of Contents	vii
List of Figures	xi
CHAPTER I INTRODUCTION	1
1.1 Background and Signification of the Research Problems.....	1
1.1.1 Introduction of SRR Algorithm.....	4
1.1.2 Literature Review.....	6
1.1.3 Insufficient Sub-Pixel Registration Accuracy Problem.....	10
1.1.4 SSR Estimation Technique Problem.....	10
1.2 Objectives of the Dissertation.....	13
1.3 The Proposed Technique and Its Novelty.....	14
1.4 Scope of the Dissertation.....	16
1.5 Expected Prospects of the Dissertation.....	18
1.6 The Dissertation Procedure.....	19
1.7 Dissertation Outline.....	21
CHAPTER II FUNDAMENTAL TECHNIQUES FOR SRR	22
2.1 Introduction of SRR.....	22
2.2 Inverse Problems.....	24
2.2.1 Definition of an Inverse Problem.....	24
2.2.2 Well-Posed and Ill-Posed Problems.....	24
2.2.3 Regularization Technique and the Solution to Ill-Posed Problems.....	25
2.2.4 Super-Resolution Reconstruction as an Ill-Posed Inverse Problem.....	26
2.2.4.1 SRR is an Inverse Problem.....	26
2.2.4.2 SRR is an Ill-Posed Problem.....	26
2.3 The Classical SRR Algorithm.....	28
2.3.1 The SRR Observation Model.....	28
2.3.2 The Classical Regularized ML for SRR Algorithm.....	30
2.4 Registration (Motion Estimation) for SRR Algorithm.....	31
2.4.1 Global Registration for SRR Algorithm.....	31
2.4.2 Regional Registration for SRR Algorithm.....	32
2.5 Estimation Technique for SRR Algorithm.....	33
2.5.1 L2 Norm Estimation for SRR Algorithm.....	33
2.5.2 L1 Norm Estimation for SRR Algorithm.....	34
2.6 Regularization Technique for SRR Algorithm.....	35

	Page
2.6.1 Laplacian Regularization for SRR Algorithm.....	35
2.6.1.1 L2 Norm Estimation with Laplacian Regularization for SRR Algorithm.....	36
2.6.1.2 L1 Norm Estimation with Laplacian Regularization for SRR Algorithm.....	36
2.6.2 MRF Regularization for SRR Algorithm	37
2.6.2.1 L2 Norm Estimation with MRF Regularization for SRR Algorithm.....	37
2.6.2.2 L1 Norm Estimation with MRF Regularization for SRR Algorithm.....	38
2.6.3 BTV Regularization for SRR Algorithm	39
2.6.3.1 L2 Norm Estimation with BTV Regularization for SRR Algorithm.....	39
2.6.3.2 L1 Norm Estimation with BTV Regularization for SRR Algorithm.....	40
CHAPTER III A FAST AFFINE BLOCK-BASED REGISTRATION AND ROBUST ESTIMATION TECHNIQUES FOR SRR.....	41
3.1 Fast Affine Block-Based Registration	
/Motion Estimation	41
3.1.1 Affine Block-Based Registration.....	42
3.1.2 Modified Three Step Search Algorithm.....	42
3.2 Robust Norm Estimation for SRR	45
3.2.1 Huber Norm Estimation for SRR.....	45
3.2.1.1 Huber Norm Estimation Definition.....	47
3.2.1.2 Huber Norm Estimation for SRR.....	47
3.2.1.3 Huber Norm Estimation for SRR With Laplacian Regularization.....	48
3.2.1.4 Huber Norm Estimation for SRR With Huber-Laplacian Regularization.....	48
3.2.2 Lorentzian Norm Estimation for SRR.....	49
3.2.2.1 Lorentzian Norm Estimation Definition...	49
3.2.2.2 Lorentzian Norm Estimation for SRR.....	50
3.2.2.3 Lorentzian Norm Estimation for SRR With Laplacian Regularization.....	50
3.2.2.4 Lorentzian Norm Estimation for SRR with Lorentzian -Laplacian Regularization.....	50
3.2.3 Tukey's Biweigh Norm Estimation for SRR.....	52
3.2.3.1 Tukey Norm Estimation Definition.....	52
3.2.3.2 Tukey Norm Estimation for SRR.....	52

	Page
3.2.3.3 Tukey Norm Estimation for SRR With Laplacian Regularization.....	53
3.2.3.4 Tukey Norm Estimation for SRR With Tukey -Laplacian Regularization.....	53
3.3 Robust Estimation for SRR using Fast Affine Block-Based Registration.....	54
3.3.1 L2 Norm Estimation for SRR using Fast Affine Block-Based Registration.....	54
3.3.1.1 L2 Norm Estimation for SRR.....	54
3.3.1.2 L2 Norm Estimation for SRR with Laplacian Regularization.....	54
3.3.2 L1 Norm Estimation for SRR using Fast Affine Block-Based Registration.....	55
3.3.2.1 L1 Norm Estimation for SRR.....	55
3.3.2.2 L1 Norm Estimation for SRR with Laplacian Regularization.....	55
3.3.3 Huber Norm Estimation for SRR using Fast Affine Block-Based Registration.....	56
3.3.3.1 Huber Norm Estimation for SRR.....	56
3.3.3.2 Huber Norm Estimation for SRR with Laplacian Regularization.....	56
3.3.4 Lorentzian Norm Estimation for SRR using Fast Affine Block-Based Registration.....	57
3.3.4.1 Lorentzian Norm Estimation for SRR.....	57
3.3.4.2 Lorentzian Norm Estimation for SRR with Laplacian Regularization.....	57
3.3.5 Tukey's Biweight Norm Estimation for SRR using Fast Affine Block-Based Registration.....	58
3.3.5.1 Tukey Norm Estimation for SRR.....	58
3.3.5.2 Tukey Norm Estimation for SRR with Laplacian Regularization.....	58
CHAPTER VI THE EXPERIMENTAL RESULTS	59
4.1 Experiments on Fast Affine Block-Based Registration.....	60
4.2 Experiments on the SRR algorithm using Fast Affine Block-Based Registration.....	65
4.2.1 Susie Sequence (The 40th Frame).....	66
4.2.2 Foreman Sequence (The 110th Frame).....	71
4.2.3 Experimental Conclusion.....	77
4.3 Experiments on Robust Estimation Technique for SRR.....	79
4.3.1 Susie Sequence (The 40th Frame).....	80

	Page
4.3.2 Lena (The Standard Image).....	91
4.3.3 Experimental Conclusion.....	101
4.4 Experiments on the SRR algorithm using robust Estimation Technique with Classical Registration.....	104
4.4.1 Susie Sequence (The 40th Frame).....	105
4.4.2 Foreman Sequence (The 110th Frame).....	110
4.4.3 Experimental Conclusion.....	117
4.5 Experiments on Robust Estimation Technique Using Affine Block-Based Registration for SRR.....	119
4.5.1 Susie Sequence (The 40th Frame).....	119
4.5.2 Foreman Sequence (The 110th Frame).....	125
4.5.3 Experimental Conclusion.....	132
CHAPTER V THE CONCLUSION	134
5.1 Conclusions of the Dissertation	134
5.2 Contributions of the Dissertation.....	137
5.2.1 A Comprehensive Survey of the Literature on the SRR.....	137
5.2.2 The Highly Accurate Sub-Pixel Images Registration on the SRR.....	137
5.2.3 The Robust Estimations on the SRR.....	138
5.2.4 The Highly Accurate Sub-Pixel Images Registration and the Robust Estimations on the SRR.....	139
5.2.5 Program Development.....	139
5.3 Future Research on SRR algorithms.....	141
REFERENCE	142
LISTS OF PUBLICATION.....	154
VIATE	157

List of Figures

	Page
Figure 1.1	Block Diagram of Observation Model4
Figure 1.2	Super-Resolution Reconstruction (SRR) Block Diagram5
Figure 1.3	Proposed Super-Resolution Reconstruction Framework....15
Figure 2.1	The Classical SRR Observation Model29
Figure 3.1	The Algorithm of the M3SS at Step 244
Figure 3.2	The Algorithm of the M3SS at Step 444
Figure 3.3	The Norm function and the Influence function46
Figure 4.1	Performance Comparison between the compensated Frame produced by the proposed M3SS and classical algorithm of Carphone sequence.....62
Figure 4.2	MCD Comparison between the compensated frame produced by the proposed and classical estimation method of Carphone sequence.....62
Figure 4.3	Performance Comparison between the compensated Frame produced by the proposed M3SS and classical algorithm of Foreman sequence.....63
Figure 4.4	MCD Comparison between the compensated frame produced by the proposed and classical estimation method of Foreman sequence.....63
Figure 4.5	Performance Comparison between the compensated Frame produced by the proposed M3SS and classical algorithm of Stefan sequence.....64
Figure 4.6	MCD Comparison between the compensated frame produced by the proposed and classical estimation method of Stefan sequence.....64
Figure 4.7	The block diagram of LR image sequence synthesis algorithm for the SRR algorithm using the proposed fast affine blockbased registration.....65
Figure 4.8	The experimental result of SRR algorithm using the proposed Registration (Susie Sequence : The 40th Frame).....68
Figure 4.9	The experimental result of SRR algorithm using the proposed Registration (Foreman Sequence : The 110th Frame).....73
Figure 4.10	The experimental result table of SRR algorithm using the proposed Registration (Susie : The 40th Frame)..77
Figure 4.11	The experimental result table of SRR algorithm using the proposed Registration (Foreman : The 110 th Frame).....78

	Page
Figure 4.12 The block diagram of LR image sequence synthesis algorithm for the SRR algorithm using proposed robust estimation).....	79
Figure 4.13 The experimental result of SRR algorithm using the proposed robust estimation technique (Susie Sequence : The 40 th Frame).....	84
Figure 4.14 The experimental result of SRR algorithm using the proposed robust estimation technique (Lena : The Standard Image).....	95
Figure 4.15 The experimental result of SRR algorithm using the proposed Registration (Susie : The 40 th Frame).....	102
Figure 4.16 The experimental result table of SRR algorithm using the proposed Registration (Lena : The Standard Image)...	103
Figure 4.17 The experimental result of the SRR algorithm using proposed robust estimation technique with classical registration (Susie : The 40 th Frame).....	107
Figure 4.18 The experimental result of the SRR algorithm using proposed robust estimation technique with classical registration (Foreman : The 110 th Frame).....	113
Figure 4.19 The experimental result of SRR algorithm using the proposed Registration (Susie : The 40 th Frame).....	117
Figure 4.20 The experimental result of SRR algorithm using the proposed Registration (Foreman : The 110 th Frame)...	118
Figure 4.21 The experimental result of the SRR algorithm using proposed robust estimation technique with proposed registration.....	122
Figure 4.22 The experimental result of the SRR algorithm using proposed robust estimation technique with proposed registration.....	128
Figure 4.23 The experimental result of SRR algorithm using the proposed Registration (Susie : The 40 th Frame).....	132
Figure 4.24 The experimental result of SRR algorithm using the proposed Registration (Foreman : The 110 th Frame)...	133

CHAPTER I

INTRODUCTION

1.1 Background and Signification of the Research Problems

A very brief overview of the enormous field of image restoration is provided here. Image restoration remains an important research topic and one of the major applications driving the theory and practice of image processing since digital computer made processing large amounts of data possible. This section is not meant to provide a review of the completed literature on image restoration, (the reader is referred to the texts [1, 17, 33, 44, 64, 80, 83, 85] for that) but to provide some perspective on how SRR (Super-Resolution Reconstruction) algorithms grew out of the existing body of research and how these new SRR algorithms define directions for future work.

The spatial resolution that represents the number of pixels per unit area in an image is the principal factor in determining the quality of an image. With the development of image processing applications, there is a great demand for high-resolution (HR) images since HR images offer not only the viewer a pleasing picture but also additional details that are important for the analysis in many applications. The most direct solution to increase spatial resolution is to reduce the pixel size (i.e., increase the number of pixels per unit area) by sensor manufacturing techniques. As the pixel size decreases, however, the amount of light available also decreases. It generates shot noise that severely degrades the image quality. To reduce the pixel size without suffering the effects of shot noise, therefore, there exists the limitation of the pixel size reduction, and the optimally limited pixel size is estimated at about $40 \mu\text{m}^2$ for a $0.35 \mu\text{m}$ CMOS processor [57, 95]. The current image sensor technology has almost reached this level. Another approach for enhancing the spatial resolution is to increase the chip size, which leads to an increase in capacitance. Since large capacitance makes it difficult to speed up a charge transfer rate, this approach is not considered effective. The high cost for high precision optics and image sensors is also an important concern in many commercial applications regarding HR imaging therefore many digital image restoration techniques have been proposed since 1970s.

Image restoration techniques are broadly categorized into two classes based on the number of observed frames. Specifically, the categorization is into the classes of single-frame and multi-frame restoration methods. The classical image restoration problem is concerned with restoration of a single output image from a single

degraded observed image and the literature on the restoration of a single input frame is extensive and spans several decades [15, 16, 17, 33, 64, 80, 83]. While the field of single frame image restoration appears to have matured, digital video has raised many new restoration problems for image processing researchers [125]. Since video typically consists of a sequence of similar, though not identical frames, it becomes possible to utilize the inter-frame motion information in processing the video data. This led to the development of image sequence processing techniques such as motion estimation [11, 39, 45, 94, 106, 108, 124, 125], image sequence interpolation [80], image registration [3, 6, 18] and standards conversion [125]. Image restoration researchers also recognized the potential of image restoration in increasing spatial resolution using the information totally contained in an image sequence as compared with that available from a single image. This led naturally to algorithms which apply motion compensation and image restoration techniques to produce high-quality and high-resolution still images from image sequences called Super-Resolution Reconstruction (SRR).

SRR algorithms [9, 20, 57, 63, 95] investigate the relative motion information between multiple low-resolution (LR) images or a video sequence and increase the spatial resolution by fusing them into a single frame. In doing so, it also removes the effect of possible blurring and noise in the LR images. In summary, the SRR algorithm estimates an HR image with finer spectral details from multiple LR observations degraded by blur, noise, and aliasing.

The major advantage of this approach is that the cost of implementation is reduced and the existing LR imaging systems can still be utilized. Thus, applications for the techniques of SRR from image sequences grow rapidly as the theory gains exposure. Continuing researches and the availability of fast computational machineries have made these methods increasingly attractive in applications requiring the highest restoration performance. SRR techniques have already been applied to problems in a number of applications such as satellite imaging, astronomical imaging, video enhancement and restoration, video standards conversion, confocal microscopy, digital mosaicing, aperture displacement cameras, medical computed tomographic imaging, diffraction tomography, video freeze frame and hard copy.

In SRR, typically, the LR images represent different “looks” at the same scene [95]. That is, LR images are subsampled (aliased) as well as shifted with sub-pixel precision. If the LR images are shifted by integer units, then each image contains the same information, and thus there is no new information that can be used to reconstruct a HR image. If

the LR images have different sub-pixel shifts from each other and if aliasing is present, however, then each image cannot be obtained from the others. In this case, the new information contained in each LR image can be exploited to obtain a HR image. To obtain different looks at the same scene, some relative scene motions must exist from frame to frame via multiple scenes or video sequences. Multiple scenes can be obtained from one camera with several captures or from multiple cameras located in different positions. These scene motions can occur due to the controlled motions in imaging systems, e.g., images acquired from orbiting satellites. The same is true of uncontrolled motions, e.g., movement of local objects or vibrating imaging systems. If these scene motions are known or can be estimated within sub-pixel accuracy and if we combine these LR images then SRR is possible.

Most of the SRR registration techniques [95] are based on the sub-pixel translation motion assumption. This implies the observed images or sequences can be modeled by global or local uniform translation thus the traditional sub-pixel registration can not be applied on the real complex motion sequences and super-resolution applications can be applied only on the sequences that have simple translation motion. In addition to image registration, the robust estimation and high accurate image estimation is also required. The traditional estimated techniques for SRR, proposed in the past literatures [9, 20, 57, 63, 94, 95] are based on the simple estimation techniques such as L1 Norm or L2 Norm Minimization. From these points of view, the SRR estimation technique and SRR sub-pixel registration for the real complex sequences is a very challenging topic because the performance of the registration and estimation techniques have a major impact on the performance of the SRR system.

This dissertation has a main objective to jointly overcome the problems of SRR application limitation (for the real complex sequences) and SRR estimation technique. The results in the dissertation would be beneficial for SRR framework design, especially in the digital image/video restoration.

1.1.1 Introduction of Super-Resolution Reconstruction Algorithm (SRR)

In this section, the fundamental knowledge of the SRR algorithm is described. This includes a block diagram of observation model and SRR algorithm.

The first step to comprehensively review the SRR problem is to formulate an observation model that relates the original HR image to the observed LR images. Several observation models have been explored in [95], and they can be broadly divided into the models for still images and for video sequence. To present a basic concept of SR reconstruction techniques, we employ the observation model for still images in [95] as shown in Figure 1.1, since it is rather straightforward to extend the still image model to the video sequence model.

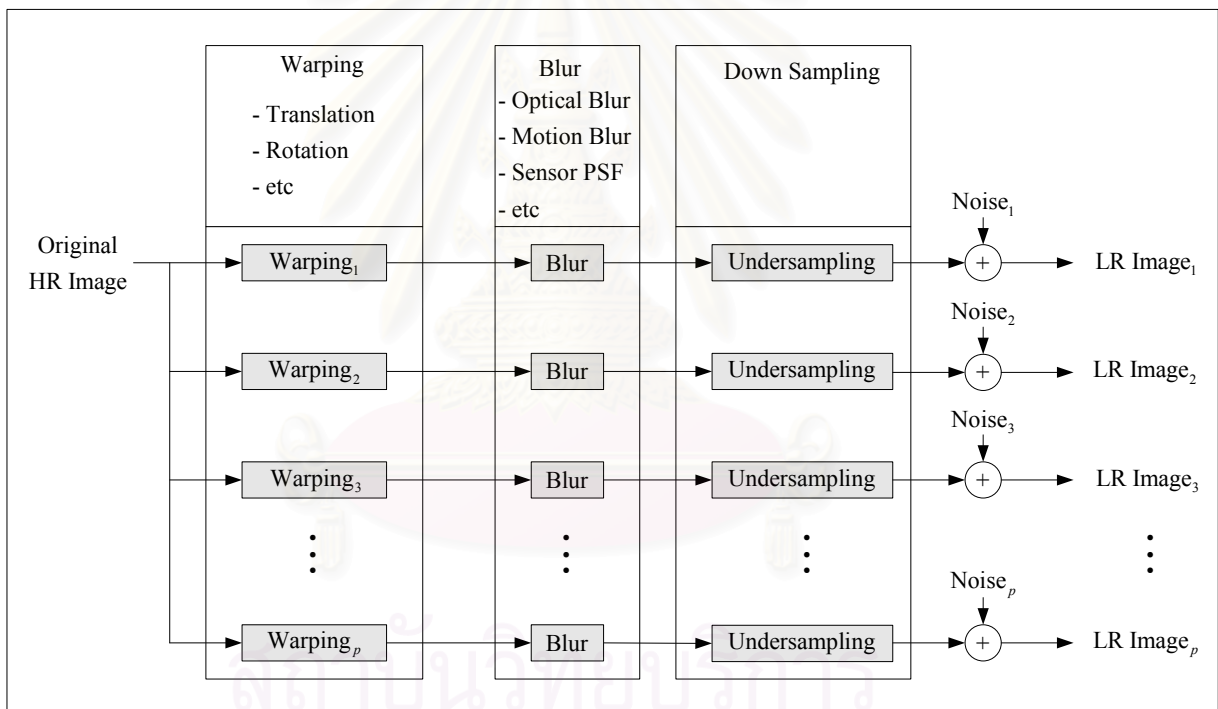


Figure 1.1: Block Diagram of Observation Model.

The motion that occurs during the image acquisition is represented by warping processes. It may contain global or local translation, rotation, and so on. Since this information is generally unknown, we need to estimate the scene motion for each frame with reference to one particular frame. The warping process performed on HR image is actually defined in terms of LR pixel spacing when we estimate it. Thus, this step requires interpolation when the fractional unit of motion is not equal to the HR sensor grid.

Blur may be caused by an optical system (e.g., out of focus, diffraction limit, aberration, etc.), relative motion between the imaging system and the original scene, and the point spread function (PSF) of the LR sensor. It can be modeled as linear space invariant (LSI) or linear space variant (LSV). In single image restoration applications, the optical or motion blur is usually considered. In the SRR, however, the finiteness of a physical dimension in LR sensors is an important factor of blur.. In the use of SRR algorithms, the characteristics of the blur are assumed to be known. However, if it is difficult to obtain this information, blur identification should be incorporated into the reconstruction procedure.

The downsampling process generates aliased LR images from the warped and blurred HR image. Although the size of LR images is the same here, in more general cases, we can address the different size of LR images by using a different downsampling matrix. Although the blur acts more or less as an anti-aliasing filter, in SR image reconstruction, it is assumed that aliasing is always present in LR images.

Most of the explored SRR algorithms [95] consist of the three stages illustrated in Figure 1.2: registration, interpolation and restoration (i.e., inverse procedure). These steps can be implemented separately or simultaneously according to the reconstruction methods adopted. The estimation methods of motion information [11, 12, 39, 40, 45, 74-78, 106, 108, 122] are referred to as registration methods [3, 6, 18], and it is extensively studied in various fields of image processing. In the registration stage, the relative shifts between LR images compared to the reference LR image are estimated with fractional pixel accuracy. Obviously, accurate sub-pixel motion estimation is a very important factor in the success of the SRR algorithm. Since the shifts between LR images are arbitrary, the registered HR image will not always match up to a uniformly spaced HR grid. Thus, nonuniform interpolation is necessary to obtain a uniformly spaced HR image from a composite of nonuniformly spaced LR images. Finally, image restoration is applied to the upsampled image to remove blurring and noise.

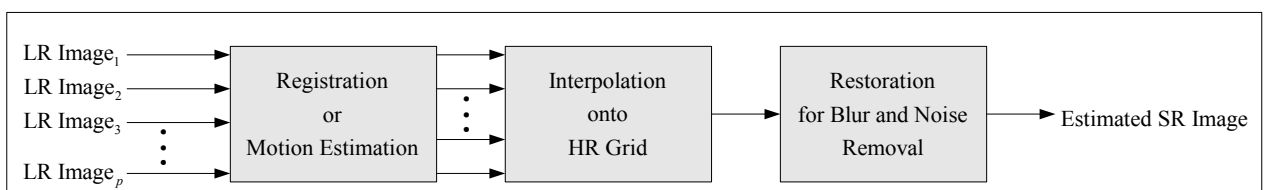


Figure 1.2: Super-Resolution Reconstruction (SRR) Block Diagram.

1.1.2 Literature Review

As stated in the beginning of this chapter, this dissertation addresses two main problems of SRR: the insufficient accuracy of the sub-pixel image registration and the non-robust estimation technique used in the SSR. In this section, the relevant research papers, published in the conferences and journals are comprehensively reviewed.

The Super-Resolution Reconstruction (SRR) idea was first presented by T. S. Huang and R. Y. Tsan [107] in 1984. They used the frequency domain approach to demonstrate the ability to reconstruct one improved resolution image from several downsampled noise-free versions of it, based on the spatial aliasing effect. Next, a frequency domain recursive algorithm for the restoration of super-resolution images from noisy and blurred measurements is proposed by S. P. Kim, N. K. Bose, and H. M. Valenzuela [102] in 1990. The algorithm using a weighted recursive least squares algorithm, is based on sequential estimation theory in the frequency-wavenumber domain, to achieve simultaneous improvement in signal-to-noise ratio and resolution from available registered sequence of low-resolution noisy frames. In 1993, S. P. Kim and Wen-Yu Su [103] also incorporated explicitly the deblurring computation into the high-resolution image reconstruction process because separate deblurring of input frames would introduce the undesirable phase and high wavenumber distortions in the DFT of those frames. Subsequently, M. K. Ng and N. K. Bose [62] proposed the analysis of the displacement errors on the convergence rate to the iterative approach for solving the transform based preconditioned system of equation in 2002 hence it is established that the used of the MAP, L2 Norm or H1 Norm regularization functional leads to a proof of linear convergence of the conjugate gradient method in terms of the displacement errors caused by the imperfect subpixel locations. Later, N. K. Bose, M. K. Ng and A. C. Yau [69] proposed the fast SRR algorithm, using MAP with MRF for blurred observation in 2006. This algorithm uses the reconditioned conjugated gradient method and FFT. Although the frequency domain methods are intuitively simple and computationally cheap, the observation model is restricted to only global translational motion and LSI blur. Due to the lack of data correlation in the frequency domain, it is also difficult to apply the spatial domain a priori knowledge for regularization.

The POCS formulation of the SRR was first suggested by Stark and Oskoui [95] in 1987. Their method was extended by Tekalp [95] to include observation noise in 1992. Although POCS is simple and can utilize a convenient inclusion of a priori information, this method has

the disadvantages of nonuniqueness of solution, slow convergence and a high computational cost. Next, A. J. Patti and Y. Altunbasak proposed [2] a SRR (Super-Resolution Reconstruction) using ML estimator with POCS-based regularization in 2001 and Y. Altunbasak, A. J. Patti, and R. M. Mersereau [126] proposed a Super-Resolution Reconstruction (SRR) for the MPEG sequences in 2002. They proposed a motion-compensated, transform-domain super-resolution procedure that directly incorporates the transform-domain quantization information by working with the compressed bit stream. Later, B. K. Gunturk and Y. Altunbasak and R. M. Mersereau [7] proposed a ML super-resolution with regularization based on compression quantization, additive noise and image prior information in 2004. Next, H. Hasegawa, T. Ono, I. Yamada and K. Sakaniwa proposed iterative SSR using the Adaptive Projected Subgradient method for MPEG sequences in 2005 [27].

The MRF or Markov/Gibbs Random Fields [35-38, 43-44, 90-91] are proposed and developed for modeling image texture during 1990-1994. Due to MRF (Markov Random Field) that can model the image characteristic especially on image texture, C. Bouman and K. Sauer [10] proposed the single image restoration algorithm using MAP estimator with the GGMRF (Generalized Gaussian-Markov Random Field) prior in 1993. Later, R. L. Stevenson, B. E. Schmitz and E. J. Delp [82] proposed the single image restoration algorithm using ML estimator with the Discontinuity Persevering Regularization in 1994. R. R. Schultz and R. L. Stevenson [88] proposed the single image restoration algorithm using MAP estimator with the HMRF (Huber-Markov Random Field) prior in 1994. Next, the Super-Resolution Reconstruction algorithm using MAP estimator (or the Regularized ML estimator), with the HMRF prior was proposed by R. R. Schultz and R. L. Stevenson [89] in 1996. The blur of the measured images is assumed to be simple averaging and the measurements additive noise is assumed to be independent and identically distributed (i.i.d.) Gaussian vector. In 2006, R. Pan and S. J. Reeves [87] proposed single image MAP estimator restoration algorithm with the efficient HMRF prior using decomposition-enabled edge-preserving image restoration in order to reduce the computational demand.

Typically, the regularized ML estimation (or MAP) [15, 16, 24, 64] is used in image restoration therefore the determination of the regularization parameter is an important issue in the image restoration. A. M. Thompson, J. C. Brown, J. W. Kay and D. M. Titterington [1] proposed the Methods of choosing the smoothing parameter in image restoration by regularized ML in 1991. Next, V. Z. Mesarovic, N. P.

Galatsanos, A. K. Katsaggelos [123] proposed the single image restoration using regularized ML for unknown linear space-invariant (LSI) point spread function (PSF) in 1995. Subsequently, D. Geman and C. Yang [14] proposed single image restoration using regularized ML with robust nonlinear regularization in 1995. This approach can be done efficiently by Monte Carlo Methods, for example by annealing FFT domain using Markov chain that alternates between (global) transitions from one array to the other. Later, M. G. Kang and A. K. Katsaggelos proposed the use of a single image regularization functional [55], which is defined in terms of restored image at each iteration step, instead of a constant regularization parameter in 1995 and proposed regularized ML for SRR [56], in which no prior knowledge of the noise variance at each frame or the degree of smoothness of the original image is required in 1997. In 1999, R. Molina, A. K. Katsaggelos, and J. Mateos [85] proposed the application of the hierarchical ML with Laplacian regularization to the single image restoration problem and derived expressions for the iterative evaluation of the two hyperparameters (regularized parameter) applying the evidence and maximum a posteriori (MAP) analysis within the hierarchical regularized ML paradigm. In 2003, R. Molina, M. Vega, J. Abad and A. K. Katsaggelos [86] proposed the mutiframe super-resolution reconstruction using ML with Laplacian regularization. The regularized parameter is defined in terms of restored image at each iteration step. Next, D. Rajan and S. Chaudhuri [21] proposed super-resolution approach, based on ML with MRF regularization, to simultaneously estimate the depth map and the focused image of a scene, both at a super-resolution from its defocused observed images in 2003. Subsequently, H. He and L. P. Kondi [29-30] proposed image resolution enhancement with adaptively weighted low-resolution images (channels) and simultaneous estimation of the regularization parameter in 2004 and proposed a generalized framework [31] of regularized image/video Iterative Blind Deconvolution/Super-Resolution (IBD-SR) algorithm using some information from the more matured blind Deconvolution techniques form image restoration in 2005. Later, they [32] proposed SRR algorithm that takes into account inaccurate estimates of the registration parameters and the point spread function in 2006. In 2006, M. Vega, R. Molina and A. K. Katsaggelos [67] proposed the problem of deconvolving color images observed with a single coupled charged device (CCD) from the super-resolution point of view. Utilizing the regularized ML paradigm, an estimate of the reconstructed image and the model parameters is generated.

M. Elad and A. Feuer [49] proposed the hybrid method combining the ML and nonellipsoid constraints for the super-resolution

restoration in 1997 and the adaptive filtering approach for the Super-Resolution Reconstruction in 1999 [50, 51]. Next, they proposed two iterative algorithms, the R-SD and the R-LMS [51], to generate the desired image sequence at the practically computational complexity in 1999. These algorithms assume the knowledge of the blur, the down-sampling, the sequences motion, and the measurements noise characteristics, and apply a sequential reconstruction process. Subsequently, the special case of Super-Resolution Reconstruction (where the warps are pure translations, the blur is space invariant and the same for all the images and the noise is white) are proposed for a fast Super-Resolution Reconstruction in 2001 [52]. Later, N. Nguyen, P. Milanfar and G. Golub [70] proposed fast SRR algorithm using regularized ML by using efficient block circulant preconditioners and the conjugate gradient method in 2001. In 2002, M. Elad [54] proposed the Bilateral Filter theory, showed how the bilateral filter can be improved and extended to treat more general reconstruction problems. Consequently, the alternate super-resolution approach, L1 Norm estimator and robust regularization based on a Bilateral Total Variance (BTV), was presented by S. Farsiu and D. Robinson [97-98] in 2004. This approach performance is superior to what proposed earlier in [49], [50] and [51] and this approach has fast convergence but this SRR algorithm effectively apply only on AWGN models. Next, they proposed a fast SRR of color images [99] using ML estimator with BTV regularization for luminance component and Tikhonov regularization for chrominance component in 2006. Subsequently, they proposed the dynamic super-resolution problem of reconstructing a high-quality set of monochromatic or color super-resolved images from low-quality monochromatic, color or mosaiced frames [100]. This approach includes a joint method for simultaneous SR, deblurring and Demosaicing. It takes into account practical color measurements encountered in video sequences. Later, we [112] proposed the SRR using a regularized ML estimator with affine block-based registration for the real image sequence. Moreover, G. Rochefort, F. Champagnat, G. L. Besnerais and Jean-Francois Giovannelli [25] proposed super-resolution approach based on regularized ML [49] for the extended original observation model devoted to the case of nonisometric interframe motion such as affine motion in 2006.

S. Baker and T. Kanade [92] proposed another super-resolution algorithm (hallucination or recognition-based super-resolution) in 2002 that attempts to recognize local features in the low-resolution image and then enhances their resolution in an appropriate manner. Due to the training data base, therefore, this algorithm performance depends

on the image type (such as face or character) and this algorithm is not robust enough to be used in typical surveillance video. J. Sun, N. N. Zheng, H. Tao and H. Y. Shum [41] proposed hallucination super-resolution (for single image) using regularization ML with primal sketches as the basic recognition elements in 2003.

During 2004 to 2006, P. Vandewalle, S. Susstrunk and M. Vetterli [75-78] have proposed a fast super-resolution reconstruction based on a non-uniform interpolation using a frequency domain registration. This method has low computation and can use in the real-time system but the degradation models are limited therefore this algorithm can apply on few applications. In 2006, M. Trimeche, R. C. Bilcu and J. Yrjanainen [65] proposed SRR algorithm using an integrated adaptive filtering method to reject the outlier image regions for which registration has failed.

1.1.3 Insufficient Sub-Pixel Registration Accuracy Problem

All the above Super-Resolution Reconstruction methods [2, 8, 20, 21, 41, 49-53, 75-78, 88-89, 92, 95-100, 102, 103, 107, 126] are restricted to globally or locally uniform translational displacement between the measured images or sequences. This implies the measured images or sequences are observed at a high temporal frequency sampling (or high frame rate) but the measured images or sequences are usually observed by the real commercial cameras at low temporal frequency sampling (or low frame rate) such as standard sequences (Foreman, Carphone, Susie, etc.). The measured images or sequences have many complex motions instead of translational motion therefore, unfortunately, the pure translation model can not represent the real complex motion effectively and image super-resolution applications can apply only on the sequences that have simple translation motion as shown in these previous literature review.

1.1.4 SSR Estimation Technique Problem

This section reviews the literature from the estimation point of view because the SRR estimation is one of the most crucial parts of the SRR research areas and directly impact to the SRR performance. Though the SRR algorithms from the reviews literature use various techniques, there are only two kinds of norm estimation (L1 and L2). L2 norm estimation has the advantage of lower variance than the L1 norm;

whereas, L1 performs better in robust to outliers because the influence function is constant and bounded.

C. Bouman and K. Sauer [10] proposed the single image restoration algorithm using ML estimator (L2 Norm) with the GGMRF (Generalized Gaussian-Markov Random Field) regularization in 1993. R. R. Schultz and R. L. Stevenson [88] proposed the single image restoration algorithm using ML estimator (L2 Norm) with the HMRF (Huber-Markov Random Field) regularization in 1994 and proposed the SRR algorithm [89] using ML estimator (L2 Norm) with the HMRF regularization in 1996. The blur of the measured images is assumed to be simple averaging and the measurements additive noise is assumed to be independent and identically distributed (i.i.d.) Gaussian vector. M. Elad and A. Feuer [49] proposed the hybrid method combining the ML estimator (L2 Norm) and nonellipsoid constraints for the Super-Resolution Reconstruction in 1997 [50]. Next, they proposed two iterative algorithms, the R-SD and the R-LMS (L2 Norm) [50, 53], to generate the desired image sequence at the practically computational complexity in 1999. These algorithms assume the knowledge of the blur, the down-sampling, the sequences motion, and the measurements noise characteristics, and apply a sequential reconstruction process. Subsequently, the special case of Super-Resolution Reconstruction (where the warps are pure translations, the blur is space invariant and the same for all the images and the noise is white) are proposed for a fast Super-Resolution Reconstruction using ML estimator (L2 Norm) in 2001 [52]. Later, N. Nguyen, P. Milanfar and G. Golub [70] proposed fast SRR algorithm using regularized ML (L2 Norm) by using efficient block circulant preconditioners and the conjugate gradient method in 2001. In 2002, A. J. Patti and Y. Altunbasak proposed [2] a SRR algorithm using ML (L2 Norm) estimator with POCS-based regularization. Y. Altunbasak, A. J. Patti, and R. M. Mersereau [126] proposed a SRR algorithm using ML (L2 Norm) estimator for the MPEG sequences in 2002. Deepu Rajan and S. Chaudhuri [21] proposed SRR using ML (L2 Norm) with MRF regularization to simultaneously estimate the depth map and the focused image of a scene in 2003. Later, we [112] proposed the SRR using a regularized ML estimator (L2 Norm) with affine block-based registration for the real image sequence. Moreover, G. Rochefort, F. Champagnat, G. L. Besnerais and Jean-Francois Giovannelli [25] proposed super-resolution approach based on regularized ML (L2 Norm) [49] for the extended original observation model devoted to the case of nonisometric interframe motion such as affine motion in 2006. In 2006, R. Pan and S. J. Reeves [87] proposed single image restoration algorithm using ML estimator (L2 Norm) with the efficient HMRF regularization

and using decomposition-enabled edge-preserving image restoration in order to reduce the computational demand.

The novel super-resolution approach, ML estimator (L1 Norm) and robust regularization based on a Bilateral Total Variance (BTV), was presented by S. Farsiu and D. Robinson [97-98] in 2004. Next, they proposed a fast SRR of color images [99] using ML estimator (L1 Norm) with BTV regularization for luminance component and Tikhonov regularization for chrominance component in 2006. Subsequently, they proposed the dynamic super-resolution problem of reconstructing a high-quality set of monochromatic or color super-resolved images from low-quality monochromatic, color or mosaiced frames [100]. This approach includes a joint method for simultaneous SR, deblurring and Demosaicing, this way taking into account practical color measurements encountered in video sequences.

The success of SRR algorithm is highly dependent on the accuracy of the model of the imaging process. However, these models are not supposed to be exactly true, as they are merely mathematically convenient formulations of some general prior information. When the data or noise model assumptions do not faithfully describe the measure data, the estimator performance degrades rapidly. Furthermore, existence of outliers defined as data points with different distributional characteristics than the assumed model will produce erroneous estimates. Most of noise models used in SRR algorithms is based on AWGN (Additive White Gaussian Noise) model; therefore, SRR algorithms can effectively apply only on the image sequence that is corrupted by AWGN. Due to this noise model, L1 norm or L2 norm error are effectively used in SRR algorithm. Unfortunately, the real noise models that corrupt the measure sequence are unknown therefore SRR algorithm using L1 norm or L2 norm may degrade the image sequence rather than enhance it. Therefore, the robust norm error is desired for SRR algorithm. This norm should be strong against several noise models. For normally distributed data, the L1 norm produces estimates with higher variance than the optimal L2 (quadratic) norm but the L2 norm is very sensitive to outliers because the influence function increases linearly and without bound.

1.2 Objectives of the Dissertation

This dissertation proposes a novel SRR (Super-Resolution Reconstruction) framework for real standard sequences that are corrupted by any noise models. The proposed sub-pixel image registration is designed to overcome the insufficient temporal sampling frequency and to register the real complex motion sequence that the traditional SSR registration can not support. To realize the implementation of the proposed sub-pixel image registration, the fast algorithm is designed to reduce the computational load for the proposed sub-pixel registration. Moreover, the novel robust estimation technique is proposed for SSR framework to increase the estimated performance and to be robust against several types of noise models.



สถาบันวิทยบริการ
จุฬาลงกรณ์มหาวิทยาลัย

1.3 The Proposed Technique and its Novelty

This dissertation proposes two novel algorithms: the highly accurate sub-pixel image registration and the robust norm for SRR algorithm. The proposed registration assumes the affine motion as the relationship between blocked images (the current frame and the reference frame). It is applicable to not only the standard sequences but also real sequences with complex motion. Therefore, it can be implemented in the previous SRR algorithms. Moreover, it can be implemented in motion estimation algorithm. To realize the implementation of the proposed sub-pixel image registration, the fast algorithm is designed to reduce the computational load for the proposed sub-pixel registration. This dissertation considers the use of a regularized maximum likelihood estimator in the image estimation process due to its high performance and low complexity [2, 10, 21, 25, 49-53, 70, 87-89, 97-100, 112, 126]. This dissertation also studies the effect of norm estimation in SRR algorithm. The L1 or L2 norms with different regularized functions are interested in this work. A novel robust norm is proposed into the model of the SRR framework using the proposed registration.

A block diagram of the proposed iterative SSR framework is illustrated in Figure 1.3. The proposed SSR framework is the iterative process composed of 2 main parts: the registration parameter estimation and image estimation. First, the registration parameters, which used to wrap all low resolution images and used in the image estimation process are estimated from low resolution images (or observed sequences) and the registration parameters. Second, all LR images, all degraded SR images, all registration information, regularized information and initialed SR image are used in the image estimation process to generate the estimated SR image.

สถาบันวิทยบริการ
จุฬาลงกรณ์มหาวิทยาลัย

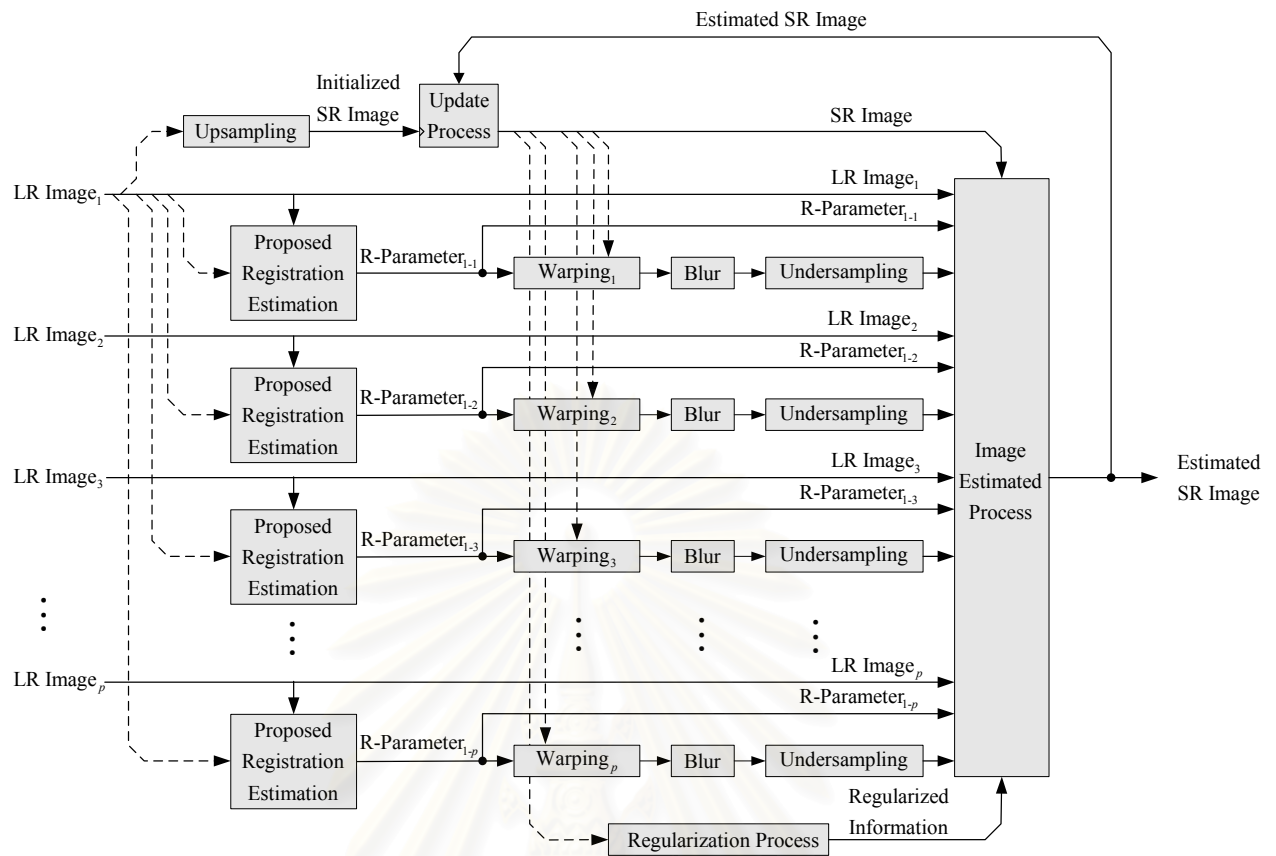


Figure 1.3: Proposed Super-Resolution Reconstruction Framework

สถาบันวิทยบริการ
จุฬาลงกรณ์มหาวิทยาลัย

1.4 Scope of the Dissertation

The research problems are the insufficient registration accuracy and the problem of image estimation techniques. The scope of these researches is as follows.

1. Study the performance and the limitation of the classical image registration applied in the SRR algorithm.
2. Develop the image sequence registration that is applicable to both the real complex sequences and standard sequences.
3. Study the performance of the proposed registration and provide a comparative study of proposed registration with other traditional registration proposed previously.
4. Provide mathematical analyses of the SRR algorithm using maximum likelihood (ML) with different regularized function such Tikhonov, MRF (Markov Random Field) and BTV (Bi-Total Variance).
5. Study the performance of the SRR using the proposed registration.
6. Develop the image estimation technique that is more accurate and robust than the existing image estimation techniques used in SRR framework.
7. Provide mathematical analyses of the SRR algorithm using proposed robust estimation technique.
8. Study the performance of the proposed image estimation technique and provide a comparative study of proposed estimation with other classical estimation technique (L1 and L2) proposed by previously.
9. Develop the SRR framework using the proposed registration and proposed estimation technique

10. Study the performance of the SRR using the proposed registration and proposed estimation technique and provide a comparative study of proposed estimation with other estimation proposed by many authors in the past.



สถาบันวิทยบริการ
จุฬาลงกรณ์มหาวิทยาลัย

1.5 Expected Prospects of the Dissertation

1. Acquire a basic knowledge of mathematical formulation models for solving the SRR problems.
2. Obtain a new registration algorithm to jointly overcome the insufficient registration accuracy; thereby, enhance the overall system performance. Thus, the SRR with the proposed registration algorithm is expected to be able to implement in the real image sequence.
3. Obtain a new estimation technique for the proposed SRR so that the SRR using the proposed estimation technique is robust to any noise models and to registration error.
4. Obtain the SRR using the proposed registration and the proposed estimation technique. Hence, the proposed SRR can be applied on real image sequence that is corrupted by any noise model.
5. Know the advantages and disadvantages of proposed SRR registration algorithm.
6. Know the advantages and disadvantages of proposed SRR estimation.
7. Know the advantages and disadvantages of the proposed SRR registration and the proposed SRR estimation techniques.
8. Understand the necessity of the registration and estimation techniques for SRR framework.

1.6 The Dissertation Procedure

1. Study previous research papers relevant to the research works of the dissertation.
 - 1.1 Study research papers relevant to the sub-pixel motion estimation/registration problem.
 - 1.2 Study research papers concerning with the robust estimation problem.
 - 1.3 Study research papers regarding the SRR.
2. Develop the highly accurate sub-pixel motion estimation/registration algorithm for the SRR (Super-Resolution Reconstruction).
3. Develop the sub-pixel motion estimation/registration simulation program.
4. Test the proposed registration algorithm by using several standard sequences such as Foreman, Carphone, Suzie and Stefan that have different moving foreground and background characteristics.
5. Develop the mathematical model for the super-resolution reconstruction using the proposed sub-pixel registration.
6. Develop the SRR simulation program using the proposed sub-pixel registration.
7. Test the SRR algorithm by using the proposed registration algorithm in several standard sequences.
8. Develop mathematical model for a robust estimation for the SRR using the proposed registration.
9. Develop the SRR simulation program using the proposed robust estimation.

10. Test the SRR using the proposed robust estimation by several standard images.
11. Develop mathematical model of the SRR using the proposed registration and the proposed robust estimation.
12. Develop the SRR simulation program using the proposed registration and the proposed robust estimation.
13. Test the SRR using the proposed robust estimation and the proposed robust estimation by several standard sequences.
14. Collect and analyze computational results obtained from simulation programs.
15. Summarize the major findings as we found in step 14 and conclude the performance of the proposed SRR framework in all concerned aspects.
16. Check whether the conclusions meet all the objectives of the research work of the dissertation.
17. Write the dissertation.

1.7 Dissertation Outline

Chapter 2 provides a concise introduction to the theory and application of fundamental techniques for SRR (Super-Resolution Reconstruction). Next, Chapter 3 describes the proposed SRR registration and the proposed SRR estimation. In chapter 4, system configurations and experimental results are elaborated. In addition, performance comparison between the proposed registration/estimation and the classical method is comprehensively demonstrated in this chapter. Finally, Chapter 5 discusses and concludes all experimental results. Contributions and suggestions of future works on SRR are given in this chapter.



สถาบันวิทยบริการ
จุฬาลงกรณ์มหาวิทยาลัย

CHAPTER II

FUNDAMENTAL TECHNIQUES

FOR SUPER-RESOLUTION RECONSTRUCTION

2.1 Introduction of SRR (Super-Resolution Reconstruction)

In this chapter, some of the background knowledge necessary for understanding and exploring the SRR (Super-Resolution Reconstruction) problem is presented.

Traditionally, the achievable resolution of any devices is constrained by both theoretical and practical (physical) limitations. SRR (Super-Resolution Reconstruction) algorithms investigate the relative motion information between multiple LR (Low Resolution) images (or a video sequence) and increase the spatial resolution by fusing them into a single frame. In doing so, it also removes the effect of possible blurring and noise in the LR images [9, 15-16, 20, 24, 57, 63, 94-95]. Recent work relates this problem to restoration theory [24, 64]. As such, the problem is shown to be an inverse problem, where an unknown image is to be reconstructed, based on measurements related to it through linear operators and additive noise. This linear relation is composed of geometric warp, blur and decimation operations. The SRR problem is modeled by using sparse matrices and analyzed from many reconstruction methods [63] such as the Non-uniform Interpolation, Frequency Domain, Maximum-Likelihood (ML), Maximum A-Posteriori (MAP), and Projection Onto Convex Sets (POCS).

Though the terminology varies considerably from field to field, SRR is broadly understood as a bandwidth extrapolation beyond the diffraction limit of the optical system. Though the use of the diffraction limit as the threshold defining SRR is common, it is often inappropriate in electronic imaging applications. SRR thus requires not only the amelioration of the degradations caused in the imaging process (the classical restoration problem), but also the extrapolation of frequency content beyond that which is present in the observed data. SRR requires the restoration of lost information or SRR refers to the restoration of a sequence of images that has information content beyond the spatial and/or temporal bandlimit of the imaging system (bandwidth extrapolation).

In Section 2.2, the theory of inverse problems that will play an important role in the chapters ahead is introduced. Next, Section 2.3 demonstrated the classical SRR algorithm. In Section 2.3, classical SRR registration/estimation is presented. Later, SRR estimation is presented in

Section 2.4. Finally, in Section 2.5, the typical SRR regularization techniques are discussed.



สถาบันวิทยบริการ
จุฬาลงกรณ์มหาวิทยาลัย

2.2 Inverse Problems

In this section, a succinct overview of some basic concepts in mathematical inverse problems is provided. The discussion here is nontechnical so that the reader may obtain an intuitive comprehension of the fundamental ideas prior to the presentation of greater detail in subsequent chapters.

2.2.1 Definition of an Inverse Problem

The inverse problem can be defined as follows [93]:

“We call two problems inverses of one another if the formulation of each involves all or part of the solution of the other. Often, for historical reasons, one of the two problems has been studied extensively for some time, while the other has never been studied and is not so well understood. In such cases, the former is called the direct problem, while the latter is the inverse problem.”

This description hints at the arbitrariness of the definition as to which problem is considered direct and which is the inverse. Considering the following classical examples clarified the terminology. The familiar example of a direct/inverse problem pair concerns polynomials. Given a polynomial of order p the direct problem is finding the p roots of the polynomial. The corresponding inverse problem is finding the polynomial given the p roots. In the case of polynomials it is clear that the direct problem is more difficult.

The above example illustrates another typical characteristic of direct/inverse problem pairs. The data for the direct problem is the desired solution of inverse problem and vice versa.

2.2.2 Well-Posed and Ill-Pose Problems

Hadamard [93], in his work on differential equations, classified a problem as “well-posed” if the solution to the problem has the following characteristic:

1. **Solution Existence:** The solution of the problem or model must exist. There may be no model that exactly fits the data and therefore no solution does exist for the approximated model. This can occur in practice because our mathematical model of the system’s physics is approximated or because the data contain noise.

2. **Solution Uniqueness:** If the solution of the problem or model is existence then the solution must be uniqueness. For some models, though exact solutions do exist, they may not be unique, even for an infinite number of exact data points. Nonunique solution is a characteristic of rank-deficient discrete linear inverse problems.

3. **Stability of the Solution Process (Continuous Dependence of the Data):** The solution of the problem must depend on the data. The process of computing an inverse solution can be, and often is, extremely unstable in that a small change in measured/observed data can lead to an enormous change in the estimated model.

In contrast, a problem which fails to satisfy any of the Hadamard conditions is said to be “ill-posed”. SRR is considered ill-posed due to the following reason: 1) No solution existence, 2) Solution Non-Uniqueness, 3) Instability of the Solution Process.

In fact, the information always losses due to the observation process therefore the information content of the solution is lower than that of the original information. This irrecoverable loss of information does not present significant difficulties for the direct problem. However, if the objective is to determine the original information from the observed information, that is, to solve the inverse problem, this information loss has serious consequences. It is not possible to reverse the process exactly and return to the original information due to the loss of information. The inverse problem fails to have a unique solution.

2.2.3 Regularization Technique and the Solution to Ill-Posed Problems

Regularization is a term which refers to methods which utilize additional information to compensate for the information loss which characterizes ill-posed problems. This additional information is typically referred to as a-priori or prior information as it cannot be derived from the observations or the observation process and must be known “before the fact”. Typically the prior information is chosen to represent desired characteristics of the solution, for example total energy, smoothness, positivity and so on. The role of the a-priori information is to constrain or reduce the space of solutions which are compatible with the observed data. A deterministic theory of regularized solutions to ill-posed problems was pioneered by A. N. Tikhonov [93].

In the Tikhonov approach, a family of approximate solutions to the inverse problem is constructed, with the family of solutions

controlled by a nonnegative real-valued regularization parameter. The solution family is constructed so that in the noise-free case, in the limit as the regularization parameter goes to zero, the exact solution to the original problem is yielded, while for noisy data, a positive value of the regularization parameter yields an optimal approximate solution. Since Tikhonov's seminal work, stochastic and set-theoretic regularization theories have been proposed. Stochastic regularization methods are applied in later chapters. In all these regularization frameworks, the inclusion of a-priori information results, by construction, in a new well-posed problem which is closely related to the original ill-posed one. This well-posed problem, the solution of which satisfies the Hadamard requirements, is formulated so that its unique solution is meaningful with respect to the original ill-posed one. It is therefore very important to ensure that the a-priori constraints used accurately reflect the required characteristics of the solution. Often physical principles are a useful guide. For instance, in an imaging application, light intensities are always nonnegative - a powerful a-priori constraint in bandlimited reconstruction scenarios.

2.2.4 Super-Resolution Reconstruction as an Ill-Posed Inverse Problem

One of the recurring issues in this work is that multiframe Super-Resolution Reconstruction is usually an ill-posed inverse problem.

2.2.4.1 Super-Resolution Reconstruction is an Inverse Problem

SRR refers to the restoration of a sequence of observed low-resolution images that has information content beyond the spatial and/or temporal bandlimit of the imaging system (bandwidth extrapolation). Hence, the corresponding inverse problem is that of determining estimate(s) of the scene given the observed image sequence and the characterization of the imaging process. Given the characteristics of the imaging process and system, the forward problem is the simulation, while the inverse problem is the restoration.

2.2.4.2 Super-Resolution Reconstruction is an Ill-Posed Problem

Recall that ill-posedness implies failure of one or more of the Hadamard conditions. The multiframe SRR problem may fail to satisfy one or more of these conditions. The failure may result from either the characteristics of the imaging system, or the observed data.

1. Nonexistence of the solution: the presence of noise in the observation process may result in an observed image sequence which,

given the imaging system characterization, is inconsistent with any scene. The result is that the system is noninvertible and the scene cannot be estimated from the observations.

2. Nonuniqueness of the solution: when the operator which characterizes the imaging process is many-to-one, there exists a nontrivial space of solutions consistent with any given observed image sequence, that is, the solution to the inverse problem is nonunique. For example, in bandlimited imaging systems, all out-of-band scene data represent the null space of the imaging process operator. Even if the imaging operator is nonsingular, a simple lack of data, which represent constraints on the solution space, is sufficient to result in the nonuniqueness of the solution. For example, consider a discretized imaging scenario with P observed low-resolution images each consisting of N pixels. These observed data provide a maximum of PN independent constraints. Assume a single superresolution image containing $M > PN$ pixels is to be estimated from the data. Since the number of unknowns exceeds the number of constraints, it is clear that there are insufficient constraints for the existence of a unique solution to the inverse problem. Furthermore, since superresolution, by definition, requires the restoration of information that is lost in the imaging process it should be expected that the solution to the superresolution restoration problem is likely to be nonunique.

3. Discontinuous dependence of the solution on the data: depending on the characteristics of the imaging system, the inverse problem may be highly sensitive to perturbations of the data. For example, consider an imaging system with a spectral response which decreases asymptotically toward zero with increasing frequency. While such a system is invertible in theory, in practice the inverse is unstable. An arbitrarily small noise component at a sufficiently high frequency leads to an arbitrarily large spurious signal in the computed restoration. In practice such restorations are typically overwhelmed by the amplification of the noise.

While, in rare circumstances, it happens that the Hadamard conditions are satisfied, in general, practical applications involving multiframe SRR are invariably ill-posed.

Despite the difficulties caused by the ill-posedness, regularized solution methods enable high quality SRR as is shown in later section. The inclusion of a-priori information is crucial to achieving this.

2.3 The Classical SRR Algorithm

In this section, the classical SRR algorithm is presented. First, the SRR observation model is described and, consequently, the classical regularized ML for the SRR algorithm is stated.

2.3.1 The SRR Observation Model

The first step to comprehensively analyze the SRR problem is to formulate an observation model that relates the original HR image to the observed LR images. The observation models can be broadly divided into the models for still images and for video sequence. To present a basic concept of SRR algorithms, we first employ the observation model for still images and, later, we extend it to the observation model for the video sequence model.

Define that a low-resolution image sequence is $\{\underline{\mathbf{Y}}_k\}$, $N_1 \times N_2$ pixels, as our measured data. A original high-resolution image $\underline{\mathbf{X}}$, $qN_1 \times qN_2$ pixels, is to be estimated from the LR sequences, where q is an integer-valued interpolation factor in both the horizontal and vertical directions. To reduce the computational complexity, each frame is separated into overlapping blocks (the shadow blocks as shown in Fig. 2.1(a) and Fig. 2.1(b)).

For convenience of notation, all overlapping blocked frames will be presented as vector, ordered column-wise lexicographically. Namely, the overlapping blocked LR frame is $\underline{Y}_k \in \mathbb{R}^{M^2}$ ($M^2 \times 1$) and the overlapping blocked HR frame is $\underline{X} \in \mathbb{R}^{q^2 M^2}$ ($L^2 \times 1$ or $q^2 M^2 \times 1$). We assume that the two images are related via the following equation

$$\underline{Y}_k = D_k H_k F_k \underline{X} + \underline{V}_k \quad ; k = 1, 2, \dots, N \quad (2.1)$$

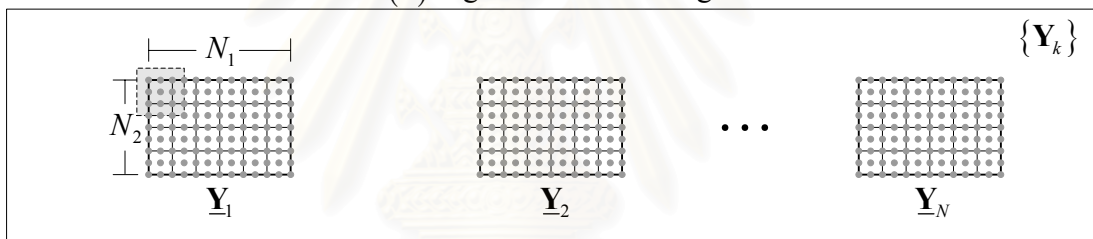
where

- \underline{X} (vector format) is the original high-resolution blocked image.
- $\underline{Y}_k(t)$ (vector format) is the blurred, decimated, down sampled and noisy blocked image
- F_k ($F \in \mathbb{R}^{q^2 M^2 \times q^2 M^2}$ and matrix format) stands for the geometric warp (Typically, Translational Motion) between the images \underline{X} and \underline{Y}_k .

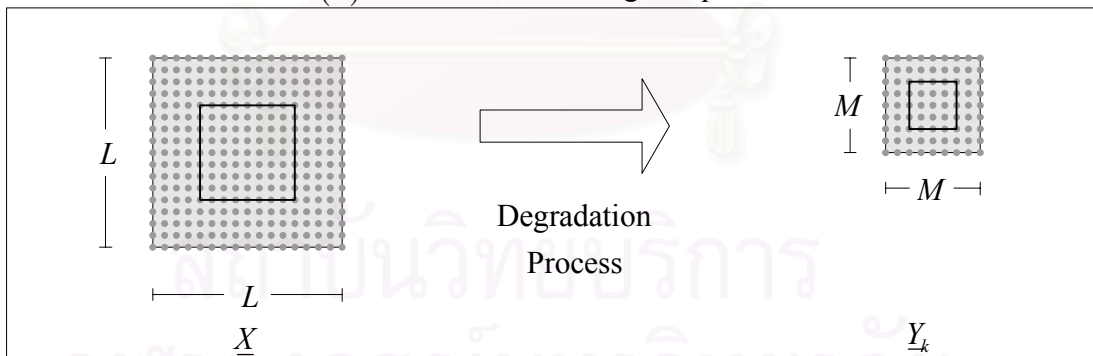
- H_k ($H_k \in \mathbb{R}^{q^2 M^2 \times q^2 M^2}$ and matrix format) is the blur matrix which is a space and time invariant.
- D_k ($D_k \in \mathbb{R}^{M^2 \times q^2 M^2}$ and matrix format) is the decimation matrix assumed constant.
- V_k ($V_k \in \mathbb{R}^{M^2}$ and vector) is a system noise.



(a) High-Resolution Image



(b) Low-Resolution Image Sequence



(c) The Relation between Overlapping Blocked HR Image and Overlapping Blocked LR Image Sequence

Figure 2.1 The Classical SRR Observation Model

2.3.2 The Classical Regularized ML for SRR Algorithm

A popular family of estimators is the ML-type estimators (Maximum Likelihood Estimators) [50, 70]. We rewrite the definition of these estimators in the super resolution reconstruction framework as the following minimization problem:

$$\hat{\underline{X}} = \underset{\underline{X}}{\text{ArgMin}} \left\{ \sum_{k=1}^N \rho(D_k H_k F_k \underline{X} - \underline{Y}_k) \right\} \quad (2.2)$$

where $\rho(\cdot)$ is a norm estimation. To minimize (2.2), the intensity at each pixel of the expected image must be close to those of the original image.



สถาบันวิทยบริการ
จุฬาลงกรณ์มหาวิทยาลัย

2.4 Registration (Motion Estimation) for SRR Algorithm

This section briefly reviews only the existing practical registration algorithms that are used in the SRR algorithm. The SRR registration can be classified into two groups: the global region registration and the local region registration.

2.4.1 Global Registration for SRR Algorithm [109, 112]

Without loss of generality, the registration will assume that the camera is stationary and the object is undergoing a rigid motion then the global region motion estimation calculates a motion vector that can represent the entity image. This estimation uses only one MV (Motion Vector) to describe all motion in the image hence it can not describe the image having a several movement objects effectively.

1. The Translation Motion Estimation [42, 125] : The translation model, the simplest model, has two motion parameters (a and b) as shown in the following equation and this model can describe only a rigid 3-D translation therefore its motion parameters are readily estimated but it cannot represent a real complex motion.

$$v_x(x, y) = a \text{ and } v_y(x, y) = b \quad (2.3)$$

where $v_x(x, y)$ and $v_y(x, y)$ represent the motion of pixel (x, y) in x and y direction, respectively.

2. The Affine Motion Estimation [25, 42, 125] : The affine model, one of the most implemented model, has six motion parameters (a, b, c, d, e and f) as shown in the following equation. This model can describe the projected 2-D model of most camera motions and a patch undergoing arbitrary 3-D rigid motion but it cannot capture either the chirping or converging effect of the projection mapping.

$$v_x(x, y) = ax + by + c \text{ and } v_y(x, y) = dx + ey + f \quad (2.4)$$

3. The Bilinear Motion Estimation [42, 125] : The bilinear motion model has eight motion parameters (a, b, c, d, e, f, g and h) and is more effective than the translation and affine model because this model can represent a perspective mapping but the estimation of the motion vector is difficult. Moreover, the computation cost is considerably high.

$$v_x(x, y) = ax + by + cxy + d \text{ and } v_y(x, y) = ex + fy + gxy + h \quad (2.5)$$

There are other complex motion models, even though these models have accuracy, computational cost are too high to implement therefore other complex motion models are rarely implemented.

2.4.2 Regional Registration for SRR Algorithm [109, 112]

This estimation separates the image plane into small regions and estimates the MV of each region, thus, this estimation can well represent the image that consists of a several moving objects.

1. The Block-Based Motion Estimation [109, 125] : The block-based motion estimation, the most ubiquitous estimation, divides the image into non-overlapping blocks and estimates the translation motion vector of each block. This method is simple to implement in both the dividing process and estimation process and is used in standard codecs. It has the drawback of giving a severe artifact error to the compensated image.

2. The Object-Based Motion Estimation [109, 125] : The object-based motion estimation divides the image into non-overlapping objects and estimates the motion vector of each object by using translation, affine or high complex motion model. Theoretically, the object-based motion estimation has the highest accuracy. However, it assumes the accurate object segmentation which does not exist and is still under researched. Therefore, this estimation method is still impractical.

2.5 Estimation Technique for SRR Algorithm

Typically, many available estimators that estimate a HR image from a set of noisy LR images are not exclusively based on the LR measurement. They are also based on many assumptions such as noise or motion models and these models are not supposed to be exactly true, as they are merely mathematically convenient formulations of some general prior information. When the fundamental assumptions of data and noise models do not faithfully describe the measured data, the estimator performance degrades. Moreover, existence of outliers defined as data points with different distributional characteristics than the assumed model will produce erroneous estimates. Estimators promising optimality for a limited class of data and noise models may not be the most effective overall approach. Often, suboptimal estimation methods that are not as sensitive to modeling and data errors may produce better and more stable results (robustness).

2.5.1 L2 Norm Estimation for SRR Algorithm

The first popular family of estimators is the L2 Norm estimators that are used in super resolution problem [49-53, 88-89]. The definition of these estimators in the super resolution context is the following minimization problem:

$$\underline{X} = \underset{\underline{X}}{\text{ArgMin}} \left\{ \sum_{k=1}^N (D_k H_k F_k \underline{X} - \underline{Y}_k)^2 \right\} \quad (2.6)$$

The L2 norm produces estimator with lower variance than the optimal L1 norm but the L2 norm is very sensitive to outliers because the influence function increases linearly and without bound.

By the steepest descent method, the solution of Equation (2.6) is defined as follows:

$$\hat{\underline{X}}_{n+1} = \hat{\underline{X}}_n + \beta \cdot \left\{ \sum_{k=1}^N F_k^T H_k^T D_k^T (\underline{Y}_k - D_k H_k F_k \hat{\underline{X}}_n) \right\} \quad (2.7)$$

where β is a scalar defining the step size in the direction of the gradient.

2.5.2 L1 Norm Estimation for SRR Algorithm

Another popular family of estimators is the L1 Norm estimators [98-100] and this norm is more robust than L2 Norm. The L1 norm is not sensitive to outliers because the influence function, $\rho'(\cdot)$, is constant and bounded but the L1 norm produces an estimator with higher variance than the optimal L2 (quadratic) norm. We rewrite the definition of these estimators in the super resolution reconstruction framework as the following minimization problem:

$$\underline{X} = \underset{\underline{X}}{\text{ArgMin}} \left\{ \sum_{k=1}^N |D_k H_k F_k \underline{X} - \underline{Y}_k| \right\} \quad (2.8)$$

By the steepest descent method, the solution of Equation (2.8) is defined as follows:

$$\hat{\underline{X}}_{n+1} = \hat{\underline{X}}_n + \beta \cdot \left\{ \left(\sum_{k=1}^N F_k^T H_k^T D_k^T \text{sign}(D_k H_k F_k \hat{\underline{X}}_n - \underline{Y}_k) \right) \right\} \quad (2.9)$$

2.6 Regularization Technique for SRR Algorithm

SRR (Super-Resolution Reconstruction), described in Section 2.2.4, is an ill-posed problem [98]. For the under-determined cases (i.e., when fewer than required frames are available), there exist an infinite number of solutions which satisfy (2.2). The solution for squared and over-determined cases is not stable, which means small amounts of noise in measurements will result in large perturbations in the final solution. Therefore, considering regularization in SRR algorithm as a mean for picking a stable solution is very useful, if not necessary. Also, regularization can help the algorithm to remove artifacts from the final answer and improve the rate of convergence. A regularization term compensates the missing measurement information with some general prior information about the desirable HR solution, and is usually implemented as a penalty factor in the generalized minimization cost function. Unfortunately, certain types of regularization cost functions work efficiently for some special types of images but are not suitable for general images.

From (2.2), we rewrite the definition of these estimators in the super resolution context as the following minimization problem:

$$\underline{X} = \underset{\underline{X}}{\text{ArgMin}} \left\{ \sum_{k=1}^N \rho(D_k H_k F_k \underline{X} - \underline{Y}_k) + \lambda \cdot \Upsilon(\underline{X}) \right\} \quad (2.10)$$

where $\Upsilon(\cdot)$ is the regularization function and λ is a scalar defining the regularization parameter.

2.6.1 Laplacian Regularization for SRR Algorithm [98-100]

In general, Tikhonov regularization $\Upsilon(\cdot)$ was replaced by matrix realization of the Laplacian kernel [98-100], the most classical and simplest regularization cost function. The Laplacian kernel is defined as

$$\Gamma = \frac{1}{8} \begin{bmatrix} 1 & 1 & 1 \\ 1 & -8 & 1 \\ 1 & 1 & 1 \end{bmatrix} \quad (2.11)$$

Combining the Laplacian regularization, we propose the solution of the super-resolution problem is as follows:

$$\underline{X} = \underset{\underline{X}}{\text{ArgMin}} \left\{ \sum_{k=1}^N \rho(D_k H_k F_k \underline{X} - \underline{Y}_k) + \lambda \cdot \rho_{REG}(\Gamma \underline{X}) \right\} \quad (2.12)$$

The most classical and simplest regularization norm function, $\rho_{REG}(\cdot)$, is $\rho_{REG}(\cdot) = (\cdot)^2$ thus the solution of the super-resolution problem is defined as

$$\underline{X} = \underset{\underline{X}}{\text{ArgMin}} \left\{ \sum_{k=1}^N \rho(D_k H_k F_k \underline{X} - \underline{Y}_k) + \lambda \cdot (\Gamma \underline{X})^2 \right\} \quad (2.13)$$

2.6.1.1 L2 Norm Estimation with Laplacian Regularization for SRR Algorithm [98-100]

By using L2 norm estimation, we rewrite the definition of these estimators in the super resolution context as the following minimization problem:

$$\underline{X} = \underset{\underline{X}}{\text{ArgMin}} \left\{ \sum_{k=1}^N (D_k H_k F_k \underline{X} - \underline{Y}_k)^2 + \lambda \cdot (\Gamma \underline{X})^2 \right\} \quad (2.14)$$

By the steepest descent method, the solution of Equation (2.14) is defined as

$$\hat{\underline{X}}_{n+1} = \hat{\underline{X}}_n + \beta \cdot \left\{ \left(\sum_{k=1}^N F_k^T H_k^T D_k^T (\underline{Y}_k - D_k H_k F_k \hat{\underline{X}}_n) \right) - \left(\lambda \cdot (\Gamma^T \Gamma) \hat{\underline{X}}_n \right) \right\} \quad (2.15)$$

2.6.1.2 L1 Norm Estimation with Laplacian Regularization for SRR Algorithm [98-100]

By using L1 norm estimation, the definition of these estimators in the super resolution context is rewritten as the following minimization problem:

$$\underline{X} = \underset{\underline{X}}{\text{ArgMin}} \left\{ \sum_{k=1}^N |D_k H_k F_k \underline{X} - \underline{Y}_k| + \lambda \cdot (\Gamma \underline{X})^2 \right\} \quad (2.16)$$

By the steepest descent method, the solution of Equation (2.16) is defined as

$$\hat{\underline{X}}_{n+1} = \hat{\underline{X}}_n + \beta \cdot \left\{ \left(\sum_{k=1}^N F_k^T H_k^T D_k^T \text{sign}(D_k H_k F_k \hat{\underline{X}}_n - \underline{Y}_k) \right) - \left(\lambda \cdot (\Gamma^T \Gamma) \hat{\underline{X}}_n \right) \right\} \quad (2.17)$$

2.6.2 MRF (Markov Random Field) Regularization for SRR Algorithm [87-89]

Due to MRF (Markov Random Field) that can model the image characteristic especially on image texture, the MRF regularization is typically used in single and multiframe image restoration. The definition of these estimators in the super resolution context is defined as the following minimization problem:

$$\underline{X} = \underset{\underline{X}}{\text{ArgMin}} \left\{ \sum_{k=1}^N \rho(D_k H_k F_k \underline{X} - \underline{Y}_k) + \left(-\frac{1}{2\beta_{MRF}} \sum_{c \in C} \rho_c(\mathbf{d}_c^t \underline{X}) \right) \right\} \quad (2.18)$$

In this expression, β_{MRF} is the temperature parameter for the Gibbs prior, and c is a local group of pixels contained within the set of all image cliques C . The quantity $\mathbf{d}_c^t \underline{X}$ is a spatial activity measure within the data, with a small value in smooth image locations and a large value at edges. Traditionally, four spatial activity measures are computed at each pixel in the high-resolution image, given by the following second-order finite differences:

$$\mathbf{d}_{m,n,1}^t \mathbf{x} = x_{m,n+1} - 2x_{m,n} + x_{m,n-1} \quad (2.19a)$$

$$\mathbf{d}_{m,n,2}^t \mathbf{x} = 0.5x_{m-1,n+1} - x_{m,n} + 0.5x_{m+1,n-1} \quad (2.19b)$$

$$\mathbf{d}_{m,n,3}^t \mathbf{x} = x_{m-1,n} - 2x_{m,n} + x_{m+1,n} \quad (2.19c)$$

$$\mathbf{d}_{m,n,4}^t \mathbf{x} = 0.5x_{m-1,n-1} - x_{m,n} + 0.5x_{m+1,n+1} \quad (2.19d)$$

Traditionally, the regularization norm function, $\rho_\alpha(\cdot)$, may be a quadratic function ($\rho_\alpha(\cdot) = (\cdot)^2$) or Huber function that is defined as

$$\rho_\alpha(x) = \rho_{HUBER}(x) = \begin{cases} x^2 & ; |x| \leq T_{HUBER} \\ T_{HUBER}^2 + 2T_{HUBER}(|x| - T_{HUBER}) & ; |x| > T_{HUBER} \end{cases} \quad (2.20)$$

where T_{HUBER} is a threshold parameter separating the quadratic and linear regions.

2.6.2.1 L2 Norm Estimation with MRF Regularization for SRR Algorithm [87-89]

By using L2 norm estimation, the definition of these estimators in the super resolution context is defined as the following minimization problem:

$$\underline{X} = \underset{\underline{X}}{\text{ArgMin}} \left\{ \sum_{k=1}^N \left((D_k \cdot H_k \cdot F_k \cdot \underline{X} - \underline{Y}_k)^2 \right) + \left(-\frac{1}{2\beta_{MRF}} \sum_{c \in C} \rho_\alpha(\mathbf{d}_c^t \underline{X}) \right) \right\} \quad (2.21)$$

By the steepest descent method, the solution of Equation (2.21) is defined as

$$\underline{\hat{X}}_{n+1} = \underline{\hat{X}}_n + \beta \cdot \left\{ \begin{array}{l} \left(\sum_{k=1}^N F_k^T H_k^T D_k^T (\underline{Y}_k - D_k H_k F_k \underline{\hat{X}}_n) \right) \\ - \left(\lambda \cdot \sum_{c \in C} \rho'_\alpha(\mathbf{d}_c^t \underline{\hat{X}}_n) \right) \end{array} \right\} \quad (2.22)$$

where $\rho'_\alpha(\cdot)$ is defined as

$$\rho'_\alpha(\cdot) = 2x \quad ; \text{if } \rho_\alpha(\cdot) \text{ is a quadratic function} \quad (2.23a)$$

$$\rho'_\alpha(\cdot) = \begin{cases} 2x & ; |x| \leq T_{HUBER} \\ 2T_{HUBER} \cdot \text{sign}(x) & ; |x| > T_{HUBER} \end{cases} ; \text{if } \rho_\alpha(\cdot) \text{ is a Huber function} \quad (2.23b)$$

2.6.2.2 L1 Norm Estimation with MRF Regularization for SRR Algorithm [87-89]

By using L1 norm estimation, the definition of these estimators in the super resolution context is defined as the following minimization problem:

$$\underline{X} = \underset{\underline{X}}{\text{ArgMin}} \left\{ \sum_{k=1}^N |D_k \cdot H_k \cdot F_k \cdot \underline{X} - \underline{Y}_k| + \left(-\frac{1}{2\beta_{MRF}} \sum_{c \in C} \rho_\alpha(\mathbf{d}_c^t \underline{X}) \right) \right\} \quad (2.24)$$

By the steepest descent method, the solution of Equation (2.24) is defined as

$$\underline{\hat{X}}_{n+1} = \underline{\hat{X}}_n + \beta \cdot \left\{ \begin{array}{l} \left(\sum_{k=1}^N F_k^T H_k^T D_k^T \text{sign}(D_k H_k F_k \underline{\hat{X}}_n - \underline{Y}_k) \right) \\ - \left(\lambda \cdot \sum_{c \in C} \rho'_\alpha(\mathbf{d}_c^t \underline{\hat{X}}_n) \right) \end{array} \right\} \quad (2.25)$$

2.6.3 BTV (Bilateral-Total Variance) Regularization [54, 98-100] for SRR Algorithm

One of the most successful regularization methods for denoising and deblurring is the total variation (TV) method [54]. The TV criterion penalizes the total amount of change in the image as measured by the L1 norm of the magnitude of the gradient. Based on the spirit of TV criterion, and a related technique called the bilateral filter [54], the robust SRR regularizer [98-100] called Bilateral TV was introduced in 2004, which is computationally cheap to implement, and preserves edges. The BTV regularization is defined as

$$\gamma(\underline{X}) = \sum_{l=-P}^P \sum_{m=0}^P \alpha^{|m|+|l|} \|\underline{X} - S_x^l S_y^m \underline{X}\| \quad (2.26)$$

where matrices (operators), S_x^l and S_y^m shift \underline{X} by l and m pixels in horizontal and vertical directions respectively, presenting several scales of derivatives. The scalar weight α , $0 < \alpha < 1$, is applied to give a spatially decaying effect to the summation of the regularization terms [33, 98-100]. Combining the BTV regularization, we rewrite the definition of these estimators in the super resolution context as the following minimization problem:

$$\underline{X} = \underset{\underline{X}}{\text{ArgMin}} \left\{ \begin{array}{l} \sum_{k=1}^N (\rho(D_k \cdot H_k \cdot F_k \cdot \underline{X} - \underline{Y}_k)) \\ + \lambda \left(\sum_{l=-P}^P \sum_{m=0}^P \alpha^{|m|+|l|} \|\underline{X} - S_x^l S_y^m \underline{X}\| \right) \end{array} \right\} \quad (2.27)$$

2.6.3.1 L2 Norm Estimation with BTV Regularization for SRR Algorithm [98-100]

By using L2 norm estimation, we rewrite the definition of these estimators in the super resolution context as the following minimization problem:

$$\underline{X} = \underset{\underline{X}}{\text{ArgMin}} \left\{ \begin{array}{l} \sum_{k=1}^N ((D_k \cdot H_k \cdot F_k \cdot \underline{X} - \underline{Y}_k)^2) \\ + \lambda \left(\sum_{l=-P}^P \sum_{m=0}^P \alpha^{|m|+|l|} \|\underline{X} - S_x^l S_y^m \underline{X}\| \right) \end{array} \right\} \quad (2.28)$$

By the steepest descent method, the solution of Equation (2.28) is defined as

$$\hat{\underline{X}}_{n+1} = \hat{\underline{X}}_n + \beta \cdot \left\{ \begin{array}{l} \left(\sum_{k=1}^N F_k^T H_k^T D_k^T (\underline{Y}_k - D_k H_k F_k \hat{\underline{X}}_n) \right) \\ -\lambda \left(\sum_{l=-P}^P \sum_{m=0}^P \alpha^{|m|+|l|} (I - S_x^l S_y^m) \cdot \text{sign}(\hat{\underline{X}} - S_x^l S_y^m \hat{\underline{X}}) \right) \end{array} \right\} \quad (2.29)$$

2.6.3.2 L1 Norm Estimation with BTV Regularization for SRR Algorithm [98-100]

By using L1 norm estimation, the definition of these estimators in the super resolution context is defined as the following minimization problem:

$$\underline{X} = \underset{\underline{X}}{\text{ArgMin}} \left\{ \begin{array}{l} \sum_{k=1}^N |D_k \cdot H_k \cdot F_k \cdot \underline{X} - \underline{Y}_k| \\ + \lambda \left(\sum_{l=-P}^P \sum_{m=0}^P \alpha^{|m|+|l|} \|\underline{X} - S_x^l S_y^m \underline{X}\| \right) \end{array} \right\} \quad (2.30)$$

By the steepest descent method, the solution of Equation (2.30) is defined as

$$\hat{\underline{X}}_{n+1} = \hat{\underline{X}}_n + \beta \cdot \left\{ \begin{array}{l} \left(\sum_{k=1}^N F_k^T H_k^T D_k^T \text{sign}(D_k H_k F_k \hat{\underline{X}}_n - \underline{Y}_k) \right) \\ -\lambda \left(\sum_{l=-P}^P \sum_{m=0}^P \alpha^{|m|+|l|} (I - S_x^l S_y^m) \cdot \text{sign}(\hat{\underline{X}} - S_x^l S_y^m \hat{\underline{X}}) \right) \end{array} \right\} \quad (2.31)$$

CHAPTER III

A FAST AFFINE BLOCK-BASED REGISTRATION AND ROBUST ESTIMATION TECHNIQUES FOR SRR

In this chapter, we first proposed the novel sub-pixel image registration that is designed to overcome the insufficient temporal sampling frequency and to register the real complex motion sequence that the traditional SSR registration can not support in Section 3.1. To realize the implementation of the proposed sub-pixel image registration, the fast algorithm is designed to reduce the computational load for the proposed sub-pixel registration. We later proposed the novel robust estimation technique for SSR framework to increase the estimated performance and to robust against the several noise models and registration error in Section 3.2. Finally, we proposed the SRR algorithm using the proposed robust norm estimation with the proposed registration in Section 3.3.

3.1 Fast Affine Block-Based Registration/Motion Estimation [109]

Due to the prosperity of the multimedia technology, the highly accurate motion estimation is crucial in high quality image processing applications such as SRR (Super-Resolution Reconstruction) algorithms. Numerical methods for solving this problem are based on the classical (or translation) block-based motion estimation algorithm but the pure translation model can not represent the real complex motion effectively.

This section aims to propose Affine Block-Based Motion Estimation which describes the complex motion more efficiently and gives excellent result on a highly accurate motion vectors in section 3.1.1, and to propose M3SS (Modified Three Step Search) algorithm that is designed to reduce a computational load in section 3.1.2. This algorithm starts by partitioning the image domain into non-overlapping small regions, called blocks, and computing the motion vector within each block by an affine model, instead of a conventional translation model. Therefore, the motion vector (MV) of each block consists of six motion (instead of two) parameters.

3.1.1 Affine Block-Based Registration

Traditionally, the classical motion estimation [109] can detect only pure translational motion along the image plane and fails to consider any complex motions that arise due to rotation, zooming, etc. An efficient way of detecting several complex motions is by using the combination of a block-base technique and an affine model. In this section, we propose a scheme for estimating affine block-based motion vectors suitable for several complex motions. The estimation can be separated to 2 stages. At the first stage of the estimation algorithm, the current and reference frames are divided into overlapping blocks (16x16). This stage divides the image into small areas in order to detect and estimate the local motions. The advantage of this stage is to reduce the computational load and allow the parallel processing. Next, the second stage computes the affine motion vector of each block between the current and the reference frame.

3.1.2 Modified Three Step Search Algorithm

The M3SS is proposed to reduce a very high computational load in affine motion vector estimation. The 3SS (Three Step Search) is one of the popular and fast algorithms used in the translational registration; therefore, this paper develops the M3SS (6 motion parameter estimation, Equation (3.1)) based on 3SS (2 motion parameter estimation Equation (3.2)).

$$mv_{x,affine}(x, y) = ax + by + c \quad \text{and}$$

$$mv_{y,affine}(x, y) = dx + ey + f \quad (3.1)$$

$$mv_{x,tran}(x, y) = a \quad \text{and} \quad mv_{y,tran}(x, y) = b \quad (3.2)$$

For the 7x7 displacement window (translational deformation) and $\pm 20^\circ$ degree (rotation, extraction or expansion deformation), the proposed M3SS algorithm utilizes a search pattern with $3^6 = 729$ check points on a search window in the first step. The point having the minimum error is used as the center of the search area in the subsequent step. The search window is reduced by half in the subsequent step until the search window equals to pre-determined resolution. (The criterion for parameter selection in this paper was based on experiments and the chosen parameters produce the highest PSNR result on 3 standard

sequences: Foreman, Carphone and Stefan [109].) The process of M3SS is described as follow:

Step 1 : Initialized the dimension of the searching area to the value depicted in Equation (3.3).

$$\begin{aligned} & [a, b, c, d, e, f] \\ & = [\pm 0.16, \pm 0.16, \pm 2 \pm 0.16, \pm 0.16, \pm 2] \end{aligned} \quad (3.3)$$

Step 2 : A minimum BDM (Block Distortion Measure) point is found from a 729 check point pattern at the center of the searching area as shown in (3.3) and this process is shown in Fig. 3.1.

Step 3 : If the search window is equal to (3.4) then the process stop otherwise go to step 4 and this process is shown in Fig. 3.2.

$$\begin{aligned} & [a, b, c, d, e, f] \\ & = [\pm 0.01, \pm 0.01, \pm 0.125 \pm 0.01, \pm 0.01, \pm 0.125] \end{aligned} \quad (3.4)$$

Step 4 : The search window is reduced by half in all dimensions of the previous search window and a minimum BDM (Block Distortion Measure) point is found from a 729 check point pattern at the center of the new searching area. It will go to step 2.

From Table 1, the total number of the M3SS check points is fixed at 3.65E+3. Compared with the classical block-based estimation method (translation block-based estimation method) at 0.25 pixel accuracy and $w=9$, the total number of the M3SS check points has just approximately 3 times more computational load than the classical FS approach.

Table 3.1 : Performance Comparison of Registration Method

Block-Based Registration Method	BMA (Block Matching Algorithm)	The Number of Search Points
Affine	FS (Full Search)	1.29E+09
	M3SS	3.65E+03
Translation	FS (Full Search : 0.25 Pixel)	1.09E+03
	FS (Full Search : 1 Pixel)	2.56E+02

```

MIN_MAD = INF
For each block
  For c = -2 : 2 : 2
    For f = -2 : 2 : 2
      For a = -0.16 : 0.16 : 0.16
        For b = -0.16 : 0.16 : 0.16
          For d = -0.16 : 0.16 : 0.16
            For e = -0.16 : 0.16 : 0.16
              - The Reference frame is transformed
                by affine MV (a,b,c,d,e,f) to be
                the transformed Frame.
              - Compute the MAD value between the
                transformed frame and current frame.
              - If the MAD is less than MIN_MAD
                then MIN_MAD is equal the MAD
                and the 1st level affine MV is
                (a,b,c,d,e,f) .
            ENDfor
          ENDfor
        ENDfor
      ENDfor
    ENDfor
  ENDfor
ENDfor

```

Figure 3.1 : The Algorithm of the M3SS at Step 2

```

(a0,b0,c0,d0,e0,f0) = previous affine MV
MIN_MAD = INF
For each block
  For c = c0-0.125 : 0.125 : c0 + 0.125
    For f = f0-0.125 : 0.125 : f0 + 0.125
      For a = a0-0.01 : 0.01 : a0+0.01
        For b = b0-0.01 : 0.01 : b0+0.01
          For d = d0-0.01 : 0.01 : d0+0.01
            For e = e0-0.01 : 0.01 : e0+0.01
              - The Reference frame is transformed
                by affine MV (a,b,c,d,e,f) to be
                the transformed Frame.
              - Compute the MAD value between the
                transformed frame and current frame.
              - If the MAD is less than MIN_MAD
                then MIN_MAD is equal the MAD
                and the best affine MV is
                (a,b,c,d,e,f) .
            ENDfor
          ENDfor
        ENDfor
      ENDfor
    ENDfor
  ENDfor
ENDfor

```

Figure 3.2 : The Algorithm of the M3SS at Step 4

3.2 Robust Norm Estimation for SRR [120]

The success of SRR algorithm is highly dependent on the accuracy of the imaging process model. Unfortunately, these models are not supposed to be exactly true, as they are merely mathematically convenient formulations of some general prior information. When the data or noise model assumptions do not faithfully describe the measure data, the estimator performance degrades. Furthermore, existence of outliers defined as data points with different distributional characteristics than the assumed model will produce erroneous estimates. Almost all noise models used in SRR algorithms are based on Additive White Gaussian Noise (AWGN) model; therefore, SRR algorithms can effectively apply only on the image sequence that is corrupted by AWGN. Due to this noise model, L1 norm or L2 norm error are effectively used in SRR algorithm. Unfortunately, the real noise models that corrupt the measure sequence are unknown therefore SRR algorithm using L1 norm or L2 norm may degrade the image sequence rather than enhance it. The robust norm error is necessary for SRR algorithm applicable to several noise models. For normally distributed data, the L1 norm produces estimates with higher variance than the optimal L2 (quadratic) norm but the L2 norm is very sensitive to outliers because the influence function increases linearly and without bound. From the robust statistical estimation [58-61], Huber, Lorentzian and Tukey-Biweight Norm are designed to be more robust than L1 and L2. While these robust norms are designed to reject outliers, these norms must be more forgiving about the remaining outliers; that is, it should increase less rapidly than L2. The norm function and their influence functions investigated in the section are shown in Figure 3.3.

3.2.1 Huber Norm Estimation for SRR [114, 119]

A robust estimation is estimated technique that is resistance to such outliers. In SRR framework, outliers are measured images or corrupted images that are highly inconsistent with the high resolution original image. Outliers may arise from several reasons such as procedural measurement error, noise or inaccurate mathematical model. Outliers should be investigated carefully; therefore, we need to analyze the outlier in a way which minimizes their effect on the estimated model. L2 norm estimation is highly susceptible to even a small number of discordant observations or outliers. For L2 norm estimation, the influence of the outlier is much larger than the other measured data because L2 norm estimation weights the error quadratically. Consequently, the robustness of L2 norm estimation is poor.

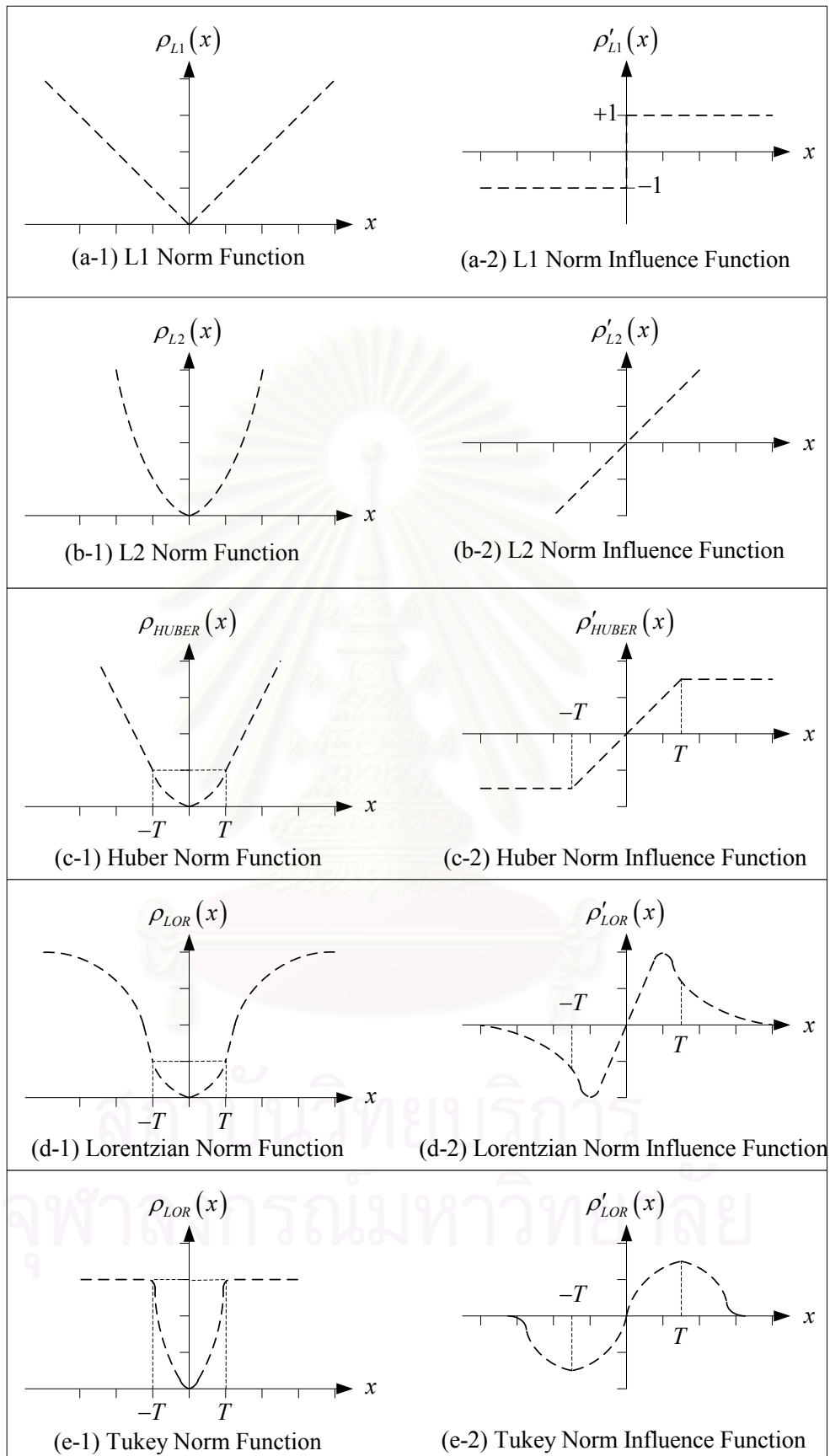


Figure 3.3 The Norm function and the Influence function

Huber's norm [58-61, 114, 119] is one of error norm from the robust statistic literature. It is equivalent to the L1 norm for large value. But, for normally distributed data, the L1 norm produces estimates with higher variance than the optimal L2 (quadratic) norm, so Huber's norm is designed to be quadratic for small values and its influence does not descend all the way to zero. The Huber norm function ($\rho(\cdot)$) and its influence function ($\rho'(\cdot)$) are shown in Figure 3.3 (c-1) and Figure 3.3 (c-2), respectively

3.2.1.1 Huber Norm Estimation Definition

In this section, we propose the novel robust SRR using Huber error norm. From (2.2), we rewrite the definition of these robust estimators in the super resolution context as the following minimization problem:

$$\underline{X} = \underset{\underline{X}}{\text{ArgMin}} \left\{ \sum_{k=1}^N \rho_{HUBER} (D_k H_k F_k \underline{X} - \underline{Y}_k) \right\} \quad (3.5)$$

$$\rho_{HUBER} (x) = \begin{cases} x^2 & ; |x| \leq T \\ T^2 + 2T(|x| + T) & ; |x| > T \end{cases} \quad (3.6)$$

where T is norm constant parameter that is a soft threshold value.

3.2.1.2 Huber Norm Estimation for SRR [114, 119]

By the steepest descent method, the solution of Equation (3.5) is defined as

$$\hat{X}_{n+1} = \hat{X}_n + \beta \cdot \left\{ \sum_{k=1}^N F_k^T H_k^T D_k^T \cdot \rho'_{HUBER} (\underline{Y}_k - D_k H_k F_k \hat{X}_n) \right\} \quad (3.7)$$

$$\rho'_{HUBER} (x) = \begin{cases} 2x & ; |x| \leq T \\ 2T \cdot \text{sign}(x) & ; |x| > T \end{cases} \quad (3.8)$$

3.2.1.3 Huber Norm Estimation for SRR with Laplacian Regularization [114, 115]

Combining the Laplacian regularization, we propose the solution of the super-resolution problem as follows:

$$\underline{X} = \underset{\underline{X}}{\text{ArgMin}} \left\{ \sum_{k=1}^N \rho_{HUBER} (D_k H_k F_k \underline{X} - \underline{Y}_k) + \lambda \cdot (\Gamma \underline{X})^2 \right\} \quad (3.9)$$

By the steepest descent method, the solution of Equation (3.9) is defined as

$$\hat{\underline{X}}_{n+1} = \hat{\underline{X}}_n + \beta \cdot \left\{ \begin{array}{l} \sum_{k=1}^N F_k^T H_k^T D_k^T \cdot \rho'_{HUBER} (\underline{Y}_k - D_k H_k F_k \hat{\underline{X}}_n) \\ -(\lambda \cdot (\Gamma^T \Gamma) \hat{\underline{X}}_n) \end{array} \right\} \quad (3.10)$$

3.2.1.4 Huber Norm Estimation for SRR with Huber-Laplacian Regularization [119]

Combining the Huber-Laplacian regularization, we propose the solution of the super-resolution problem as follows:

$$\underline{X} = \underset{\underline{X}}{\text{ArgMin}} \left\{ \sum_{k=1}^N \rho_{HUBER} (D_k H_k F_k \underline{X} - \underline{Y}_k) + \lambda \cdot \psi_{HUBER} (\Gamma \underline{X}) \right\} \quad (3.11)$$

$$\psi_{HUBER} (x) = \begin{cases} x^2 & ; |x| \leq T_g \\ T_g^2 + 2T_g (|x| - T_g) & ; |x| > T_g \end{cases} \quad (3.12)$$

By the steepest descent method, the solution of Equation (3.12) is defined as

$$\hat{\underline{X}}_{n+1} = \hat{\underline{X}}_n + \beta \cdot \left\{ \begin{array}{l} \sum_{k=1}^N F_k^T H_k^T D_k^T \cdot \rho'_{HUBER} (\underline{Y}_k - D_k H_k F_k \hat{\underline{X}}_n) \\ -(\lambda \cdot \Gamma^T \cdot \psi'_{HUBER} (\Gamma \hat{\underline{X}}_n)) \end{array} \right\} \quad (3.13)$$

$$\psi'_{HUBER} (x) = \begin{cases} 2x & ; |x| \leq T_g \\ 2T_g \cdot \text{sign}(x) & ; |x| > T_g \end{cases} \quad (3.14)$$

3.2.2 Lorentzian Norm Estimation for SRR [113, 115, 116, 120]

This section first reviews the main concepts of Lorentzian norm estimation technique and later develops the Lorentzian norm estimation for SRR framework.

3.2.2.1 Lorentzian Norm Estimation Definition

Much can be improved if the influence is bounded in one way or another. This is exactly the general idea of applying a robust error norm. Instead of using the sum of squared differences (2.6), this error norm should be selected such that above a given level of x , its influence is ruled out. In addition, one would like to have $\rho(x)$ being smooth so that numerical minimization of (2.2) is not too difficult. The one of suitable choices (among other) is so-called Lorentzian error norm [58-61]. In this section, we propose the novel robust SRR using Lorentzian error norm. From (2.2), the definition of these robust estimators in the super resolution is defined context as the following minimization problem:

$$\underline{X} = \underset{\underline{X}}{\text{ArgMin}} \left\{ \sum_{k=1}^N \rho_{\text{LOR}}(D_k H_k F_k \underline{X} - \underline{Y}_k) \right\} \quad (3.15)$$

$$\rho_{\text{LOR}}(x) = \log \left[1 + \frac{1}{2} \left(\frac{x}{T} \right)^2 \right] \quad (3.16)$$

For values of x smaller than T , the function follows the L2 norm. For values larger than T , the function gets saturated. Consequently for small value of x , the derivative of $\rho'(x) = \partial\{\rho(x)\}/\partial x$ of $\rho(x)$ is nearly a constant. But for large values of x (for outliers), it becomes nearly zero. Therefore, in a Gauss-Newton style of optimization, the Jacobian matrix is virtually zero for outliers. Only residuals that are about as large as T or smaller than that play a role.

From L1 and L2 norm estimation point of view, Lorentzian's norm is equivalent to the L1 norm for large value. But, for normally distributed data, the L1 norm produces estimates with higher variance than the optimal L2 (quadratic) norm, so Lorentzian's norm is designed to be quadratic for small values and be bound for large values. The Lorentzian norm function ($\rho(\cdot)$) and its influence function ($\rho'(\cdot)$) are shown in Figure 3.3 (c-1) and Figure 3.3 (c-2) respectively.

3.2.2.2 Lorentzian Norm Estimation for SRR [113, 115, 116, 120]

By the steepest descent method, the solution of Equation (3.15) is defined as

$$\underline{\hat{X}}_{n+1} = \underline{\hat{X}}_n + \beta \cdot \left\{ \sum_{k=1}^N F_k^T H_k^T D_k^T \cdot \rho'_{LOR}(\underline{Y}_k - D_k H_k F_k \underline{\hat{X}}_n) \right\} \quad (3.17)$$

$$\rho'_{LOR}(x) = \frac{2x}{2T^2 + x^2} \quad (3.18)$$

3.2.2.3 Lorentzian Norm Estimation for SRR with Laplacian Regularization [113, 115, 116, 120]

Combining the Laplacian regularization, we propose the solution of the super-resolution problem as follows:

$$\underline{X} = \underset{\underline{X}}{\text{ArgMin}} \left\{ \sum_{k=1}^N \rho_{LOR}(D_k H_k F_k \underline{X} - \underline{Y}_k) + \lambda \cdot (\Gamma \underline{X})^2 \right\} \quad (3.19)$$

By the steepest descent method, the solution of Equation (3.19) is defined as

$$\underline{\hat{X}}_{n+1} = \underline{\hat{X}}_n + \beta \cdot \left\{ \begin{array}{l} \sum_{k=1}^N F_k^T H_k^T D_k^T \cdot \rho'_{LOR}(\underline{Y}_k - D_k H_k F_k \underline{\hat{X}}_n) \\ -(\lambda \cdot (\Gamma^T \Gamma) \underline{\hat{X}}_n) \end{array} \right\} \quad (3.20)$$

3.2.2.4 Lorentzian Norm Estimation for SRR with Lorentzian-Laplacian Regularization [113, 120]

Combining the Lorentzian-Laplacian regularization, we propose the solution of the super-resolution problem as follows:

$$\underline{X} = \underset{\underline{X}}{\text{ArgMin}} \left\{ \sum_{k=1}^N \rho_{LOR}(D_k H_k F_k \underline{X} - \underline{Y}_k) + \lambda \cdot \psi_{LOR}(\Gamma \underline{X}) \right\} \quad (3.21)$$

$$\psi_{LOR}(x) = \log \left[1 + \frac{1}{2} \left(\frac{x}{T_g} \right)^2 \right] \quad (3.22)$$

By the steepest descent method, the solution of Equation (3.21) is defined as

$$\hat{\underline{X}}_{n+1} = \hat{\underline{X}}_n + \beta \cdot \left\{ \begin{array}{l} \sum_{k=1}^N F_k^T H_k^T D_k^T \cdot \rho'_{LOR}(\underline{Y}_k - D_k H_k F_k \hat{\underline{X}}_n) \\ -(\lambda \cdot \Gamma^T \cdot \psi'_{LOR}(\Gamma \hat{\underline{X}}_n)) \end{array} \right\} \quad (2.23)$$

$$\psi'_{LOR}(x) = \frac{2x}{2T_g^2 + x^2} \quad (2.24)$$



สถาบันวิทยบริการ
จุฬาลงกรณ์มหาวิทยาลัย

3.2.3 Tukey's Biweight Estimation Norm for SRR [117]

This section first reviews the main concepts of Tukey's Biweight norm estimation technique and later develops the Tukey's Biweight norm estimation for SRR framework.

3.2.3.1 Tukey's Biweight Norm Estimation Definition

Tukey's Biweight norm [58-61, 117] is another error norm from the robust statistic literature. It is more robust than L1 and L2 norm. While the Lorentzian norm is more robust than L2 (quadratic norm), its influence does not descend all the way to zero. Tukey's Biweight norm is a more robust from the robust statistics literature whose value does descend to zero. We propose the novel robust SRR using Tukey's Biweight error norm. From (2.2), we rewrite the definition of these robust estimators in the super resolution context as the following minimization problem:

$$\underline{X} = \underset{\underline{X}}{\text{ArgMin}} \left\{ \sum_{k=1}^N \rho_{TUKEY} (D_k H_k F_k \underline{X} - \underline{Y}_k) \right\} \quad (3.25)$$

$$\rho_{TUKEY}(x) = \begin{cases} \frac{x^2}{T^2} - \frac{x^4}{T^4} + \frac{x^6}{3T^6} & ; |x| \leq T \\ \frac{1}{3} & ; otherwise \end{cases} \quad (3.26)$$

3.2.3.2 Tukey's Biweight Norm Estimation for SRR

By the steepest descent method, the solution of Equation (3.25) is defined as

$$\hat{X}_{n+1} = \hat{X}_n + \beta \cdot \left\{ \sum_{k=1}^N F_k^T H_k^T D_k^T \cdot \rho'_{TUKEY} (\underline{Y}_k - D_k H_k F_k \hat{X}_n) \right\} \quad (3.27)$$

$$\rho'_{TUKEY}(x) = \begin{cases} x \left[1 - (x/T)^2 \right]^2 & ; |x| \leq T \\ 0 & ; otherwise \end{cases} \quad (3.28)$$

3.2.3.3 Tukey's Biweight Norm Estimation for SRR with Laplacian Regularization

Combining the Laplacian regularization, we propose the solution of the super-resolution problem as follows:

$$\underline{X} = \underset{\underline{X}}{\text{ArgMin}} \left\{ \sum_{k=1}^N \rho_{TUKEY} (D_k H_k F_k \underline{X} - \underline{Y}_k) + \lambda \cdot (\Gamma \underline{X})^2 \right\} \quad (3.29)$$

By the steepest descent method, the solution of Equation (3.29) is defined as

$$\underline{\hat{X}}_{n+1} = \underline{\hat{X}}_n + \beta \cdot \left\{ \begin{array}{l} \sum_{k=1}^N F_k^T H_k^T D_k^T \cdot \rho'_{TUKEY} (\underline{Y}_k - D_k H_k F_k \underline{\hat{X}}_n) \\ -(\lambda \cdot (\Gamma^T \Gamma) \underline{\hat{X}}_n) \end{array} \right\} \quad (3.30)$$

3.2.3.4 Tukey's Biweight Norm Estimation for SRR with Tukey-Laplacian Regularization

Combining the Tukey-Laplacian regularization, we propose the solution of the super-resolution problem as follows:

$$\underline{X} = \underset{\underline{X}}{\text{ArgMin}} \left\{ \sum_{k=1}^N \rho_{TUKEY} (D_k H_k F_k \underline{X} - \underline{Y}_k) + \lambda \cdot \psi_{TUKEY} (\Gamma \underline{X}) \right\} \quad (3.31)$$

$$\psi_{TUKEY} (x) = \begin{cases} \frac{x^2}{T_g^2} - \frac{x^4}{T_g^4} + \frac{x^6}{3T_g^6} & ; |x| \leq T_g \\ \frac{1}{3} & ; otherwise \end{cases} \quad (3.32)$$

By the steepest descent method, the solution of Equation (3.31) is defined as

$$\underline{\hat{X}}_{n+1} = \underline{\hat{X}}_n + \beta \cdot \left\{ \begin{array}{l} \sum_{k=1}^N F_k^T H_k^T D_k^T \cdot \rho'_{TUKEY} (\underline{Y}_k - D_k H_k F_k \underline{\hat{X}}_n) \\ -(\lambda \cdot \Gamma^T \cdot \psi'_{TUKEY} (\Gamma \underline{\hat{X}}_n)) \end{array} \right\} \quad (3.33)$$

$$\psi'_{TUKEY} (x) = \begin{cases} x \left[1 - (x/T_g)^2 \right]^2 & ; |x| \leq T_g \\ 0 & ; otherwise \end{cases} \quad (3.34)$$

3.3 Robust Estimation for SRR using Fast Affine Block-Based Registration [110-112, 118, 121-122]

In this section, we proposed the SRR algorithm using the proposed robust estimation (Huber, Lorentzian and Tukey's Biweight norm) with affine block-based registration for applying on the real image sequences that have complex motion and that is corrupted by the several noise models. Therefore, we propose the definition of the SRR using affine block-based registration as the following minimization problem:

$$\underline{X} = \underset{\underline{X}}{\text{ArgMin}} \left\{ \sum_{k=1}^N \rho(D_k H_k G_k \underline{X} - \underline{Y}_k) \right\} \quad (3.35)$$

where $\rho(\cdot)$ is the norm estimation and the G_k stands for the geometric warp operator (affine) between the images \underline{X} and \underline{Y}_k . [25, 109]

3.3.1 L2 Norm Estimation for SRR using Fast Affine Block-Based Registration [111, 112, 118]

3.3.1.1 L2 Norm Estimation for SRR

In this section, we propose the novel SRR using L2 error norm with fast affine block-based registration. From (3.35), we propose the definition of these robust estimators in the super resolution context as the following minimization problem:

$$\underline{X} = \underset{\underline{X}}{\text{ArgMin}} \left\{ \sum_{k=1}^N (D_k H_k G_k \underline{X} - \underline{Y}_k)^2 \right\} \quad (3.36)$$

By the steepest descent method, the solution of Equation (3.36) is defined as

$$\hat{\underline{X}}_{n+1} = \hat{\underline{X}}_n + \beta \cdot \left\{ \sum_{k=1}^N G_k^T H_k^T D_k^T \cdot (\underline{Y}_k - D_k H_k G_k \hat{\underline{X}}_n) \right\} \quad (3.37)$$

3.3.1.2 L2 Norm Estimation for SRR with Laplacian Regularization

Combining the Laplacian regularization, we propose the solution of the super-resolution problem as follows:

$$\underline{X} = \underset{\underline{X}}{\text{ArgMin}} \left\{ \sum_{k=1}^N \rho(D_k H_k G_k \underline{X} - \underline{Y}_k) + \lambda \cdot (\Gamma \underline{X})^2 \right\} \quad (3.38)$$

By the steepest descent method, the solution of Equation (3.38) is defined as

$$\hat{\underline{X}}_{n+1} = \hat{\underline{X}}_n + \beta \cdot \left\{ \begin{array}{l} \sum_{k=1}^N G_k^T H_k^T D_k^T \cdot (\underline{Y}_k - D_k H_k G_k \hat{\underline{X}}_n) \\ -(\lambda \cdot (\Gamma^T \Gamma) \hat{\underline{X}}_n) \end{array} \right\} \quad (3.39)$$

3.3.2 L1 Norm Estimation for SRR using Fast Affine Block-Based Registration [110]

3.3.2.1 L1 Norm Estimation for SRR

In this section, we propose the novel SRR using L1 error norm with fast affine block-based registration. From (3.35), we propose the definition of these robust estimators in the super resolution context as the following minimization problem:

$$\underline{X} = \underset{\underline{X}}{\text{ArgMin}} \left\{ \sum_{k=1}^N |D_k H_k G_k \underline{X} - \underline{Y}_k| \right\} \quad (3.40)$$

By the steepest descent method, the solution of Equation (3.40) is defined as

$$\hat{\underline{X}}_{n+1} = \hat{\underline{X}}_n + \beta \cdot \left\{ \sum_{k=1}^N G_k^T H_k^T D_k^T \cdot \text{sign}(D_k H_k G_k \hat{\underline{X}}_n - \underline{Y}_k) \right\} \quad (3.41)$$

3.3.2.2 L1 Norm Estimation for SRR with Laplacian Regularization

Combining the Laplacian regularization, we propose the solution of the super-resolution problem as follows:

$$\underline{X} = \underset{\underline{X}}{\text{ArgMin}} \left\{ \sum_{k=1}^N |D_k H_k G_k \underline{X} - \underline{Y}_k| + \lambda \cdot (\Gamma \underline{X})^2 \right\} \quad (3.42)$$

By the steepest descent method, the solution of Equation (3.42) is defined as

$$\hat{\underline{X}}_{n+1} = \hat{\underline{X}}_n + \beta \cdot \left\{ \begin{array}{l} \sum_{k=1}^N G_k^T H_k^T D_k^T \cdot \text{sign}(D_k H_k G_k \hat{\underline{X}}_n - \underline{Y}_k) \\ -(\lambda \cdot (\Gamma^T \Gamma) \hat{\underline{X}}_n) \end{array} \right\} \quad (3.43)$$

3.3.3 Huber Norm Estimation for SRR using Fast Affine Block-Based Registration

3.3.3.1 Huber Norm Estimation for SRR

In this section, we propose the novel robust SRR using Huber error norm. From (3.35), we propose the definition of these robust estimators in the super resolution context as the following minimization problem:

$$\underline{X} = \underset{\underline{X}}{\text{ArgMin}} \left\{ \sum_{k=1}^N \rho_{HUBER} (D_k H_k G_k \underline{X} - \underline{Y}_k) \right\} \quad (3.44)$$

By the steepest descent method, the solution of Equation (3.44) is defined as

$$\hat{\underline{X}}_{n+1} = \hat{\underline{X}}_n + \beta \cdot \left\{ \sum_{k=1}^N G_k^T H_k^T D_k^T \cdot \rho'_{HUBER} (\underline{Y}_k - D_k H_k G_k \hat{\underline{X}}_n) \right\} \quad (3.45)$$

3.3.3.2 Huber Norm Estimation for SRR with Laplacian Regularization

Combining the Laplacian regularization, we propose the solution of the super-resolution problem as follows:

$$\underline{X} = \underset{\underline{X}}{\text{ArgMin}} \left\{ \sum_{k=1}^N \rho_{HUBER} (D_k H_k G_k \underline{X} - \underline{Y}_k) + \lambda \cdot (\Gamma \underline{X})^2 \right\} \quad (3.46)$$

By the steepest descent method, the solution of Equation (3.46) is defined as

$$\hat{\underline{X}}_{n+1} = \hat{\underline{X}}_n + \beta \cdot \left\{ \begin{array}{l} \sum_{k=1}^N G_k^T H_k^T D_k^T \cdot \rho'_{HUBER} (\underline{Y}_k - D_k H_k G_k \hat{\underline{X}}_n) \\ -(\lambda \cdot (\Gamma^T \Gamma) \hat{\underline{X}}_n) \end{array} \right\} \quad (3.47)$$

3.3.4 Lorentzian Norm Estimation for SRR using Fast Affine Block-Based Registration [122]

3.3.4.1 Lorentzian Norm Estimation for SRR

In this section, we propose the novel robust SRR using Lorentzian error norm. From (3.35), we propose the definition of these robust estimators in the super resolution context as the following minimization problem:

$$\underline{X} = \underset{\underline{X}}{\text{ArgMin}} \left\{ \sum_{k=1}^N \rho_{LOR} (D_k H_k G_k \underline{X} - \underline{Y}_k) \right\} \quad (3.48)$$

By the steepest descent method, the solution of Equation (3.48) is defined as

$$\hat{\underline{X}}_{n+1} = \hat{\underline{X}}_n + \beta \cdot \left\{ \sum_{k=1}^N G_k^T H_k^T D_k^T \cdot \rho'_{LOR} (\underline{Y}_k - D_k H_k G_k \hat{\underline{X}}_n) \right\} \quad (3.49)$$

3.3.4.2 Lorentzian Norm Estimation for SRR with Laplacian Regularization

Combining the Laplacian regularization, we propose the solution of the super-resolution problem as follows:

$$\underline{X} = \underset{\underline{X}}{\text{ArgMin}} \left\{ \sum_{k=1}^N \rho_{LOR} (D_k H_k G_k \underline{X} - \underline{Y}_k) + \lambda \cdot (\Gamma \underline{X})^2 \right\} \quad (3.50)$$

By the steepest descent method, the solution of Equation (3.50) is defined as

$$\hat{\underline{X}}_{n+1} = \hat{\underline{X}}_n + \beta \cdot \left\{ \begin{aligned} & \sum_{k=1}^N G_k^T H_k^T D_k^T \cdot \rho'_{LOR} (\underline{Y}_k - D_k H_k G_k \hat{\underline{X}}_n) \\ & - (\lambda \cdot (\Gamma^T \Gamma) \hat{\underline{X}}_n) \end{aligned} \right\} \quad (3.51)$$

3.3.5 Tukey's Biweight Norm Estimation for SRR using Fast Affine Block-Based Registration [121]

3.3.5.1 Tukey's Biweight Norm Estimation for SRR

In this section, we propose the novel robust SRR using Tukey's Biweight error norm. From (3.35), we propose the definition of these robust estimators in the super resolution context as the following minimization problem:

$$\underline{X} = \underset{\underline{X}}{\text{ArgMin}} \left\{ \sum_{k=1}^N \rho_{TUKEY} (D_k H_k G_k \underline{X} - \underline{Y}_k) \right\} \quad (3.52)$$

By the steepest descent method, the solution of Equation (3.52) is defined as

$$\hat{\underline{X}}_{n+1} = \hat{\underline{X}}_n + \beta \cdot \left\{ \sum_{k=1}^N G_k^T H_k^T D_k^T \cdot \rho'_{TUKEY} (\underline{Y}_k - D_k H_k G_k \hat{\underline{X}}_n) \right\} \quad (3.53)$$

3.3.5.2 Tukey's Biweight Norm Estimation for SRR with Laplacian Regularization

Combining the Laplacian regularization, we propose the solution of the super-resolution problem as follows:

$$\underline{X} = \underset{\underline{X}}{\text{ArgMin}} \left\{ \sum_{k=1}^N \rho_{TUKEY} (D_k H_k G_k \underline{X} - \underline{Y}_k) + \lambda \cdot (\Gamma \underline{X})^2 \right\} \quad (3.54)$$

By the steepest descent method, the solution of Equation (3.54) is defined as

$$\hat{\underline{X}}_{n+1} = \hat{\underline{X}}_n + \beta \cdot \left\{ \begin{array}{l} \sum_{k=1}^N G_k^T H_k^T D_k^T \cdot \rho'_{TUKEY} (\underline{Y}_k - D_k H_k G_k \hat{\underline{X}}_n) \\ -(\lambda \cdot (\Gamma^T \Gamma) \hat{\underline{X}}_n) \end{array} \right\} \quad (3.55)$$

CHAPTER IV

THE EXPERIMENTAL RESULTS

The purpose of this chapter is to analyze how the proposed registration (fast affine block-based) and the proposed robust norm estimation (Huber, Lorentzian and Tukey) can affect the performance of the SRR algorithm.

In this chapter, five cases are studied. In the first case, the performance of registration approaches is evaluated. Section 4.1 presents the experiments and results obtained by the proposed registration (fast affine block-based) and the classical registration (translation block-based) in order to analyze the proposed registration accuracy [109]. Next, Section 4.2 presents the experiments and results obtained by the SRR algorithm using the proposed registration and the classical registration to demonstrate the effect of the proposed registration on the SRR performance on the standard sequence such as Susie and Foreman Sequence [110-112, 118]. Third, Section 4.3 analyzes how the proposed robust norm estimation impacts the performance of SRR algorithm. This section presents the experiments and results obtained the SRR algorithms using the proposed robust norm estimation (Huber norm, Lorentzian norm and Tukey norm) compared with the classical SRR algorithm using L1 and L2 norm [113-117, 119-120]. Section 4.4 analyzes the performance of proposed norm estimation hence this section presents the experiments and results obtained the SRR algorithms using the proposed robust norm estimation with the classical registration compared with the classical SRR algorithm using L1 and L2 norm. Finally, Section 4.5 presents the experiments and results obtained by the SRR algorithm using the proposed robust norm estimation with fast affine block-based registration [121-122].

สถาบันวิทยบริการ
จุฬาลงกรณ์มหาวิทยาลัย

4.1 Experiments on Fast Affine Block-Based Registration [109]

This section investigates the accuracy performance of the proposed registration (affine block-based) compared with the classical registration (translation block-based). This experiment intends to study the registration accuracy that is traditionally used in the SRR algorithm and the proposed registration accuracy. This section presents the experiments and results obtained by the classical registration using FS (Full Search) and proposed registration using M3SS (Modified Three Step Search) as proposed in section 3.1. These experiments are implemented in MATLAB. Three standard video sequences (Carphone, Foreman and Stefan) in QCIF format (176x144) were used as the test sequences which can be categorized by moving characteristic. First, Carphone sequence has only a moving foreground but the background is almost stationary. Second, Foreman sequence has both slightly moving foreground and background. Finally, Stefan sequence has both dramatically moving foreground and background. For the classical registration using FS (Full Search), the search window $w=9$ and the block size is fixed at 16×16 . For the proposed registration using M3SS (Modified Three Step Search), the search window $w=7$ and the block size is fixed at 16×16 [109]. The performance of the estimation algorithm is evaluated quantitatively. To quantitatively measure the accuracy of the proposed methodology, the PSNR (Peak Signal to Noise Ratio) [125] is used to measure the error between the compensated frame and the current frame. The PSNR is defined as

$$PSNR = 10 \times \log_{10} \left(\frac{\psi_{MAX}^2}{(\psi_{current} - \psi_{compensated})^2} \right) \quad (4.1)$$

where - $\psi_{current}$ is the current frame

- $\psi_{compensated}$ is the compensated frame

- ψ_{MAX} is the peak (maximum) intensity value of the video signal.

4.1.1 Carphone Sequence

The performance comparison between the M3SS and classical method (1st Frame-35th Frame) is depicted in Figure 4.1 and we can observe that the PSNR of the M3SS method is 5-6 dB higher than that of the classical method.

The simulation results of the Carphone sequence (14th Frame and 15th Frame) are displayed in figure 4.2. The PSNR between

the current frame and the classical compensated frame for the 16x16 pixel block size is 29.3762 dB and the MCD (Motion Compensated Difference) of the classical method is shown in figure 4.2 (d). The PSNR between the current frame and the M3SS compensated frame is 35.1235 dB as shown in Figure 4.2 (e). From this result, we can observe that the MCD of the M3SS is obviously better than the classical method.

4.1.2 Foreman Sequence

The performance comparison between the proposed M3SS algorithm and the classical algorithm (101st Frame-135th Frame) is depicted in figure 4.3 and we can observe that the proposed M3SS algorithm has outstandingly better result than the classical method.

Figure 4.4 shows the simulation results of the Foreman sequence (115th Frame and 116th Frame) and the PSNR between the current frame and the classical compensated frame is 29.3762 dB as shown in Fig. 4.4 (d). Next, the PSNR between the current frame and the M3SS compensated frame is 34.4652 dB and the MCD of the M3SS method is shown in figure 4.4 (e).

4.1.3 Stefan Sequence

The performance comparison between the proposed M3SS algorithm and the classical algorithm (101st Frame-135th Frame) is depicted in Figure 4.5 and we can observe that the proposed M3SS algorithm has dramatically better result than the classical method about 4-5 dB.

The Stefan sequence (16th Frame) is shown in Figure 4.6 (a) and the Stefan sequence (17th Frame) is shown in Figure 4.6 (b). The absolute difference between the 16th Frame and 17th Frame are shown in Figure 4.6 (c) and the PSNR between the two frames is 18.5385 dB. The PSNR between the current frame and the classical compensated frame is 18.5385 dB and the MCD (Motion Compensated Difference) of the classical method is shown in Figure 4.6 (d). Next, the PSNR between the current frame and the M3SS compensated frame is 25.5609 dB and the MCD of the M3SS method is shown in Figure 4.6 (e).

Although all three experimental results demonstrate that the proposed registration require higher computation than the classical registration but the proposed registration have obviously better PSNR performance compared to the classical registration.

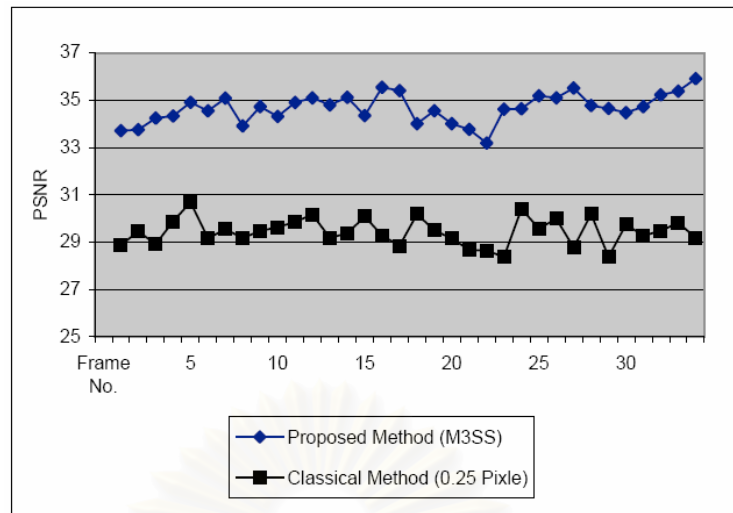


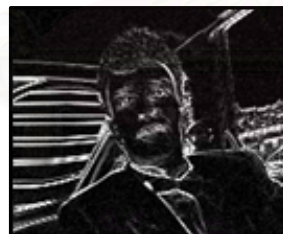
Figure 4.1 : Performance Comparison between the compensated frame produced by the proposed M3SS and classical algorithm of Carphone sequence



(a) Reference Frame (fr.14)



(b) Current Frame (fr.15)



(c) Frame Difference ($\times 10$)
(PSNR = 18.5385 dB)



(d) MCD of the Classical Method ($\times 10$)
(fr.15)
(PSNR = 29.3762 dB)



(e) MCD of the M3SS Method ($\times 10$)
(fr.15)
(PSNR = 35.1235 dB)

Figure 4.2 : MCD Comparison between the compensated frame produced by the proposed and classical estimation method of Carphone sequence

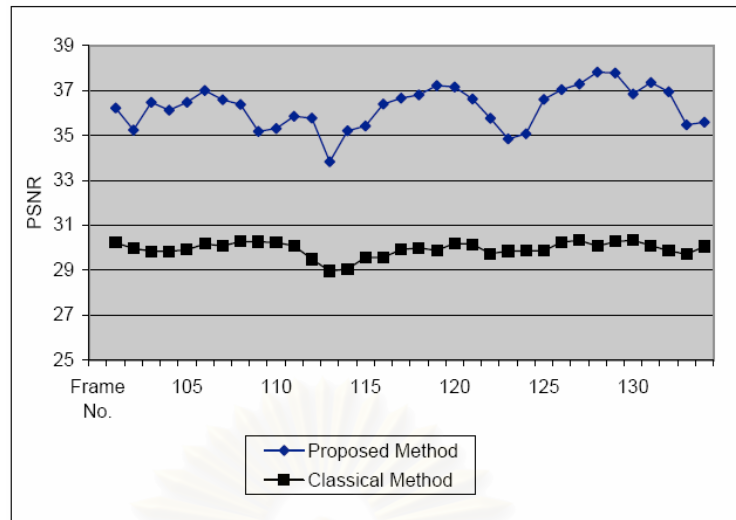


Figure 4.3 : Performance Comparison between the compensated frame produced by the proposed M3SS and classical algorithm of Foreman sequence

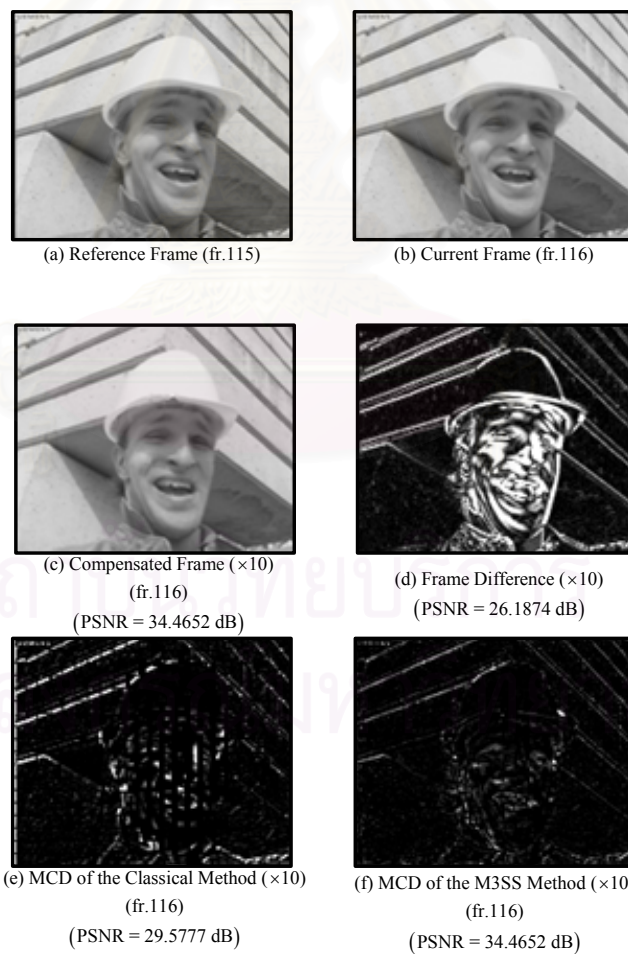


Figure 4.4 : MCD Comparison between the compensated frame produced by the proposed and classical estimation method of Foreman sequence

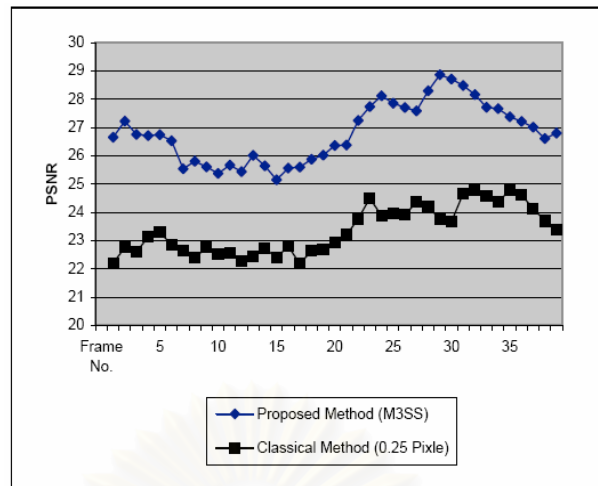


Figure 4.5 : Performance Comparison between the compensated frame produced by the proposed M3SS and classical algorithm of Stefan sequence

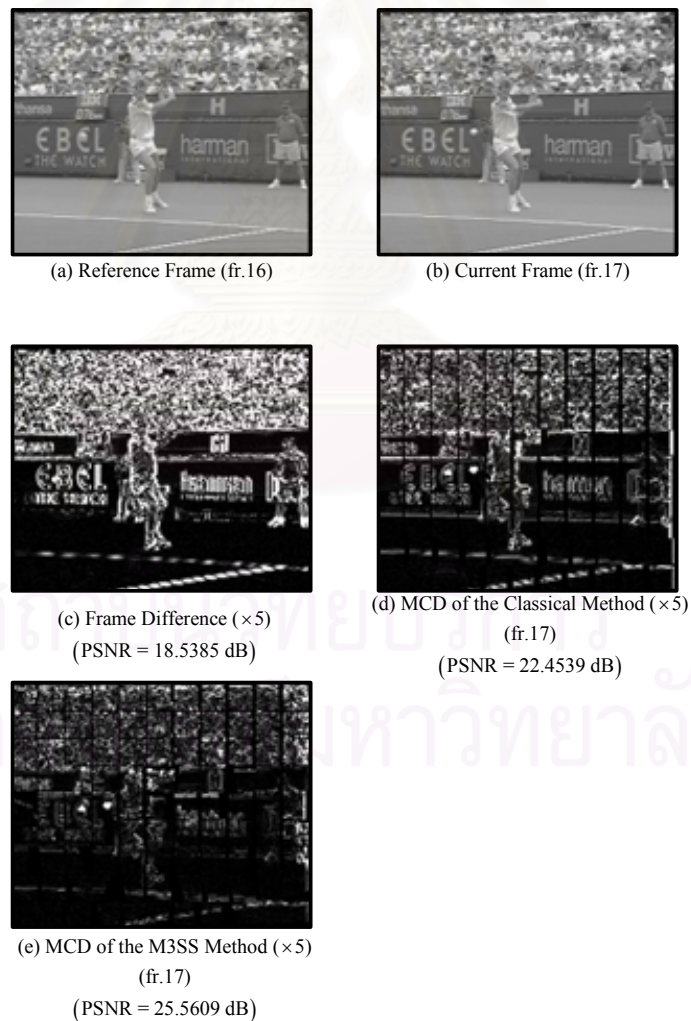


Figure 4.6 : MCD Comparison between the compensated frame produced by the proposed and classical estimation method of Stefan sequence

4.2 Experiments on the SRR algorithm using Fast Affine Block-Based Registration [110-112, 118]

This section presents the experiments and results obtained by the SRR algorithm using proposed fast affine block-based registration that are calculated by Equation (3.39) and Equation (3.43) respectively. To demonstrate the proposed registration performance, the results of L1 norm SRR with the classical translation block-based registration calculated by Equation (2.17) and the results of L2 norm SRR with the classical translation block-based registration calculated by Equation (2.15) are presented in order to compare the performance.

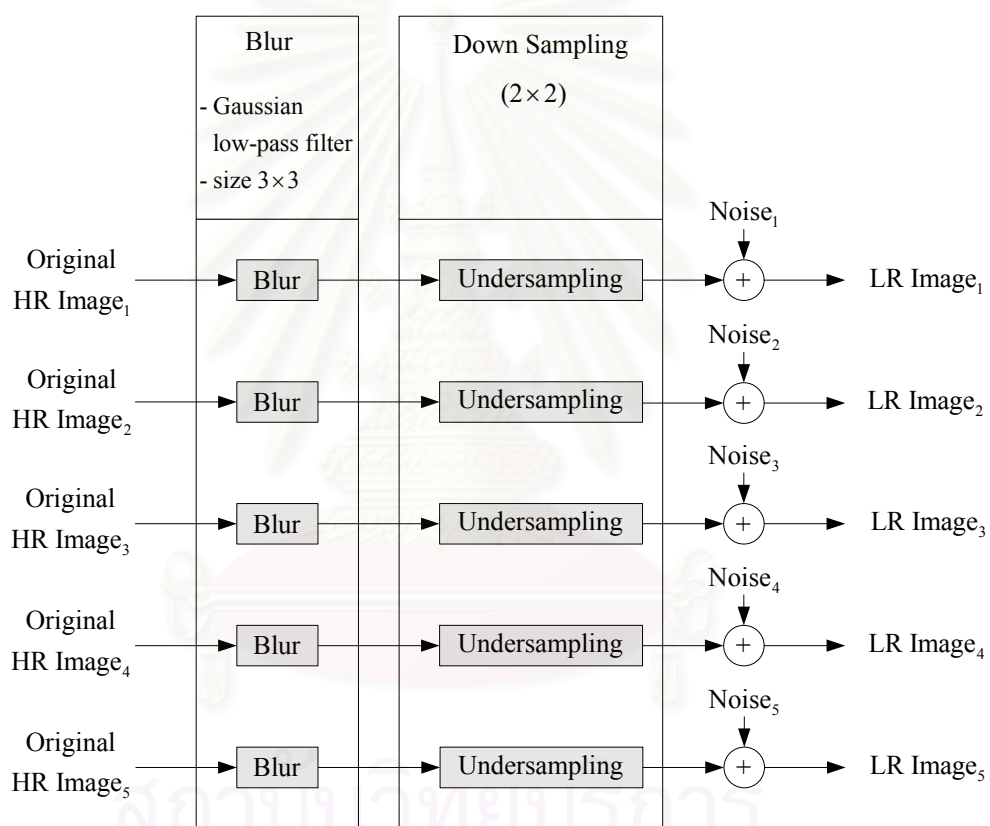


Figure 4.7 : The block diagram of LR image sequence synthesis algorithm for the SRR algorithm using the proposed fast affine block-based registration

The experiment was implemented in MATLAB and the block size of LR images is fixed at 8x8 (or 16x16 for overlapping block) and the search window is 7 for fast affine block-based registration [109] and 5 Frames for ML estimation process. The 38th- 42nd frame Susie sequence and the 108th- 112th frame Foreman sequence, which are QCIF format (176x144), are used in these experiments to generate the high resolution : 40th frame Susie and 110th frame Foreman respectively. Both

sequences are in QCIF format and have complex-edge characteristic. Then, to simulate the effect of camera PSF, the images were convolved with a symmetric Gaussian low-pass filter with the size of 3×3 and standard deviation of one. The blurred images were subsampled by the factor of 2 in each direction (88×72) and the blurred subsampled images were corrupted by Gaussian noise. The LR image sequence synthesis algorithm is shown in Figure 4.7.

The criterion for parameter selection in this experiment was to choose parameters which produce both most visually appealing results and highest PSNR. Therefore, to ensure fairness, each experiment was repeated several times with different parameters and the best result of each experiment was chosen [97-100].

4.2.1 Susie Sequence (The 40th Frame)

4.2.1.1 Noiseless

The original HR image is shown in Fig. 4.8 (a-1) and one of corrupted LR images is shown in Fig. 4.8 (a-2). The result of L1 estimator using classical registration, L2 estimator using classical registration, L1 estimator using proposed registration and L2 estimator using proposed registration are shown in Figs. 4.8(a-3) - 4.8(a-6), respectively. (The below image on our experiment result of each subfigure is the absolute difference between it's correspond upper image to the original HR image. The difference is magnified by 5.)

4.2.1.2 AWGN (Additive White Gaussian Noise)

This experiment is a 5 AWGN cases at SNR=25, 22.5, 20, 17.5 and 15dB respectively and the original HR images are shown in Figs. 4.8(b-1) - (f-1) respectively. The corrupted images at SNR=25, 22.5, 20, 17.5 and 15dB are showed in Figs. 4.8(b-2) - 4.8(f-2) respectively. The result of L1 estimator using classical registration, L2 estimator using classical registration, L1 estimator using proposed registration and L2 estimator using proposed registration are shown in Figs. 4.8(b-3) - 4.8(b-6) for SNR=25dB, Figs. 4.8(c-3) - 4.8(c-6) for SNR=22.5dB, Figs. 4.8(d-3) - 4.8(d-6) for SNR=20dB, Figs. 4.8(e-3) - 4.8(e-6) for SNR=17.5dB and Figs. 4.8(f-3) - 4.8(f-6) for SNR=15dB, respectively.

4.2.1.3 Poisson Noise

This experiment is a poisson Noise cases. The original HR image is shown in Fig. 4.8(g-1) and one of corrupted LR images is shown

in Fig. 4.8(g-2). The result of L1 estimator using classical registration, L2 estimator using classical registration, L1 estimator using proposed registration and L2 estimator using proposed registration are shown in Figs. 4.8(g-3) - 4.8(g-6).

4.2.1.4 Salt&Pepper Noise

This experiment is a 3 Salt&Pepper Noise cases at $D=0.005$, $D=0.010$ and $D=0.015$ respectively (D is the noise density) and the original HR images are shown in Figs. 4.8(h-1) – (j-1). The corrupted images at $D=0.005$, $D=0.010$ and $D=0.015$ are showed in Fig. 4.8(h-2), Fig. 4.8(i-2) and Fig. 4.8(j-2), respectively. The result of L1 estimator using classical registration, L2 estimator using classical registration, L1 estimator using proposed registration and L2 estimator using proposed registration are shown in Figs. 4.8(h-3) - 4.8(h-6) for $D=0.005$, Fig. 4.8(i-3) - 4.8(i-6) for $D=0.010$ and Fig. 4.8(j-3) - 4.8(j-6) for $D=0.015$, respectively.

4.2.1.5 Speckle Noise

The last experiment is a 3 Speckle Noise cases for 40th frame Susie sequence at $V=0.01$, $V=0.02$ and $V=0.03$ respectively (V is the noise variance) and the original HR images are shown in Fig. 4.8(k-1) –4.8(m-1). The corrupted images at $V=0.01$, $V=0.02$ and $V=0.03$ are showed in Fig. 4.8(k-2), Fig. 4.8(l-2) and Fig. 4.8(m-2), respectively. The result of L1 estimator using classical registration, L2 estimator using classical registration, L1 estimator using proposed registration and L2 estimator using proposed registration are shown in Figs. 4.8(k-3) - 4.8(k-6) for $V=0.01$, Figs. 4.8(l-3) - 4.8(l-6) for $V=0.02$ and Figs. 4.8(m-3) - 4.8(m-6) for $V=0.03$ respectively.

From all experimental results of Susie Sequence (40th Frame), the SRR algorithm using L1 norm with the proposed registration gives the higher PSRN than the SRR algorithm using L1 norm with the classical registration. Moreover, the SRR algorithm using L2 norm with the proposed registration gives the higher PSRN than the SRR algorithm using L2 norm with the classical registration. Next, the SRR algorithm using L1 norm gives the higher PSRN than the SRR algorithm using L2 norm because L2 norm is more sensitive the outliers such as the registration error (and the L2 influence function increases linearly and without bound) than L1 norm. Moreover, the SRR algorithm using L2 norm with the classical registration can not increase the PSNR due to noise and registration error.



Figure 4.8 : The experimental result of SRR algorithm using the proposed Registration (Susie Sequence : The 40th Frame)

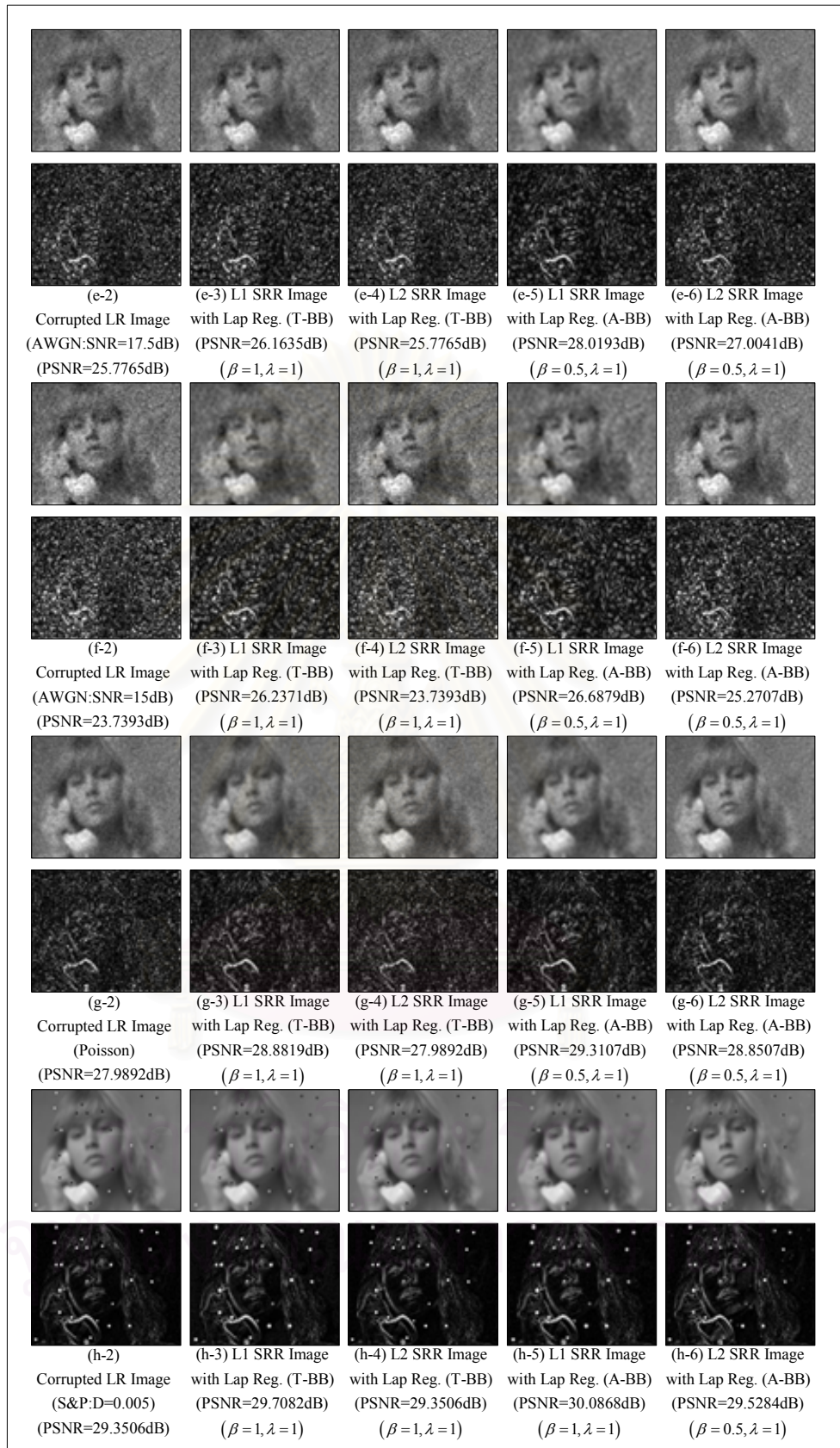


Figure 4.8 : The experimental result of SRR algorithm using the proposed Registration (Susie Sequence : The 40th Frame) (Con.)

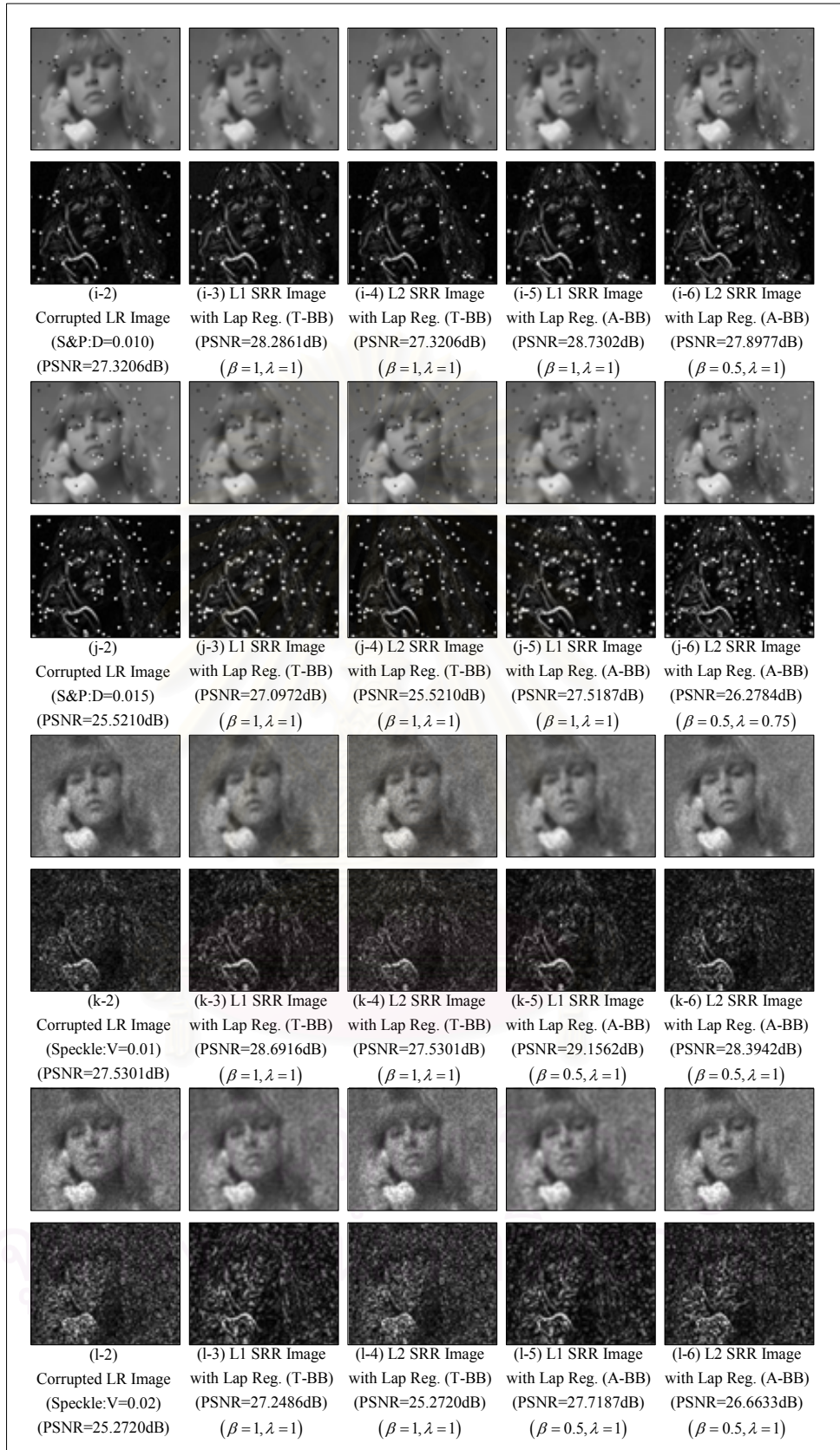


Figure 4.8 : The experimental result of SRR algorithm using the proposed Registration (Susie Sequence : The 40th Frame) (Con.)

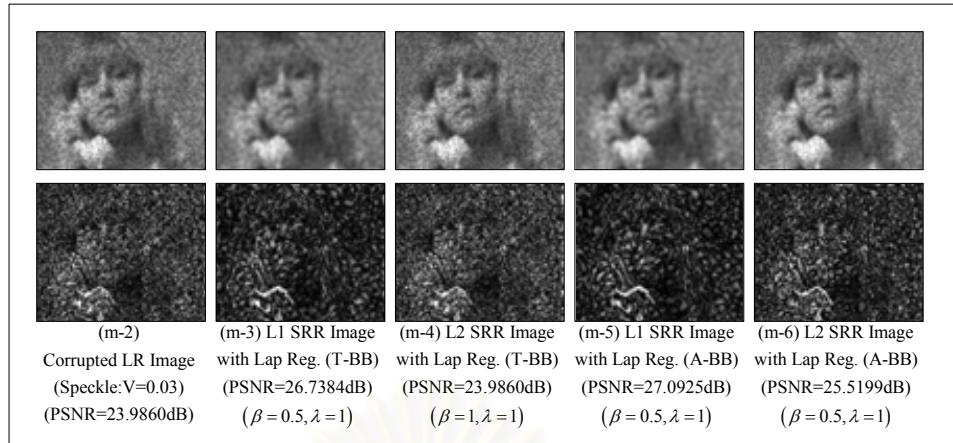


Figure 4.8 : The experimental result of SRR algorithm using the proposed Registration (Susie Sequence : The 40th Frame) (Con.)

4.2.2 Foreman Sequence (The 110th Frame)

4.2.2.1 Noiseless

The original HR image is shown in Fig. 4.9 (a-1) and one of corrupted LR images is shown in Fig. 4.9 (a-2). The result of L1 estimator using classical registration, L2 estimator using classical registration, L1 estimator using proposed registration and L2 estimator using proposed registration are shown in Figs. 4.9(a-3) - 4.9(a-6).

4.2.2.2 AWGN (Additive White Gaussian Noise)

This experiment is a 5 AWGN cases at SNR=25, 22.5, 20, 17.5 and 15dB, respectively and the original HR images are shown in Figs. 4.9(b-1) - 4.9(f-1) respectively. The corrupted images at SNR=25, 22.5, 20, 17.5 and 15dB are showed in Figs. 4.9(b-2) - 4.9(f-2) respectively. The result of L1 estimator using classical registration, L2 estimator using classical registration, L1 estimator using proposed registration and L2 estimator using proposed registration are shown in Figs. 4.9(b-3) - 4.9(b-6) for SNR=25dB, Figs. 4.9(c-3) - 4.9(c-6) for SNR=22.5dB, Figs. 4.9(d-3) - 4.9(d-6) for SNR=20dB, Figs. 4.9(e-3) - 4.9(e-6) for SNR=17.5dB and Figs. 4.9(f-3) - 4.9(f-6) for SNR=15dB respectively.

4.2.2.3 Poisson Noise

This experiment is a poisson Noise cases. The original HR image is shown in Fig. 4.9(g-1) and one of corrupted LR images is shown

in Fig. 4.9(g-2). The result of L1 estimator using classical registration, L2 estimator using classical registration, L1 estimator using proposed registration and L2 estimator using proposed registration are shown in Figs. 4.9(g-3) - 4.9(g-6).

4.2.2.4 Salt&Pepper Noise

This experiment is a 3 Salt&Pepper Noise cases at $D=0.005$, $D=0.010$ and $D=0.015$ respectively (D is the noise density) and the original HR images are shown in Figs. 4.9(h-1) – 4.9(j-1) respectively. The corrupted images at $D=0.005$, $D=0.010$ and $D=0.015$ are showed in Fig. 4.9(h-2), Fig. 4.9(i-2) and Fig. 4.9(j-2) respectively. The result of L1 estimator using classical registration, L2 estimator using classical registration, L1 estimator using proposed registration and L2 estimator using proposed registration are shown in Figs. 4.9(h-3) - 4.9(h-6) for $D=0.005$, Figs. 4.9(i-3) - 4.9(i-6) for $D=0.010$ and Figs. 4.9(j-3) - 4.9(j-6) for $D=0.015$ respectively.

4.2.2.5 Speckle Noise

The last experiment is a 3 Speckle Noise cases for 40th frame Foreman sequence at $V=0.01$, $V=0.02$ and $V=0.03$ respectively (V is the noise variance) and the original HR images are shown in Fig. 4.9(k-1) – Fig. 4.9(m-1) respectively. The corrupted images at $V=0.01$, $V=0.02$ and $V=0.03$ are showed in Fig. 4.9(k-2), Fig. 4.9(l-2) and Fig. 4.9(m-2) respectively. The result of L1 estimator using classical registration, L2 estimator using classical registration, L1 estimator using proposed registration and L2 estimator using proposed registration are shown in Figs. 4.9(k-3) - 4.9(k-6) for $V=0.01$, Figs. 4.9(l-3) - 4.9(l-6) for $V=0.02$ and Figs. 4.9(m-3) - 4.9(m-6) for $V=0.03$ respectively.

From all experimental results of Foreman Sequence (110th Frame), the SRR algorithm using L1 norm with the proposed registration gives the higher PSNR than the SRR algorithm using L1 norm with the classical registration. Moreover, the SRR algorithm using L2 norm with the proposed registration gives the higher PSNR than the SRR algorithm using L2 norm with the classical registration. Next, the SRR algorithm using L1 norm gives the higher PSNR than the SRR algorithm using L2 norm because L2 norm is more sensitive the outliers such as the registration error (and the L2 influence function increases linearly and without bound) than L1 norm. Moreover, the SRR algorithm using L2 norm with the classical registration can not increase the PSNR due to noise and registration error.

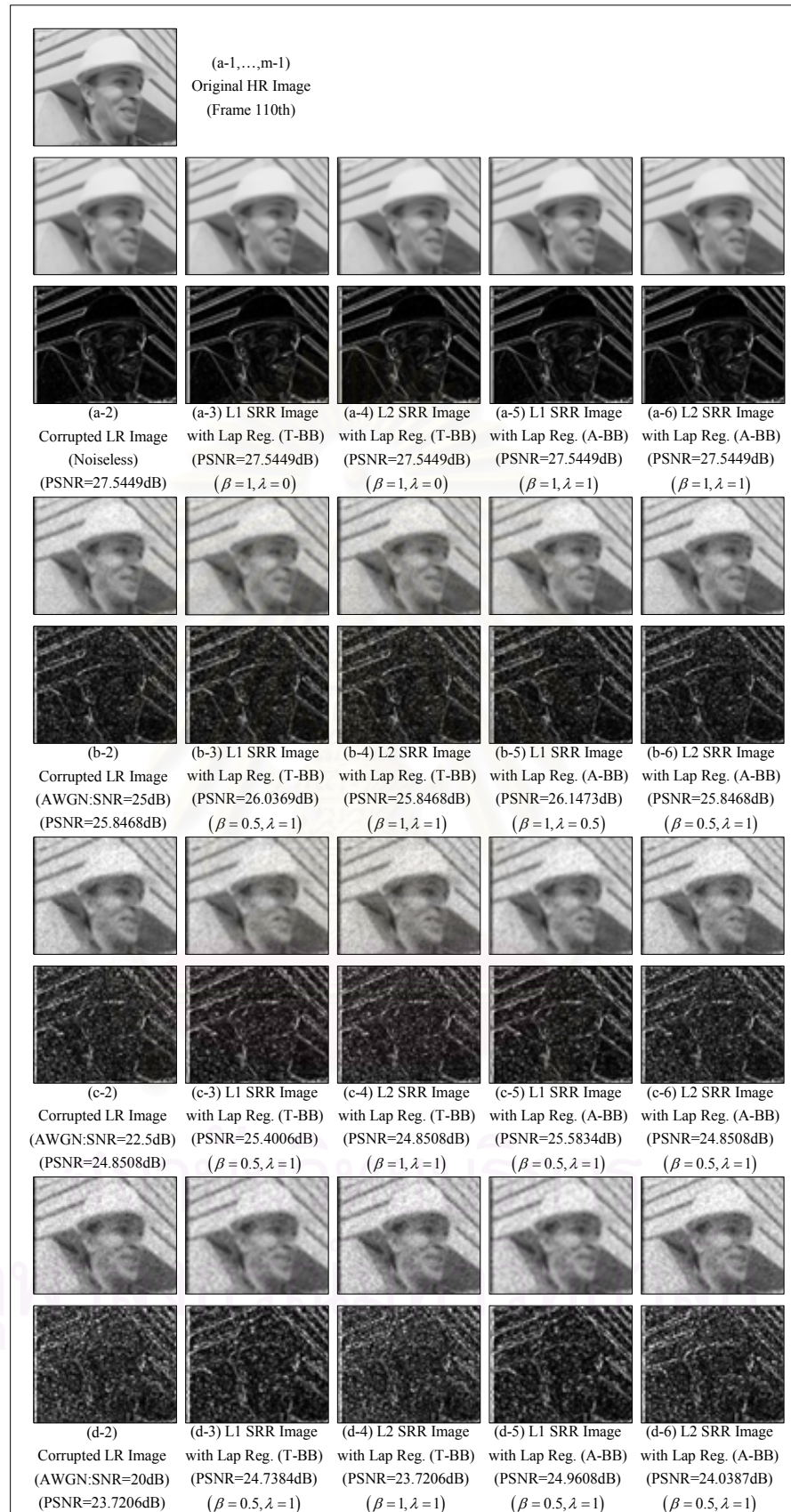


Figure 4.9 : The experimental result of SRR algorithm using the proposed Registration (Foreman Sequence : The 110th Frame)

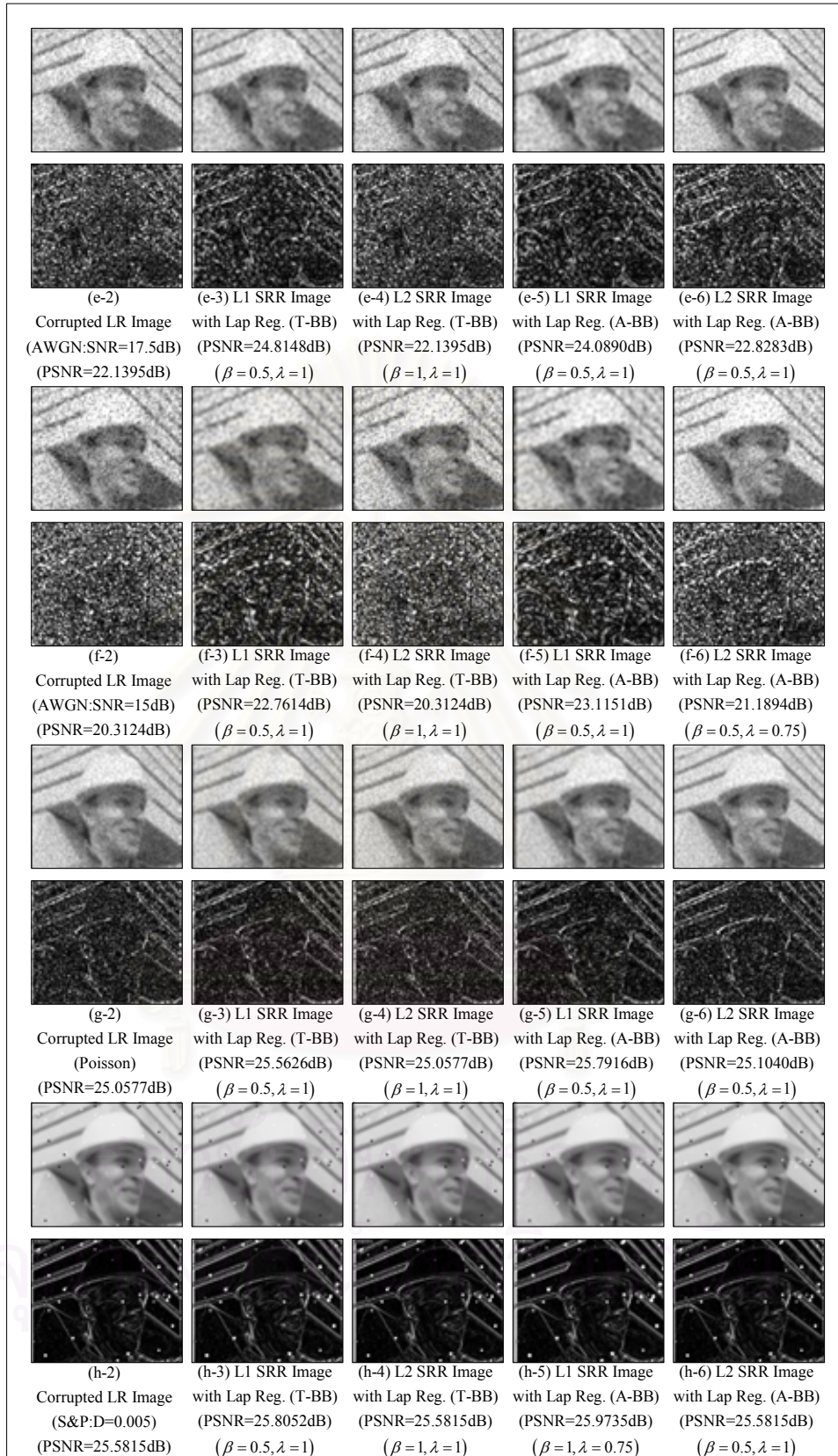


Figure 4.9 : The experimental result of SRR algorithm using the proposed Registration (Foreman Sequence : The 110th Frame) (Con.)

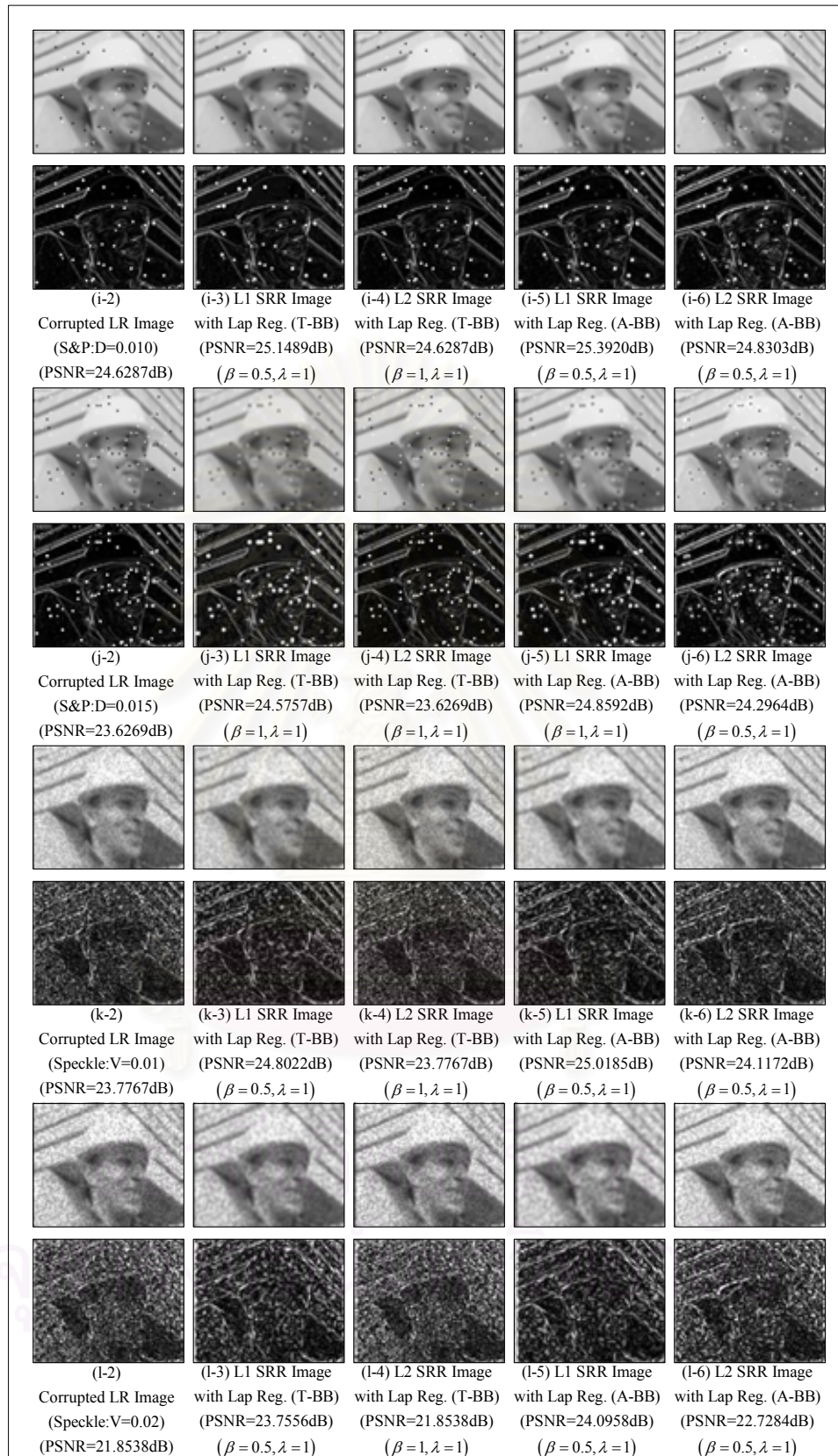


Figure 4.9 : The experimental result of SRR algorithm using the proposed Registration (Foreman Sequence : The 110th Frame) (Con.)

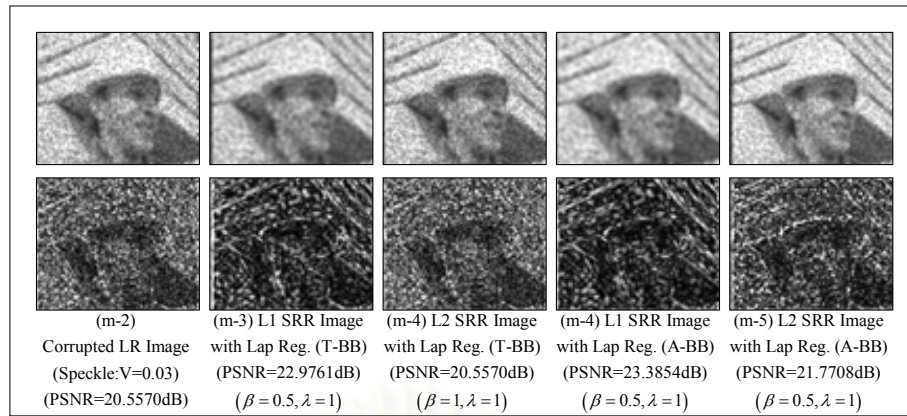


Figure 4.9 : The experimental result of SRR algorithm using the proposed Registration (Foreman Sequence : The 110th Frame) (Con.)

สถาบันวิทยบริการ
จุฬาลงกรณ์มหาวิทยาลัย

4.2.3 Experimental Conclusion on the SRR algorithm using Fast Affine Block-Based Registration

From all experimental results of both Susie Sequence (40th Frame) and Foreman Sequence (110th Frame) shown in Fig. 4.9 and Fig. 4.10 respectively, all comparatively experimental results are concluded as follow:

- For the same norm estimation technique, the SRR algorithm with the proposed registration gives the higher PSNR than the SRR algorithm with the classical registration.
- The SRR algorithm using L1 norm with the proposed registration gives the highest PSNR.
- The SRR algorithm using L1 norm gives the higher PSNR than the SRR algorithm using L2 norm because L2 norm is more sensitive the outliers such as the registration error (and the L2 influence function increases linearly and without bound) than L1 norm.
- The SRR algorithm using L2 norm with the classical registration can not increase the PSNR because the registration error is high and L2 norm is more sensitive the outliers.

PSNR (dB)	Noise Model												
	Noiseless	AWGN:SNR=25dB	AWGN:SNR=22.5dB	AWGN:SNR=20dB	AWGN:SNR=17.5dB	AWGN:SNR=15dB	Poisson	S&P:D=0.005	S&P:D=0.010	S&P:D=0.015	Speckle:V=0.01	Speckle:V=0.02	Speckle:V=0.03
Corrupted LR Image	32.169	30.149	29.057	27.574	25.777	23.739	27.989	29.351	27.321	25.521	27.53	25.272	23.986
L1 SRR Image with Lap Reg. (T-BB)	32.169	30.382	29.663	28.8	26.164	26.237	28.882	29.708	28.286	27.097	28.692	27.249	26.738
L2 SRR Image with Lap Reg. (T-BB)	32.169	30.149	29.057	27.574	25.777	23.739	27.989	29.351	27.321	25.521	27.53	25.272	23.986
L1 SRR Image with Lap Reg. (A-BB)	32.169	30.662	30.019	29.13	28.019	26.688	29.311	30.087	28.73	27.519	29.156	27.719	27.093
L2 SRR Image with Lap Reg. (A-BB)	32.169	30.235	29.432	28.375	27.004	25.271	28.851	29.528	27.898	26.278	28.394	26.663	25.52

Figure 4.10 (a) : The experimental result table of SRR algorithm using the proposed Registration (Susie : The 40th Frame)

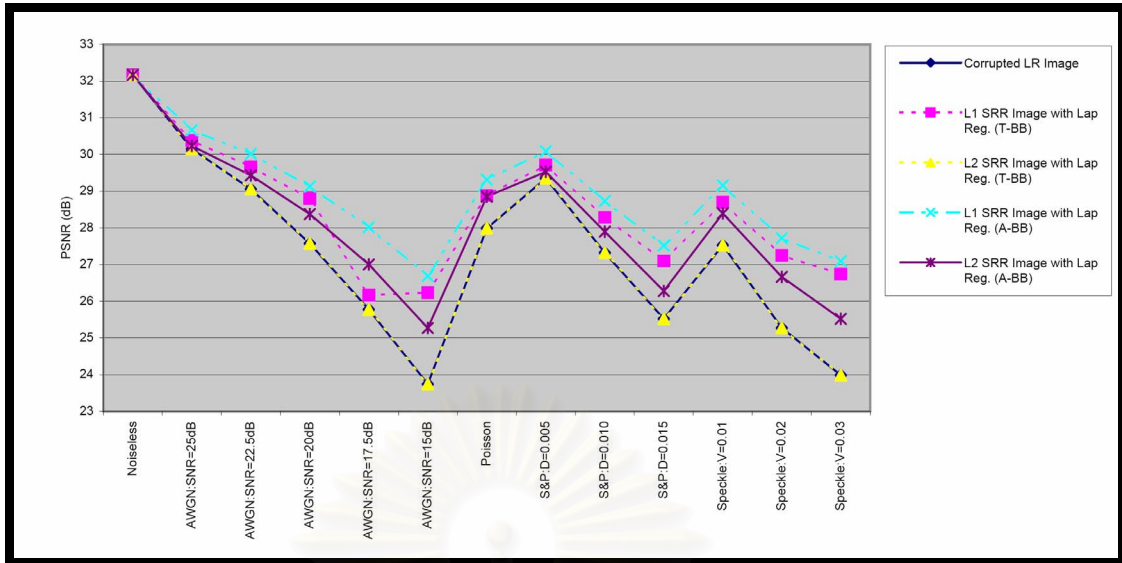


Figure 4.10 (b) : The experimental result of SRR algorithm using the proposed Registration (Susie : The 40th Frame)

PSNR (dB)	Noise Model												
	Noiseless	AWGN:SNR=25dB	AWGN:SNR=22.5dB	AWGN:SNR=20dB	AWGN:SNR=17.5dB	AWGN:SNR=15dB	Poisson	S&P: D=0.005	S&P: D=0.010	S&P: D=0.015	Speckle: V=0.01	Speckle: V=0.02	Speckle: V=0.03
Corrupted LR Image	27.545	25.847	24.851	23.721	22.14	20.312	25.058	25.582	24.629	23.627	23.777	21.854	20.557
L1 SRR Image with Lap Reg. (T-BB)	27.545	26.037	25.401	24.738	24.815	22.761	25.563	25.805	25.149	24.576	24.802	23.756	22.976
L2 SRR Image with Lap Reg. (T-BB)	27.545	25.847	24.851	23.721	22.14	20.312	25.058	25.582	24.629	23.627	23.777	21.854	20.557
L1 SRR Image with Lap Reg. (A-BB)	27.545	26.147	25.583	24.961	24.089	23.115	25.792	25.974	25.392	24.859	25.019	24.096	23.385
L2 SRR Image with Lap Reg. (A-BB)	27.545	25.847	24.851	24.039	22.828	21.189	25.104	25.582	24.83	24.296	24.117	22.728	21.771

Figure 4.11 (a) : The experimental result table of SRR algorithm using the proposed Registration (Foreman : The 110th Frame)

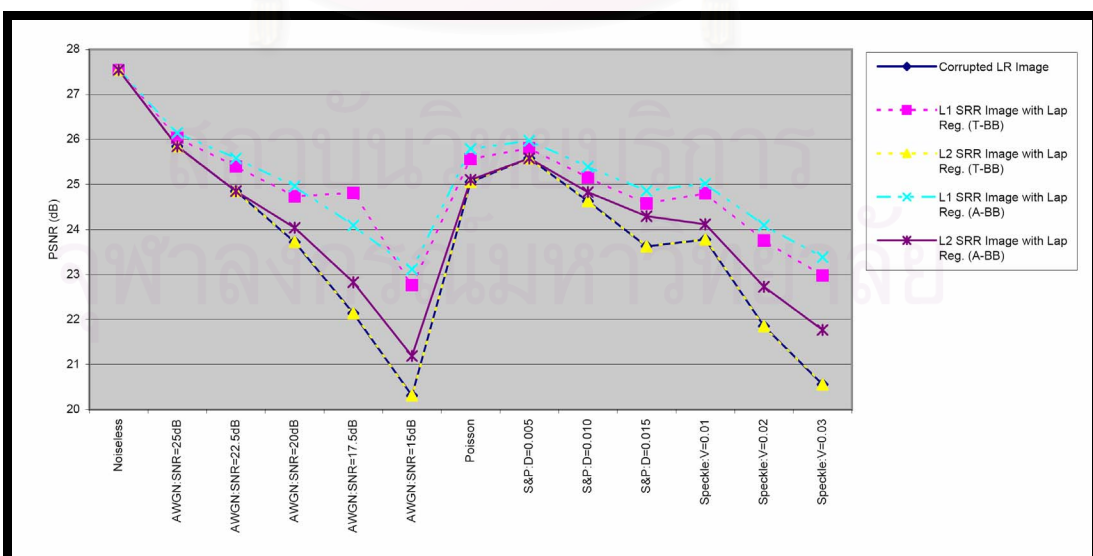


Figure 4.11 (b) : The experimental result of SRR algorithm using the proposed Registration (Foreman : The 110th Frame)

4.3 Experiments on Robust Estimation Technique for SRR [113-117, 119-120]

This section presents the experiments and results obtained by the SRR algorithm methods using the proposed robust estimation (Huber, Lorentzian and Tukey norm) with Laplacian, Huber-Laplacian and Lorentzian-Laplacian and Tukey-Laplacian regularization that are calculated by Equation (3.10), (3.13), (3.20), (3.23), (3.30) and (3.33) respectively. To demonstrate the performance of the SRR algorithm using proposed robust estimation, the results of SRR algorithm using classical L2 norm SRR with Laplacian and BTV regularization calculated by Equation (2.15) and (2.29) and the results of SRR algorithm using classical L1 norm SRR with Laplacian and BTV regularization calculated by Equation (2.17) and (2.31) are presented in order to compare the performance.

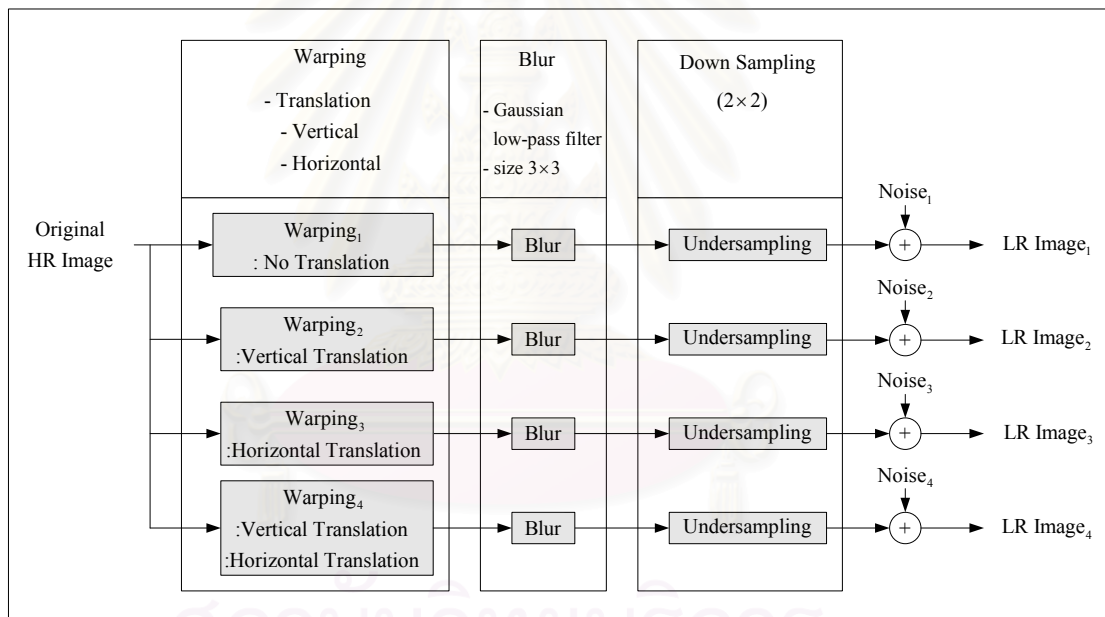


Figure 4.12 : The block diagram of LR image sequence synthesis algorithm for the SRR algorithm using proposed robust estimation.

These experiments are implemented in MATLAB and the block size is fixed at 8x8 (or 16x16 for overlapping block). The 40th frame Susie sequence in QCIF format (176x144) and the Lena (Standard Image : 256x256) are used in these experiments. For the LR image sequence generation, we shifted this original HR image by a pixel in the vertical direction. Then, to simulate the effect of camera PSF, this shifted image was convolved with a symmetric Gaussian low-pass filter of the size 3x3 with the standard deviation equal to one. The resulting image was subsampled by the factor of 2 in each direction. The same approach

with different motion vectors (shifts) in vertical and horizontal directions was used to produce four LR images from the original scene. We added difference noise model to the resulting LR frames. The LR image sequence algorithm is shown in Figure 4.12. For the SRR algorithm, we use four LR frames to generate the high resolution image by the different SRR methods.

The criterion for parameter selection in this experiment was to choose parameters which produce both most visually appealing results and highest PSNR. Therefore, to ensure fairness, each experiment was repeated several times with different parameters and the best result of each experiment was chosen [97-100].

4.3.1 Susie Sequence (The 40th Frame)

4.3.1.1 Noiseless

The original HR image is shown in Fig. 4.13(a-1) and one of corrupted LR images is shown in Fig. 4.13(a-2). Next, the result of implementing the SRR algorithm using L1 estimator with Laplacian Regularization, L1 estimator with BTV Regularization, L2 estimator with Laplacian Regularization, L2 estimator with BTV Regularization are shown in Figs. 4.13(a-3) - 4.13(a-6) respectively. The result of the SRR algorithm using Huber estimator with Laplacian Regularization, Huber estimator with Huber-Laplacian Regularization, Lorentzian estimator with Laplacian Regularization, Lorentzian estimator with Lorentzian-Laplacian Regularization, Tukey estimator with Laplacian Regularization and Tukey estimator with Tukey-Laplacian Regularization are shown in Figs. 4.13(a-7) - 4.13(a-12) respectively.

The results indicates that Huber, Lorentzian and Tukey estimator efficiently reconstruct the noiseless image than L1 and L2 estimator about 1-3 dB respectively.

4.3.1.2 AWGN (Additive White Gaussian Noise)

This experiment is a 5 AWGN cases at SNR=25, 22.5, 20, 17.5 and 15dB respectively and the original HR images are shown in Fig. 4.13(b-1) - Fig. 4.13(f-1) respectively. The corrupted images at SNR=25, 22.5, 20, 17.5 and 15dB are showed in Fig. 4.13(b-2) - Fig. 4.13(f-2) respectively.

At the high SNR (SNR=25dB, 22.5dB and 20dB) or low noise power, the L2 estimator result (with Laplacian and BTV Regularization) give slightly higher PSNR than Huber and Lorentzian

estimator result. However, L2, Huber and Lorentzian estimator result have higher PSNR than L1 estimator result. At SNR=25dB, SNR=22.5dB, SNR=20dB, the result of L1 estimator with Laplacian Regularization, L1 estimator with BTV Regularization, L2 estimator with Laplacian Regularization, L2 estimator with BTV Regularization, Huber estimator with Laplacian Regularization, Huber estimator with Huber-Laplacian Regularization, Lorentzian estimator with Laplacian Regularization, Lorentzian estimator with Lorentzian-Laplacian Regularization, Tukey estimator with Laplacian Regularization and Tukey estimator with Tukey-Laplacian Regularization are shown in Fig. 4.13(b-3) - Fig. 4.13(b-12), Fig. 4.13(c-3) - Fig. 4.13(c-12) and Fig. 4.13(d-3) - Fig. 4.13(d-12) respectively.

At low SNR (SNR=17.5dB and SNR=15dB) or high noise power, the Huber and Lorentzian estimator result give the best performance than L2 estimator result (with Laplacian and BTV Regularization) and L1 estimator result (with Laplacian and BTV Regularization). At SNR=17.5dB and SNR=15dB, the result of L1 estimator with Laplacian Regularization, L1 estimator with BTV Regularization, L2 estimator with Laplacian Regularization, L2 estimator with BTV Regularization, Huber estimator with Laplacian Regularization, Huber estimator with Huber-Laplacian Regularization, Lorentzian estimator with Laplacian Regularization, Lorentzian estimator with Lorentzian-Laplacian Regularization, Tukey estimator with Laplacian Regularization and Tukey estimator with Tukey-Laplacian Regularization are shown in Fig. 4.13(e-3) - Fig. 4.13(e-12) and Fig. 4.13(f-3) - Fig. 4.13(f-12) respectively.

From the result, the L2 estimator gives the best result for SRR estimating at low noise power because the AWGN distributional characteristic is a quadratic model that similar to L2 model. However, at high noise power, the Huber and Lorentzian estimator give the better result than L2 estimator since the L2 norm is very sensitive to outliers where the influence function increases linearly and without bound.

4.3.1.3 Poisson Noise

The original HR image is shown in Fig. 4.13(g-1) and one of corrupted LR images is shown in Fig. 4.13(g-2). The Huber estimator (with Huber-Laplacian Regularization) and Lorentzian estimator (with Lorentzian-Laplacian Regularization) give the highest PSNR from experimental results.

The result of L1 estimator with Laplacian Regularization, L1 estimator with BTV Regularization, L2 estimator with Laplacian Regularization, L2 estimator with BTV Regularization, Huber estimator with Laplacian Regularization, Huber estimator with Huber-Laplacian Regularization, Lorentzian estimator with Laplacian Regularization, Lorentzian estimator with Lorentzian-Laplacian Regularization, Tukey estimator with Laplacian Regularization and Tukey estimator with Tukey-Laplacian Regularization are shown in Fig. 4.13(g-3) - Fig. 4.13(g-12) respectively.

From the result, the Huber and Lorentzian estimator give the best result since the power of noise is slightly high and the distribution of noise is not a quadratic model (the L2 estimator can not estimate the nonquadratic model effectively).

4.3.1.4 Salt&Pepper Noise

This experiment is a 3 Salt&Pepper Noise cases at $D=0.005$, $D=0.010$ and $D=0.015$ respectively and the original HR images are shown in Fig. 4.13(h-1) – Fig. 4.13(j-1) respectively. The corrupted images at $D=0.005$, $D=0.010$ and $D=0.015$ are showed in Fig. 4.13(h-2), Fig. 4.13(i-2) and Fig. 4.13(j-2) respectively. The Huber, Lorentzian and Tukey estimator results give dramatically higher PSNR than L1 estimator result (with Laplacian and BTV Regularization result) and L2 estimator result (with Laplacian and BTV Regularization result).

At $D=0.005$, $D=0.010$ and $D=0.015$, the result of L1 estimator with Laplacian Regularization, L1 estimator with BTV Regularization, L2 estimator with Laplacian Regularization, L2 estimator with BTV Regularization, Huber estimator with Laplacian Regularization, Huber estimator with Huber-Laplacian Regularization, Lorentzian estimator with Laplacian Regularization, Lorentzian estimator with Lorentzian-Laplacian Regularization, Tukey estimator with Laplacian Regularization and Tukey estimator with Tukey-Laplacian Regularization are shown in Fig. 4.13(h-3) - Fig. 4.13(h-12), Fig. 4.13(i-3) - Fig. 4.13(i-12) and Fig. 4.13(j-3) - Fig. 4.13(j-12) respectively.

From the results, the Huber, Lorentzian and Tukey estimator outperform the other estimators when the image is corrupted by Salt&Pepper Noise about 4-5 dB. The Huber, Lorentzian and Tukey estimators give the better result for SRR estimating than L1 or L2 estimator because these robust estimators are designed to be robust and reject outliers. Their norms are more forgiving outliers; that is, the norm should increase less rapidly than L2.

4.3.1.5 Speckle Noise

The last experiment is a 3 Speckle Noise cases for 40th frame Susie sequence at $V=0.01$, $V=0.02$ and $V=0.03$ respectively. The original HR images are shown in Fig. 4.13(k-1) – Fig. 4.13(m-1) respectively. The corrupted images at $V=0.01$, $V=0.02$ and $V=0.03$ are shown in Fig. 4.13(k-2), Fig. 4.13(l-2) and Fig. 4.13(m-2) respectively.

At low noise power ($V=0.01$), the L2 estimator result (with Laplacian and BTV Regularization) give slightly higher PSNR than Huber and Lorentzian estimator results. However, L2, Huber and Lorentzian estimator result have higher PSNR than L1 estimator result (with Laplacian and BTV Regularization). The result of L1 estimator with Laplacian Regularization, L1 estimator with BTV Regularization, L2 estimator with Laplacian Regularization, L2 estimator with BTV Regularization, Huber estimator with Laplacian Regularization, Huber estimator with Huber-Laplacian Regularization, Lorentzian estimator with Laplacian Regularization, Lorentzian estimator with Lorentzian-Laplacian Regularization, Tukey estimator with Laplacian Regularization and Tukey estimator with Tukey-Laplacian Regularization are shown in Fig. 4.13(k-3) - Fig. 4.13(k-12) respectively.

At high noise power ($V=0.02$ and $V=0.03$), the Huber and Lorentzian estimator result give the best performance than L2 estimator result (with Laplacian and BTV Regularization), L1 estimator result (with Laplacian and BTV Regularization). At $V=0.02$ and $V=0.03$, the result of L1 estimator with Laplacian Regularization, L1 estimator with BTV Regularization, L2 estimator with Laplacian Regularization, L2 estimator with BTV Regularization, Huber estimator with Laplacian Regularization, Huber estimator with Huber-Laplacian Regularization, Lorentzian estimator with Laplacian Regularization, Lorentzian estimator with Lorentzian-Laplacian Regularization, Tukey estimator with Laplacian Regularization and Tukey estimator with Tukey-Laplacian Regularization are shown in Fig. 4.13(l-3) - Fig. 4.13(l-12) and Fig. 4.13(m-3) - Fig. 4.13(m-12) respectively.

From the results, the Huber and Lorentzian estimator efficiently reconstruct the image that is corrupted by Speckle Noise at high noise power. It performs better than L1 and L2 estimator because Huber and Lorentzian estimator is more robust against the high power outliers than L1 and L2 estimators.

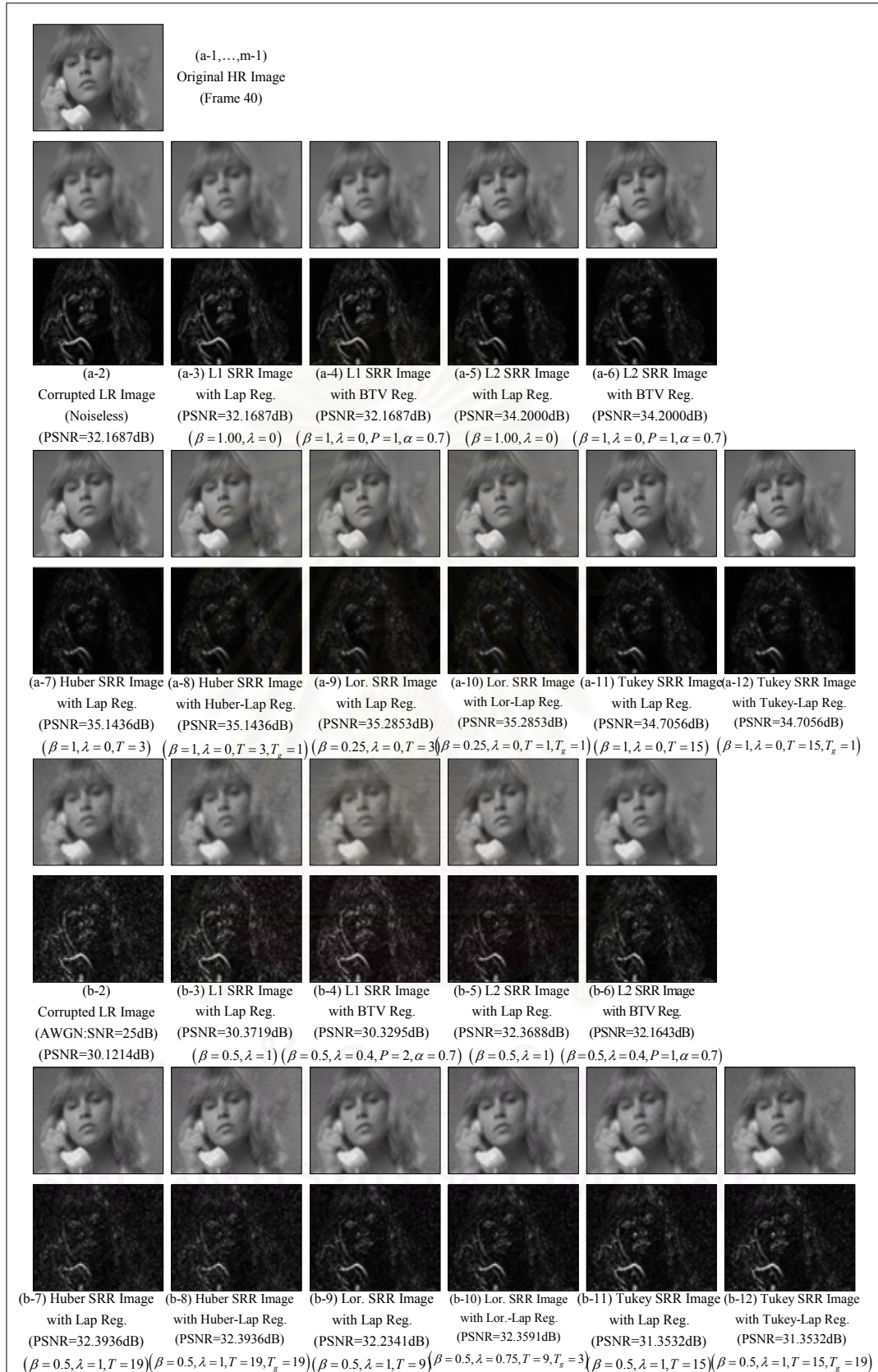


Figure 4.13 : The experimental result of SRR algorithm using the proposed robust estimation technique (Susie Sequence : The 40th Frame)



Figure 4.13 : The experimental result of SRR algorithm using the proposed robust estimation technique (Susie Sequence : The 40th Frame)
(Con.)



Figure 4.13 : The experimental result of SRR algorithm using the proposed robust estimation technique (Susie Sequence : The 40th Frame)
(Con.)

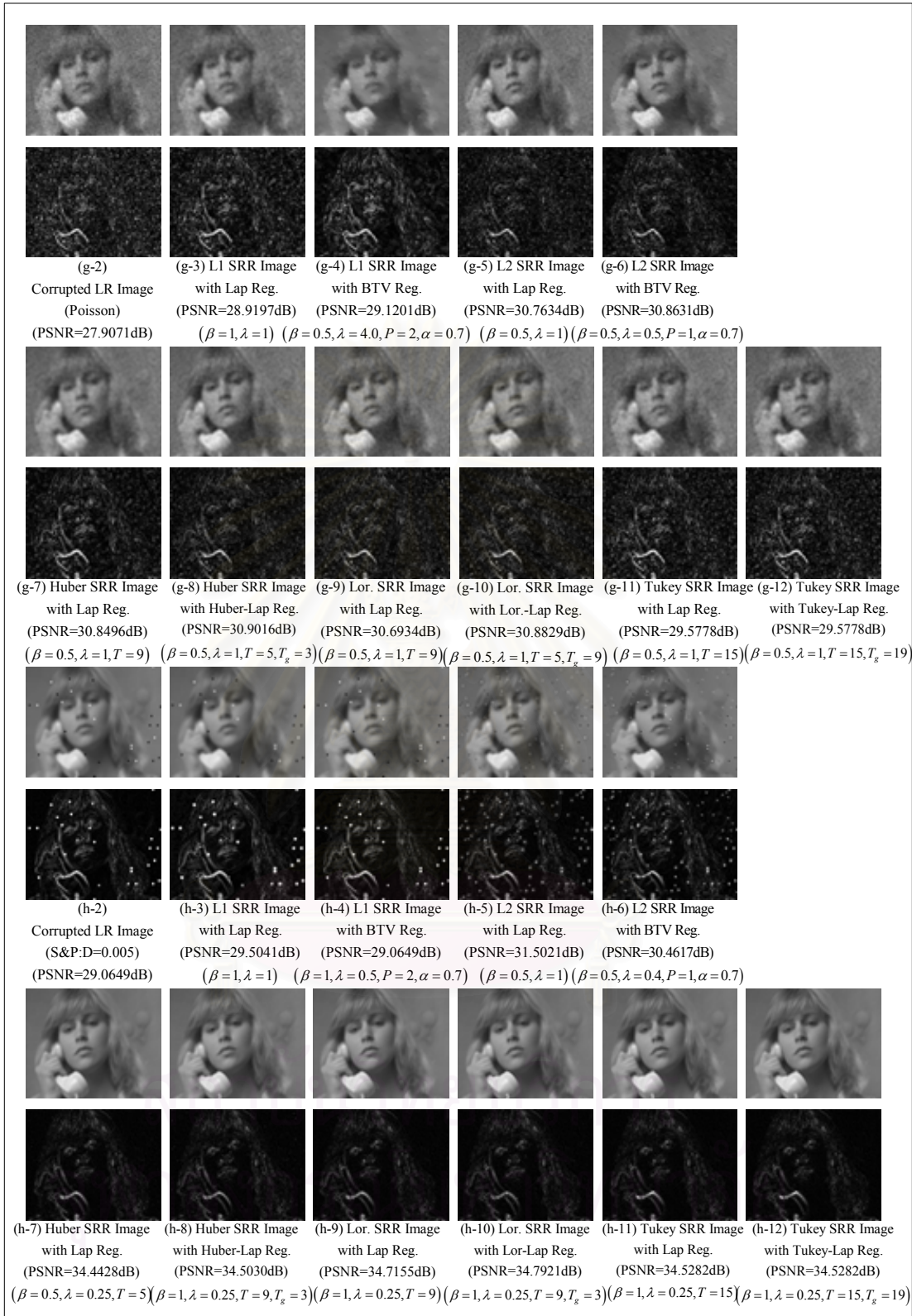


Figure 4.13 : The experimental result of SRR algorithm using the proposed robust estimation technique (Susie Sequence : The 40th Frame)
(Con.)



Figure 4.13 : The experimental result of SRR algorithm using the proposed robust estimation technique (Susie Sequence : The 40th Frame) (Con.)



Figure 4.13 : The experimental result of SRR algorithm using the proposed robust estimation technique (Susie Sequence : The 40th Frame)
(Con.)

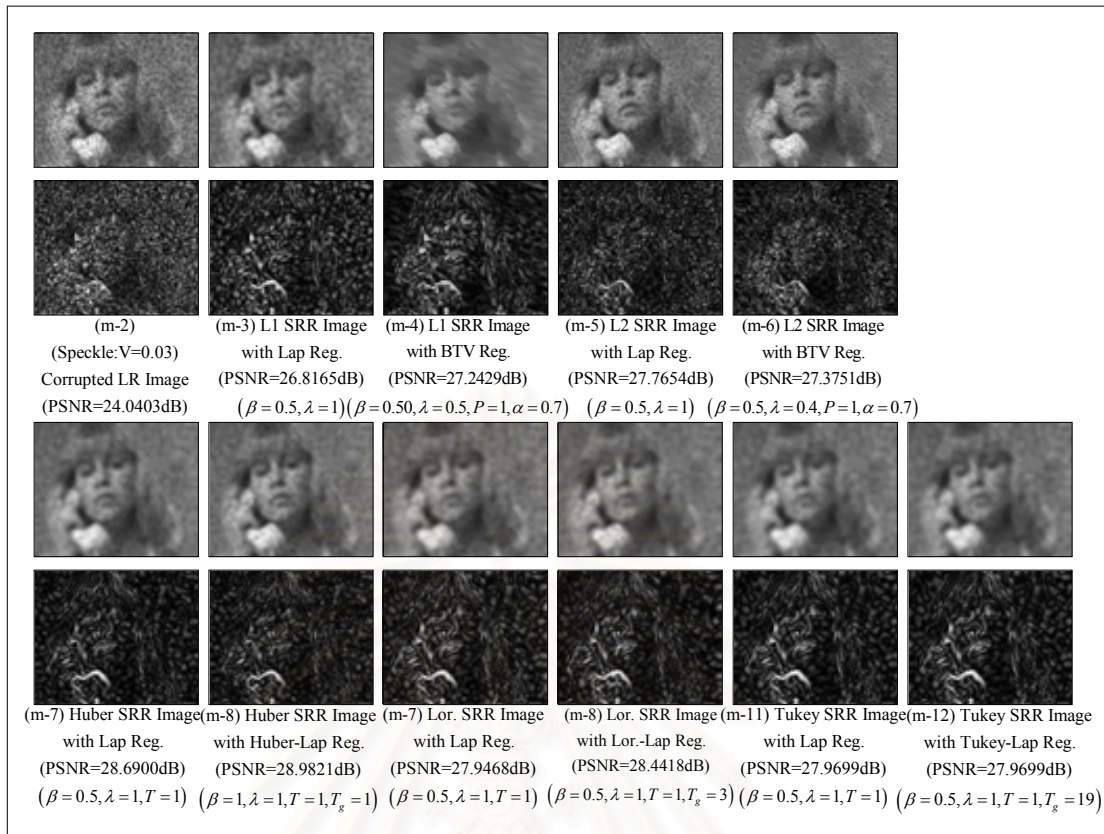


Figure 4.13 : The experimental result of SRR algorithm using the proposed robust estimation technique (Susie Sequence : The 40th Frame)
(Con.)

4.3.2 Lena : (The Standard Image)

4.3.2.1 Noiseless

The original HR image is shown in Fig. 4.14(a-1) and one of corrupted LR images is shown in Fig. 4.14(a-2). Next, the result of implementing the SRR algorithm using L1 estimator with Laplacian Regularization, L1 estimator with BTV Regularization, L2 estimator with Laplacian Regularization, L2 estimator with BTV Regularization are shown in Fig. 4.14(a-3) - Fig. 4.14(a-6) respectively. The result of the SRR algorithm using Huber estimator with Laplacian Regularization, Huber estimator with Huber-Laplacian Regularization, Lorentzian estimator with Laplacian Regularization, Lorentzian estimator with Lorentzian-Laplacian Regularization, Tukey estimator with Laplacian Regularization and Tukey estimator with Tukey-Laplacian Regularization are shown in Fig. 4.14(a-7) - Fig. 4.14(a-12) respectively.

From the results, Huber, Lorentzian and Tukey estimator give the better reconstruction of the noiseless image than L1 and L2 estimator approximately 1-3 dB higher PSNR.

4.3.2.2 AWGN (Additive White Gaussian Noise)

This experiment is a 5 AWGN cases at SNR=25, 22.5, 20, 17.5 and 15dB respectively and the original HR images are shown in Fig. 4.14(b-1) - Fig. 4.14(f-1) respectively. The corrupted images at SNR=25, 22.5, 20, 17.5 and 15dB are showed in Fig. 4.14(b-2) - Fig. 4.14(f-2) respectively.

From the result, the Huber and Lorentzian estimator result give the best performance than L2 estimator result (with Laplacian and BTV Regularization) and L1 estimator result (with Laplacian and BTV Regularization). At SNR=25dB, SNR=22.5dB, SNR=20dB, SNR=17.5dB and SNR=15dB, the result of L1 estimator with Laplacian Regularization, L1 estimator with BTV Regularization, L2 estimator with Laplacian Regularization, L2 estimator with BTV Regularization, Huber estimator with Laplacian Regularization, Huber estimator with Huber-Laplacian Regularization, Lorentzian estimator with Laplacian Regularization, Lorentzian estimator with Lorentzian-Laplacian Regularization, Tukey estimator with Laplacian Regularization and Tukey estimator with Tukey-Laplacian Regularization are shown in Fig. 4.14(b-3) - Fig. 4.14(b-12), Fig. 4.14(c-3) - Fig. 4.14(c-12), Fig. 4.14(d-3) - Fig. 4.14(d-12), Fig. 4.14(e-3) - Fig. 4.14(e-12) and Fig. 4.14(f-3) - Fig. 4.14(f-12) respectively.

From the result, the Huber and Lorentzian estimator will give the better result than L2 estimator since the L2 norm is very sensitive to outliers. The influence function of L2 increases linearly and without bound.

4.3.2.3 Poisson Noise

The original HR image is shown in Fig. 4.14(g-1) and one of corrupted LR images is shown in Fig. 4.14(g-2). The Huber estimator (with Huber-Laplacian Regularization) and Lorentzian estimator (with Lorentzian-Laplacian Regularization) give the highest PSNR from experimental results.

The result of L1 estimator with Laplacian Regularization, L1 estimator with BTV Regularization, L2 estimator with Laplacian Regularization, L2 estimator with BTV Regularization, Huber estimator with Laplacian Regularization, Huber estimator with Huber-Laplacian Regularization, Lorentzian estimator with Laplacian Regularization, Lorentzian estimator with Lorentzian-Laplacian Regularization, Tukey estimator with Laplacian Regularization and Tukey estimator with Tukey-Laplacian Regularization are shown in Fig. 4.14(g-3) - Fig. 4.14(g-12) respectively.

From the result, the Huber and Lorentzian estimator give the best result than L1 and L2 estimator since the power of noise is slight high and the distribution of noise is not quadratic model which the L2 estimator can not estimate the effectively.

4.3.2.4 Salt&Pepper Noise

This experiment is a 3 Salt&Pepper Noise cases at $D=0.005$, $D=0.010$ and $D=0.015$ respectively and the original HR images are shown in Fig. 4.14(h-1) – Fig. 4.14(j-1) respectively. The corrupted images at $D=0.005$, $D=0.010$ and $D=0.015$ are showed in Fig. 4.14(h-2), Fig. 4.14(i-2) and Fig. 4.14(j-2) respectively. The Huber, Lorentzian and Tukey estimator results give dramatically higher PSNR than L1 estimator result (with Laplacian and BTV Regularization result) and L2 estimator result (with Laplacian and BTV Regularization result).

At $D=0.005$, $D=0.010$ and $D=0.015$, the result of L1 estimator with Laplacian Regularization, L1 estimator with BTV Regularization, L2 estimator with Laplacian Regularization, L2 estimator with BTV Regularization, Huber estimator with Laplacian Regularization, Huber estimator with Huber-Laplacian Regularization, Lorentzian estimator with Laplacian Regularization, Lorentzian estimator

with Lorentzian-Laplacian Regularization, Tukey estimator with Laplacian Regularization and Tukey estimator with Tukey-Laplacian Regularization are shown in Fig. 4.14(h-3) - Fig. 4.14(h-12), Fig. 4.14(i-3) - Fig. 4.14(i-12) and Fig. 4.14(j-3) - Fig. 4.14(j-12) respectively.

From the results, the Huber, Lorentzian and Tukey estimator give the far better reconstruction than L1 and L2 estimator with approximately 4-5 dB higher PSNR. The Huber, Lorentzian and Tukey estimators give the better result for SRR estimating than L1 or L2 estimator because these robust estimators are designed to be robust and reject outliers. The norms are more forgiving on outliers; that is, they should increase less rapidly than L2.

4.3.2.5 Speckle Noise

The last experiment is a 2 Speckle Noise cases for 40th frame Susie sequence at $V=0.03$ and $V=0.05$ respectively and the original HR images are shown in Fig. 4.14(k-1) – Fig. 4.14(l-1) respectively. The corrupted images at $V=0.03$ and $V=0.05$ are showed in Fig. 4.14(k-2), and Fig. 4.14(l-2) respectively.

At low noise power ($V=0.03$), the L2 estimator result (with Laplacian and BTV Regularization) give slightly higher PSNR than Huber and Lorentzian estimator results. However, L2, Huber and Lorentzian estimator result have higher PSNR than L1 estimator result (with Laplacian and BTV Regularization). The result of L1 estimator with Laplacian Regularization, L1 estimator with BTV Regularization, L2 estimator with Laplacian Regularization, L2 estimator with BTV Regularization, Huber estimator with Laplacian Regularization, Huber estimator with Huber-Laplacian Regularization, Lorentzian estimator with Laplacian Regularization, Lorentzian estimator with Lorentzian-Laplacian Regularization, Tukey estimator with Laplacian Regularization and Tukey estimator with Tukey-Laplacian Regularization are shown in Fig. 4.14(k-3) - Fig. 4.14(k-12) respectively.

At high noise power ($V=0.05$), the Huber and Lorentzian estimator result give the better performance than L2 estimator result (with Laplacian and BTV Regularization), L1 estimator result (with Laplacian and BTV Regularization). The result of L1 estimator with Laplacian Regularization, L1 estimator with BTV Regularization, L2 estimator with Laplacian Regularization, L2 estimator with BTV Regularization, Huber estimator with Laplacian Regularization, Huber estimator with Huber-Laplacian Regularization, Lorentzian estimator with Laplacian Regularization, Lorentzian estimator with Lorentzian-Laplacian

Regularization, Tukey estimator with Laplacian Regularization and Tukey estimator with Tukey-Laplacian Regularization are shown in Fig. 4.14(1-3) - Fig. 4.14(1-12).

From the results, the Huber and Lorentzian estimator efficiently reconstruct the image that is corrupted by Speckle Noise at high noise power. It was better than L1 and L2 estimator because Huber and Lorentzian estimator is more robust for estimation to the high power outlier than L1 and L2 estimator.



สถาบันวิทยบริการ
จุฬาลงกรณ์มหาวิทยาลัย



Figure 4.14 : The experimental result of SRR algorithm using the proposed robust estimation technique (Lena : The Standard Image)



Figure 4.14 : The experimental result of SRR algorithm using the proposed robust estimation technique (Lena : The Standard Image) (Con.)



Figure 4.14 : The experimental result of SRR algorithm using the proposed robust estimation technique (Lena : The Standard Image) (Con.)



Figure 4.14 : The experimental result of SRR algorithm using the proposed robust estimation technique (Lena : The Standard Image) (Con.)



Figure 4.14 : The experimental result of SRR algorithm using the proposed robust estimation technique (Lena : The Standard Image) (Con.)



Figure 4.14 : The experimental result of SRR algorithm using the proposed robust estimation technique (Lena : The Standard Image) (Con.)

4.3.3 Experimental Conclusion on Robust Estimation Technique for SRR

From all experimental results of both Susie Sequence (40th Frame) and Lena (The Standard Image) shown in Fig. 4.15 and Fig. 4.16 respectively, all comparatively experimental results are concluded as follow:

- The SRR algorithm using Huber and Lorentzian norm with the proposed registration gives the highest PSRN especially for high power noise.
- For Salt&Pepper Noise cases, the Huber, Lorentzian and Tukey estimator give the far better reconstruction than L1 and L2 estimator because these robust estimators are designed to be robust and reject outliers. The norms are more forgiving on outliers; that is, they should increase less rapidly than L2.
- The SRR algorithm using Tukey norm gives the lower PSRN than the Huber, Lorentzian and L2 norm because Tukey norm is excessively robust against the outliers (and the Tukey influence function equal zero) therefore some information losses.
- The SRR algorithm using L1 norm with the proposed registration gives the lowest PSRN because the L1 norm is excessively robust against the outliers.

PSNR (dB)	Noise Model												
	Noiseless	AWGN:SNR=25dB	AWGN:SNR=22.5dB	AWGN:SNR=20dB	AWGN:SNR=17.5dB	AWGN:SNR=15dB	Poisson	S&P:D=0.005	S&P:D=0.010	S&P:D=0.015	Speckle:V=0.01	Speckle:V=0.02	Speckle:V=0.03
Corrupted LR Image	32.169	30.121	29.023	27.532	25.733	23.709	27.907	29.065	26.445	25.276	27.617	25.356	24.04
L1 SRR Image with Lap Reg	32.169	30.372	29.648	28.7	27.577	26.264	28.92	29.504	27.759	26.925	28.829	27.553	26.817
L1 SRR Image with BTV Reg	32.169	30.372	29.532	28.903	27.758	26.906	29.12	29.065	26.445	25.276	28.866	27.828	27.243
L2 SRR Image with Lap Reg	34.2	32.369	31.638	30.69	29.338	27.667	30.763	31.502	29.84	28.761	30.614	28.941	27.765
L2 SRR Image with BTV Reg	34.2	32.164	31.594	31.006	29.409	27.842	30.863	30.462	28.034	26.867	30.613	28.886	27.375
Huber SRR Image with Lap Reg	35.144	32.394	31.681	30.752	30.045	29.198	30.85	34.443	34.417	34.362	30.462	29.375	28.69
Huber SRR Image with Huber-Lap Reg	35.144	32.394	31.681	30.799	30.145	29.296	30.902	34.503	34.459	34.504	30.469	29.717	28.982
Lor. SRR Image with Lap Reg	35.285	32.234	31.475	30.547	29.471	28.152	30.693	34.716	34.719	34.699	29.85	28.502	27.947
Lor. SRR Image with Lor-Lap Reg	35.285	32.359	31.617	30.749	29.691	28.439	30.883	34.792	34.778	34.7	30.129	28.978	28.442
Tukey SRR Image with Lap Reg	34.706	31.353	30.498	29.359	28.604	27.693	29.578	34.528	34.517	34.502	29.361	28.482	27.97
Tukey SRR Image with Tukey-Lap Reg	34.706	31.353	30.498	29.359	28.604	27.693	29.578	34.528	34.517	34.502	29.634	28.482	27.97

Figure 4.15 (a) : The experimental result table of SRR algorithm using the proposed Registration (Susie : The 40th Frame)

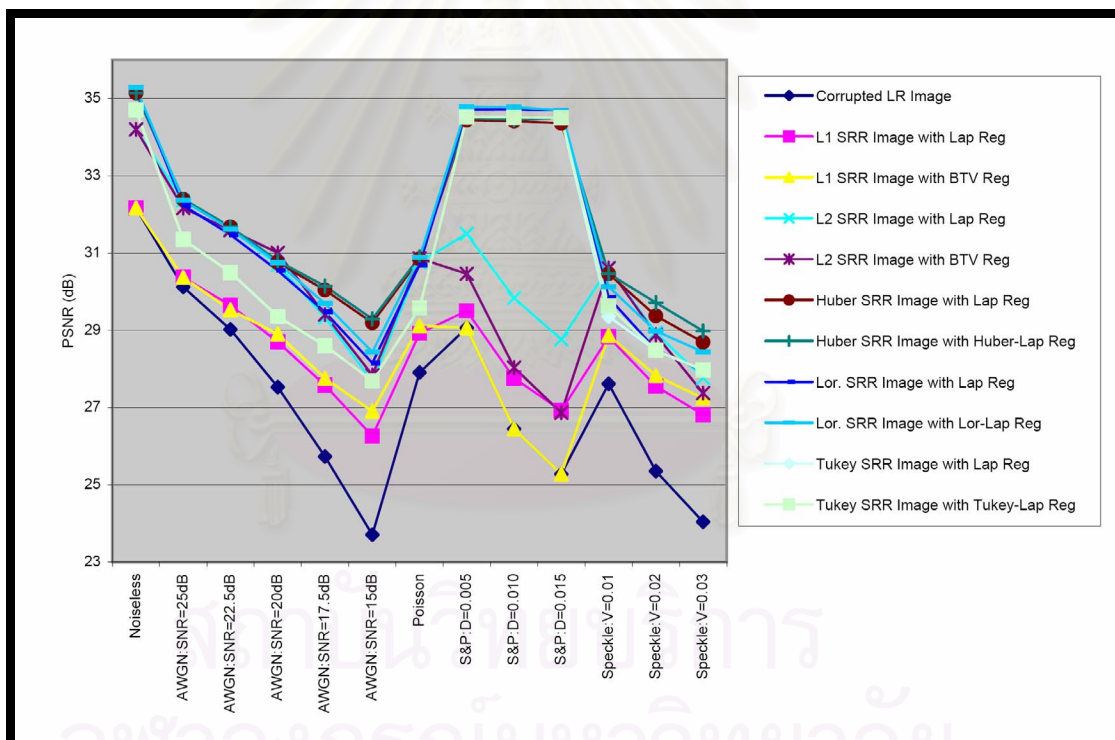


Figure 4.15 (b) : The experimental result of SRR algorithm using the proposed Registration (Susie : The 40th Frame)

PSNR (dB)	Noise Model											
	Noiseless	AWGN:SNR=25dB	AWGN:SNR=22.5dB	AWGN:SNR=20dB	AWGN:SNR=17.5dB	AWGN:SNR=15dB	Poisson	S&P:D=0.005	S&P:D=0.010	S&P:D=0.015	Speckle:V=0.03	Speckle:V=0.05
Corrupted LR Image (dB)	28.863	27.888	27.242	26.219	24.96	23.355	26.512	26.858	25.268	24.219	23.529	21.799
L1 SRR Image with Lap Reg	28.863	27.949	27.492	26.785	26.035	25.149	26.96	27.115	26.057	25.353	25.313	24.422
L1 SRR Image with BTV Reg	28.863	27.888	27.397	26.72	26.007	25.264	26.876	26.858	25.268	24.22	25.217	24.51
L2 SRR Image with Lap Reg	30.855	29.658	29.161	28.602	27.815	26.641	28.719	28.85	28.035	27.319	26.696	25.317
L2 SRR Image with BTV Reg	30.855	29.58	29.078	28.52	27.964	26.771	28.685	28.144	26.798	25.824	26.273	23.958
Huber SRR Image with Lap Reg	32.019	29.722	29.194	28.631	27.873	27.195	28.728	30.946	30.933	30.912	26.672	26.06
Huber SRR Image with Huber-Lap Reg	32.019	29.803	29.196	28.631	27.881	27.212	28.733	31.335	31.111	31.023	26.884	26.26
Lor. SRR Image with Lap Reg	31.957	29.736	29.193	28.561	27.762	26.757	28.674	31.184	31.052	30.023	26.07	25.314
Lor. SRR Image with Lor-Lap Reg	31.957	29.771	29.218	28.638	27.915	26.795	28.747	31.212	31.075	31.063	26.385	25.609
Tukey SRR Image with Lap Reg	31.589	29.133	28.446	27.58	26.572	25.889	27.788	31.315	31.342	31.279	25.883	25.289
Tukey SRR Image with Tukey-Lap Reg	31.589	29.232	28.48	27.58	26.572	25.889	27.816	31.315	31.342	31.279	25.883	25.289

Figure 4.16 (a) : The experimental result table of SRR algorithm using the proposed Registration (Lena : The Standard Image)

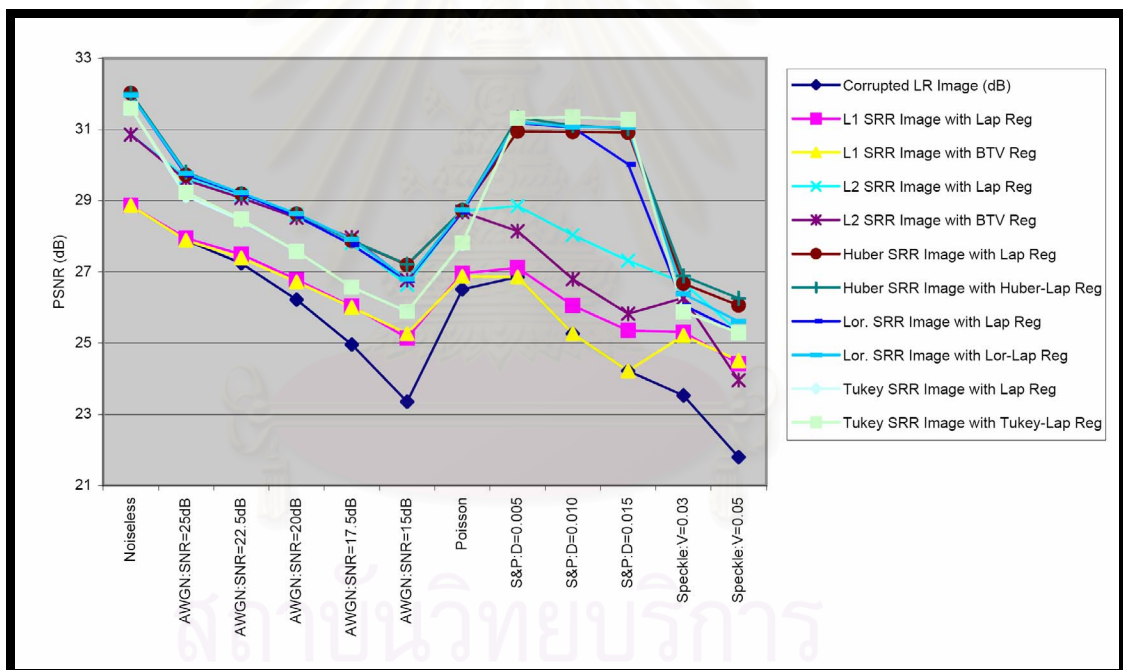


Figure 4.16 (b) : The experimental result of SRR algorithm using the proposed Registration (Lena : The Standard Image)

4.4 Experiments on the SRR Algorithm using Robust Estimation Technique with Classical Registration

The objective of this experiment is to demonstrate the performance of the proposed robust norm regarding to the SRR performance. The SRR algorithm is applied to the image sequence using the classical registration (the translation block-based registration). This section presents the experiments and results obtained by the SRR algorithm using Huber, Lorentzian and Tukey norm with the classical registration. Later, the results of SRR algorithm using L1 and L2 are presented for performance comparison.

The experiment was implemented in MATLAB and the block size of LR images is fixed at 8x8 (or 16x16 for overlapping block) and the search window is 9x9 for classical registration and 5 Frames for ML estimation process. The 38th- 42nd frame Susie sequence and the 108th- 112th frame Foreman sequence in QCIF format (176x144), are used in these experiments to reconstruct the high resolution image of the 40th frame of Susie and the 110th frame of Foreman respectively. Both sequences have complex-edge characteristic. Then, to simulate the effect of camera PSF, the images were convolved with a symmetric Gaussian low-pass filter with size of 3x3 and standard deviation of one. The blurred images were subsampled by the factor of two in each direction (88x72) and the blurred subsampled images were corrupted by Gaussian noise. The LR image sequence synthesis algorithm is shown in Figure 4.7.

The criterion for parameter selection in this experiment was to choose parameters which produce both most visually appealing results and highest PSNR. Therefore, to ensure fairness, each experiment was repeated several times with different parameters and the best result of each experiment was chosen [97-100].

4.4.1 Susie Sequence (The 40th Frame)

4.4.1.1 Noiseless

The original HR image is shown in Fig. 4.17(a-1) and one of corrupted LR images is shown in Fig. 4.17(a-2). Next, the result of implementing the SRR algorithm using L1 estimator, L2 estimator, Huber estimator, Lorentzian estimator and Tukey estimator are shown in Figs. 4.17(a-3) - 4.17(a-7) respectively. From the results, Huber estimator can

reconstruct the noiseless image slightly better than L1 and L2 estimator respectively.

4.4.1.2 AWGN (Additive White Gaussian Noise)

This experiment is a 5 AWGN cases at SNR=25, 22.5, 20, 17.5 and 15dB respectively and the original HR images are shown in Fig. 4.17(b-1) - Fig. 4.17(f-1) respectively. The corrupted images at SNR=25, 22.5, 20, 17.5 and 15dB are showed in Fig. 4.17(b-2) - Fig. 4.17(f-2) respectively.

At the high SNR (SNR=25 and 22.5dB) or low noise power, the Huber estimator result gives slightly higher PSNR than Lorentzian and Tukey estimator result. However, all three estimator results have higher PSNR than L1 and L2 estimator result. At SNR=25dB and SNR=22.5dB, the result of implementing the SRR algorithm using L1 estimator, L2 estimator, Huber estimator, Lorentzian estimator and Tukey estimator are shown in Figs. 4.17(b-3) - 4.17(b-7) and Figs. 4.17(c-3) - 4.17(c-7) respectively.

At low SNR (SNR=20dB, 17.5dB and 15dB) or high noise power, the Tukey estimator result give the best performance than Huber and Lorentzian estimator result. All three robust estimator results have higher PSNR than L1 and L2 estimator result. At SNR=20dB, SNR=17.5dB and SNR=15dB, the result of implementing the SRR algorithm using L1 estimator, L2 estimator, Huber estimator, Lorentzian estimator and Tukey estimator are shown in Fig. 4.17(d-3) - Fig. 4.17(d-7), Fig. 4.17(e-3) - Fig. 4.17(e-7) and Fig. 4.17(f-3) - Fig. 4.17(f-7) respectively.

From the result, all proposed robust estimators gives the better result for SRR estimating than classical L1 and L2 estimator. The result demonstrated the higher resistance to the registration error of the proposed robust estimators.

4.4.1.3 Poisson Noise

The original HR image is shown in Fig. 4.17(g-1) and one of corrupted LR images is shown in Fig. 4.17(g-2). The Lorentzian estimator result gives the highest PSNR. Huber, Lorentzian and Tukey estimator result have higher PSNR than L1 and L2 estimator result. The result of implementing the SRR algorithm using L1 estimator, L2 estimator, Huber estimator, Lorentzian estimator and Tukey estimator are shown in Figs. 4.17(g-3) - 4.17(g-7) respectively. From the results, Huber

estimator reconstructs the noiseless image slightly better than L1 and L2 estimator respectively.

From the result, all proposed robust estimators gives the better SRR result than L1 and L2 estimators because all proposed robust estimators are more resistant to the registration error.

4.4.1.4 Salt&Pepper Noise

This experiment is a 3 Salt&Pepper Noise cases at $D=0.005$, $D=0.010$ and $D=0.015$ respectively and the original HR images are shown in Fig. 4.17(h-1) – Fig. 4.17(j-1) respectively. The corrupted images at $D=0.005$, $D=0.010$ and $D=0.015$ are showed in Fig. 4.17(h-2), Fig. 4.17(i-2) and Fig. 4.17(j-2) respectively. The results of Huber, Lorentzian and Tukey have higher PSNR than these of L1 and L2 estimator. At $D=0.005$, $D=0.010$ and $D=0.015$, the result of implementing the SRR algorithm using L1 estimator, L2 estimator, Huber estimator, Lorentzian estimator and Tukey estimator are shown in Figs. 4.17(h-3) - 4.17(h-8), Figs. 4.17(i-3) - 4.17(i-8) and Figs 4.17(j-4) - 4.17(j-8) respectively. From the result, all proposed robust estimators give the better result for SRR estimating than L1 and L2 estimator because all proposed robust estimators are more resistant to the registration error.

4.4.1.5 Speckle Noise

The last experiment is a 3 Speckle Noise cases for 40th frame Susie sequence at $V=0.01$, $V=0.02$ and $V=0.03$ respectively and the original HR images are shown in Figs. 4.17(k-1) –4.17(m-1) respectively. The corrupted images at $V=0.01$, $V=0.02$ and $V=0.03$ are showed in Fig. 4.17(k-2), Fig. 4.17(l-2) and Fig. 4.17(m-2) respectively. The Huber, Lorentzian and Tukey give higher PSNR than L1 and L2 estimator results. At $V=0.01$, $V=0.02$ and $V=0.03$, the result of implementing the SRR algorithm using L1 estimator, L2 estimator, Huber estimator, Lorentzian estimator and Tukey estimator are shown in Figs. 4.17(k-3) - 4.17(k-8), Figs. 4.17(l-3) - 4.17(l-8) and Figs. 4.17(m-4) - 4.17(m-8) respectively.

From the result, all proposed robust estimators give the better SRR result than L1 and L2 estimator because all proposed robust estimators are more resistance to the registration error. Moreover, L2 estimator can not enhancement the image corrupted by Speckle noise because the L2 norm is very sensitive to outliers (registration error) where the influence function increases linearly and without bound.



Figure 4.17 : The experimental result of the SRR algorithm using proposed robust estimation technique with classical registration



Figure 4.17 : The experimental result of the SRR algorithm using proposed robust estimation technique with classical registration (Susie Sequence : The 40th frame) (Con.)



Figure 4.17 : The experimental result of the SRR algorithm using proposed robust estimation technique with classical registration (Susie Sequence : The 40th frame) (Con.)

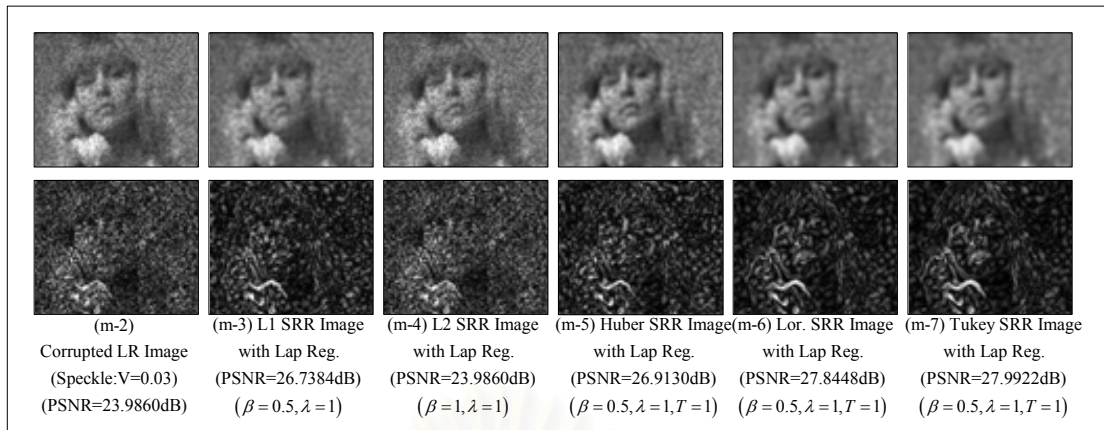


Figure 4.17 : The experimental result of the SRR algorithm using proposed robust estimation technique with classical registration (Susie Sequence : The 40th frame) (Con.)

4.4.2 Foreman Sequence (The 110th Frame)

4.4.2.1 Noiseless

The original HR image is shown in Fig. 4.18(a-1) and one of corrupted LR images is shown in Fig. 4.18(a-2). The SRR result using L1 estimator, L2 estimator, Huber estimator, Lorentzian estimator and Tukey estimator are shown in Figs. 4.18(a-3) - 4.18(a-7) respectively. From the results, Huber estimator can reconstruct the noiseless image slightly better than L1 and L2 estimator.

4.4.2.2 AWGN (Additive White Gaussian Noise)

This experiment is a 5 AWGN cases at SNR=25, 22.5, 20, 17.5 and 15dB respectively and the original HR images are shown in Fig. 4.18(b-1) - Fig. 4.18(f-1) respectively. The corrupted images at SNR=25, 22.5, 20, 17.5 and 15dB are showed in Fig. 4.18(b-2) - Fig. 4.18(f-2) respectively.

At the high SNR (SNR=25 and 22.5dB) or low noise power, the Huber estimator results have slightly higher PSNR than Lorentzian and Tukey estimator result. Huber, Lorentzian and Tukey estimator result have higher PSNR than L1 and L2 estimator result. At SNR=25dB and SNR=22.5dB, the result of implementing the SRR algorithm using L1 estimator, L2 estimator, Huber estimator, Lorentzian estimator and Tukey estimator are shown in Figs. 4.18(b-3) - 4.18(b-7) and Figs. 4.18(c-3) - 4.18(c-7) respectively.

At low SNR (SNR=20dB, 17.5dB and 15dB) or high noise power, the Tukey estimator result give the best performance than Huber and Lorentzian estimator result. Huber, Lorentzian and Tukey estimator result have higher PSNR than L1 and L2 estimator result. At SNR=20dB, 17.5dB and 15dB, the result of implementing the SRR algorithm using L1 estimator, L2 estimator, Huber estimator, Lorentzian estimator and Tukey estimator are shown in Figs. 4.18(d-3) - 4.18(d-7), Figs. 4.18(e-3) - 4.18(e-7) and Figs. 4.18(f-3) - 4.18(f-7) respectively.

From the result, all proposed robust estimators have the better SRR result than L1 and L2 estimator because all proposed robust estimators are more resistant to the registration error.

4.4.2.3 Poisson Noise

The original HR image is shown in Fig. 4.18(g-1) and one of corrupted LR images is shown in Fig. 4.18(g-2). The Lorentzian estimator result gives the highest PSNR than Huber, Tukey, L1 and L2 estimator. Huber, Lorentzian and Tukey estimator result have higher PSNR than L1 and L2 estimator result. The result of implementing the SRR algorithm using L1 estimator, L2 estimator, Huber estimator, Lorentzian estimator and Tukey estimator are shown in Figs. 4.18(g-3) - 4.18(g-7) respectively. From the results, Huber estimator can reconstruct the noiseless image slightly better than L1 and L2 estimator respectively.

From the result, all proposed robust estimators gives the better SRR than L1 and L2 estimators because all proposed robust estimators are more resistant to the registration error.

4.4.2.4 Salt&Pepper Noise

This experiment is a 3 Salt&Pepper Noise cases at $D=0.005$, $D=0.010$ and $D=0.015$ respectively and the original HR images are shown in Figs. 4.18(h-1) –4.18(j-1) respectively. The corrupted images at $D=0.005$, $D=0.010$ and $D=0.015$ are showed in Figs. 4.18(h-2), Fig. 4.18(i-2) and Fig. 4.18(j-2) respectively. The Huber, Lorentzian and Tukey give higher PSNR than L1 and L2 estimator results.

At $D=0.005$, $D=0.010$ and $D=0.015$, the result of implementing the SRR algorithm using L1 estimator, L2 estimator, Huber estimator, Lorentzian estimator and Tukey estimator are shown in Figs. 4.18(h-3) - 4.18(h-8), Figs. 4.18(i-3) - 4.18(i-8) and Figs. 4.18(j-4) - 4.18(j-8) respectively. From the result, all proposed robust estimators give the better SRR result than L1 and L2 estimators because all proposed robust estimators are more resistant to the registration error.

4.4.2.5 Speckle Noise

The last experiment is a 3 Speckle Noise cases for 40th frame Foreman sequence at $V=0.01$, $V=0.02$ and $V=0.03$ respectively and the original HR images are shown in Fig. 4.18(k-1) – Fig. 4.18(m-1) respectively. The corrupted images at $V=0.01$, $V=0.02$ and $V=0.03$ are showed in Fig. 4.18(k-2), Fig. 4.18(l-2) and Fig. 4.18(m-2) respectively. The Huber, Lorentzian and Tukey give higher PSNR than L1 and L2 estimator results. At $V=0.01$, $V=0.02$ and $V=0.03$, the result of implementing the SRR algorithm using L1 estimator, L2 estimator, Huber estimator, Lorentzian estimator and Tukey estimator are shown in Figs. 4.18(k-3) - 4.18(k-8), Figs. 4.18(l-3) - 4.18(l-8) and Figs. 4.18(m-4) - 4.18(m-8) respectively.

From the result, all proposed robust estimators gives the better SRR results than L1 and L2 estimators because all proposed robust estimators are more resistant to the registration error. Moreover, L2 estimator can not enhancement the image corrupted by Speckle noise because the L2 norm is very sensitive to outliers (registration error) where the influence function increases linearly and without bound.

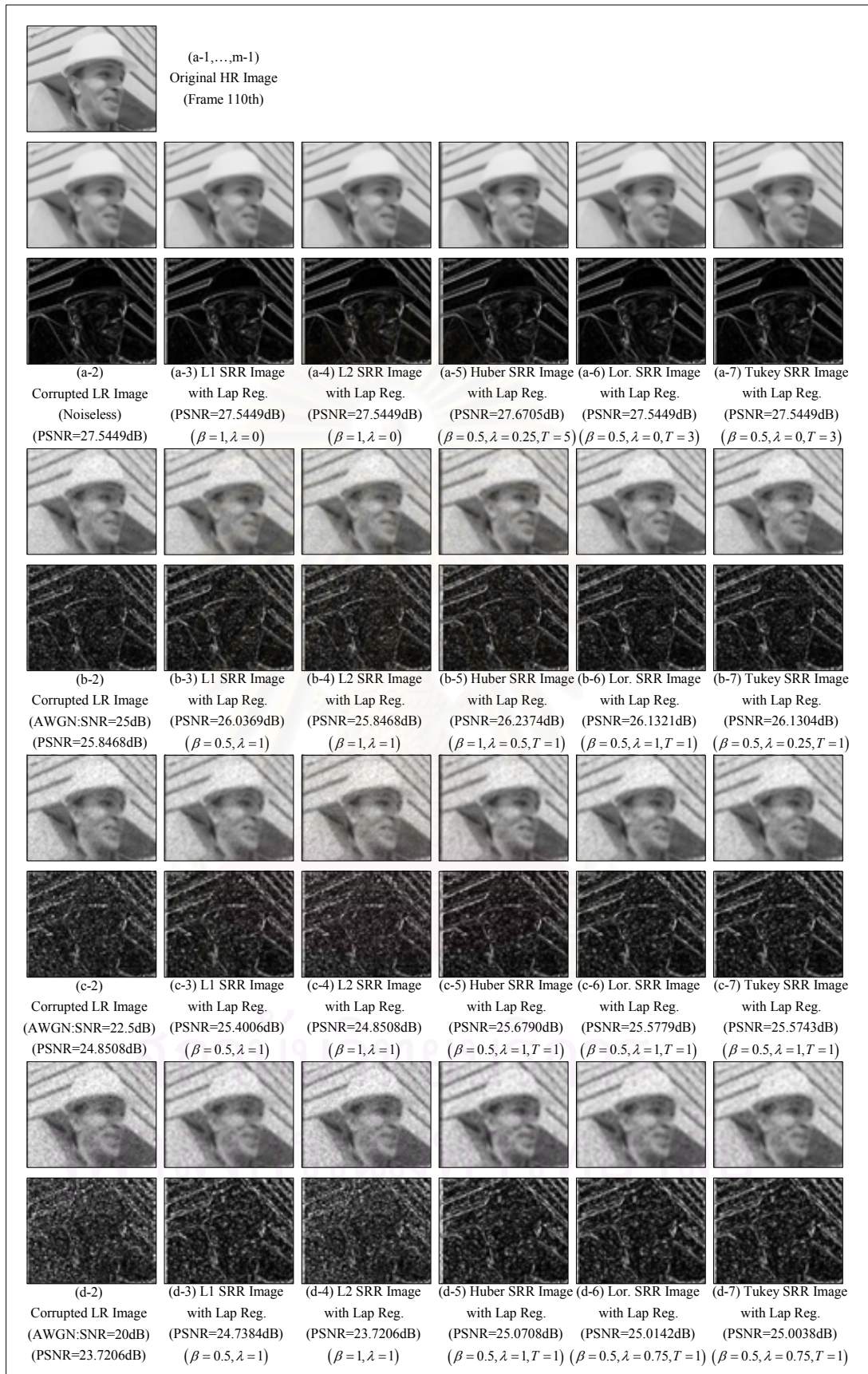


Figure 4.18 : The experimental result of the SRR algorithm using proposed robust estimation technique with classical registration



Figure 4.18 : The experimental result of the SRR algorithm using proposed robust estimation technique with classical registration (Foreman Sequence : The 110th frame)) (Con.)

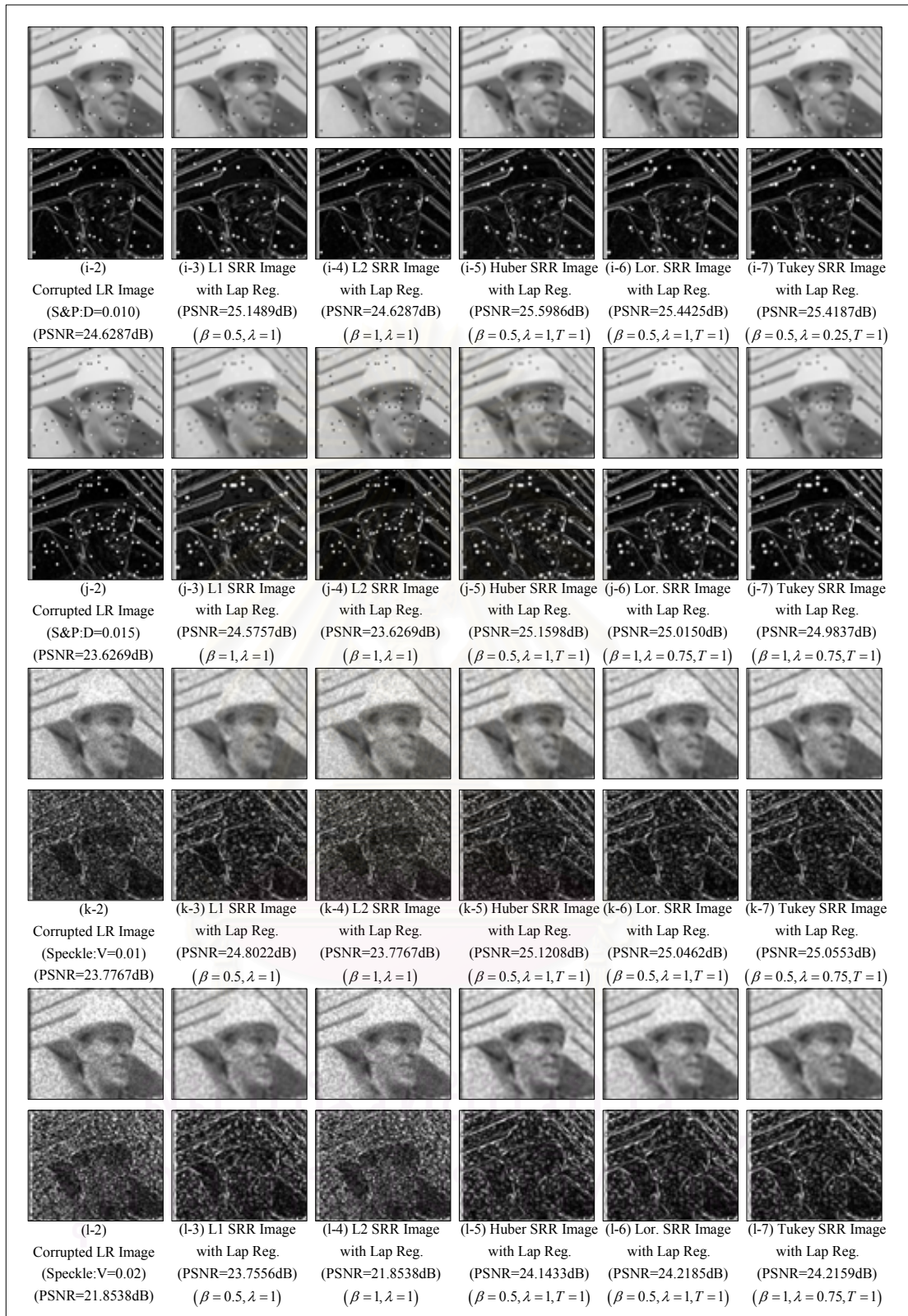


Figure 4.18 : The experimental result of the SRR algorithm using proposed robust estimation technique with classical registration (Foreman Sequence : The 110th frame)) (Con.)

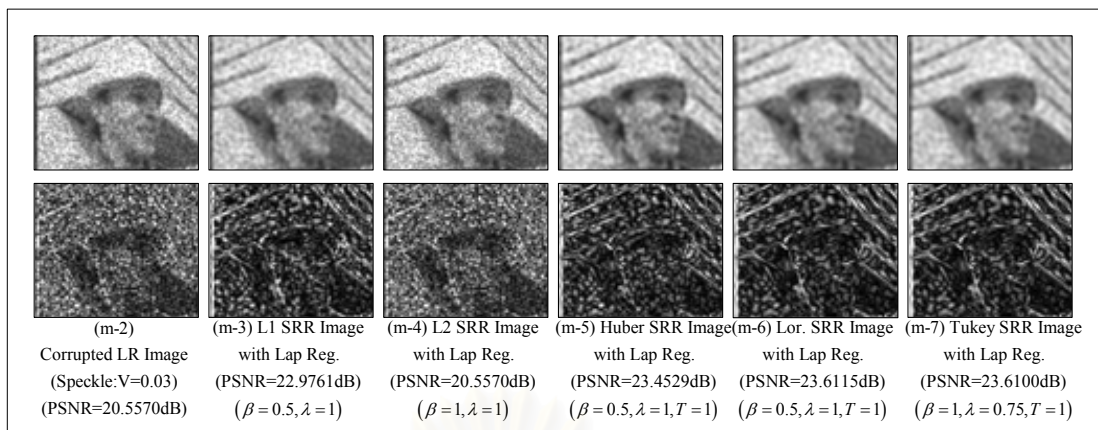


Figure 4.18 : The experimental result of the SRR algorithm using proposed robust estimation technique with classical registration (Foreman Sequence : The 110th frame)) (Con.)

สถาบันวิทยบริการ
จุฬาลงกรณ์มหาวิทยาลัย

4.4.3 Experimental Conclusion on the SRR Algorithm using Robust Estimation Technique with Classical Registration

From all experimental results of both Susie Sequence (40th Frame) and Foreman Sequence (110th Frame) shown in Fig. 4.19 and Fig. 4.20 respectively, all comparatively experimental results are concluded as follow:

- The SRR algorithm using Huber, Lorentzian and Tukey norm with the classical registration gives the highest PSNR because these robust estimators are designed to be robust and reject outliers (registration error). The norms are more forgiving on outliers; that is, they should increase less rapidly than L1 and L2.
- The SRR algorithm using L1 norm gives the higher PSNR than the SRR algorithm using L2 norm because L2 norm is more sensitive the outliers such as the registration error (and the L2 influence function increases linearly and without bound) than L1 norm.
- The SRR algorithm using L2 norm with the classical registration can not increase the PSNR because the registration error is high and L2 norm is more sensitive the outliers.

PSNR (dB)	Noise Model												
	Noiseless	AWGN:SNR=25dB	AWGN:SNR=22.5dB	AWGN:SNR=20dB	AWGN:SNR=17.5dB	AWGN:SNR=15dB	Poisson	S&P:D=0.005	S&P:D=0.010	S&P:D=0.015	Speckle:V=0.01	Speckle:V=0.02	Speckle:V=0.03
Corrupted LR Image	32.169	30.149	29.057	27.574	25.777	23.739	27.989	29.351	27.321	25.521	27.53	25.272	23.986
L1 SRR Image with Lap Reg	32.169	30.382	29.663	28.8	26.164	26.237	28.882	29.708	28.286	27.097	28.692	27.249	26.738
L2 SRR Image with Lap Reg	32.169	30.149	29.057	27.574	25.777	23.739	27.989	29.351	27.321	25.521	27.53	25.272	23.986
Huber SRR Image with Lap Reg	32.223	30.766	30.095	29.205	28.148	26.849	29.396	30.181	29.007	27.925	29.153	27.615	26.913
Lor. SRR Image with Lap Reg	32.169	30.656	30.064	29.413	28.582	27.629	29.482	30.13	29.133	28.227	29.294	28.202	27.845
Tukey SRR Image with Lap Reg	32.169	30.634	30.052	29.43	28.566	27.662	29.441	30.109	29.156	28.394	29.329	28.315	27.992

Figure 4.19 (a) : The experimental result table of SRR algorithm using the proposed Registration (Susie : The 40th Frame)

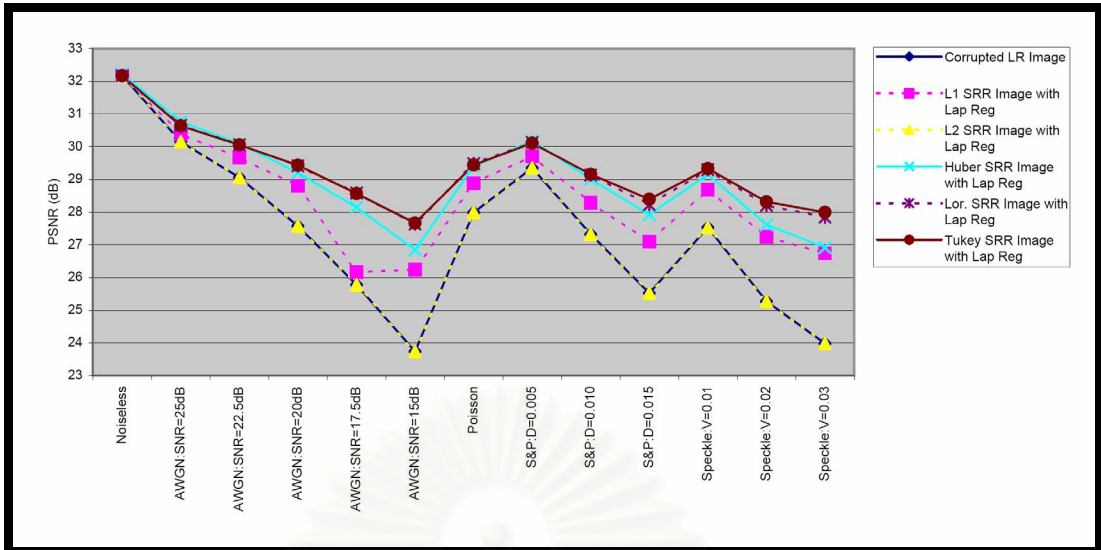


Figure 4.19 (b) : The experimental result of SRR algorithm using the proposed Registration (Susie : The 40th Frame)

PSNR (dB)	Noise Model												
	Noiseless	AWGN:SNR=25dB	AWGN:SNR=22.5dB	AWGN:SNR=20dB	AWGN:SNR=17.5dB	AWGN:SNR=15dB	Poisson	S&P:D=0.005	S&P:D=0.010	S&P:D=0.015	Speckle:V=0.01	Speckle:V=0.02	Speckle:V=0.03
Corrupted LR Image (dB)	27.545	25.847	24.851	23.721	22.14	20.312	25.058	25.582	24.629	23.627	23.777	21.854	20.557
L1 SRR Image with Lap Reg	27.545	26.037	25.401	24.738	24.815	22.761	25.563	25.805	25.149	24.576	24.802	23.756	22.976
L2 SRR Image with Lap Reg	27.545	25.847	24.851	23.721	22.14	20.312	25.058	25.582	24.629	23.627	23.777	21.854	20.557
Huber SRR Image with Lap Reg	27.671	26.237	25.679	25.071	24.221	23.307	25.871	26.085	25.599	25.16	25.121	24.143	23.453
Lor. SRR Image with Lap Reg	27.545	26.132	25.578	25.014	24.251	23.474	25.775	25.971	25.443	25.015	25.046	24.219	23.612
Tukey SRR Image with Lap Reg	27.545	26.13	25.574	25.004	24.24	23.458	25.763	25.946	25.419	24.984	25.055	24.216	23.61

Figure 4.20 (a) : The experimental result table of SRR algorithm using the proposed Registration (Foreman : The 110th Frame)

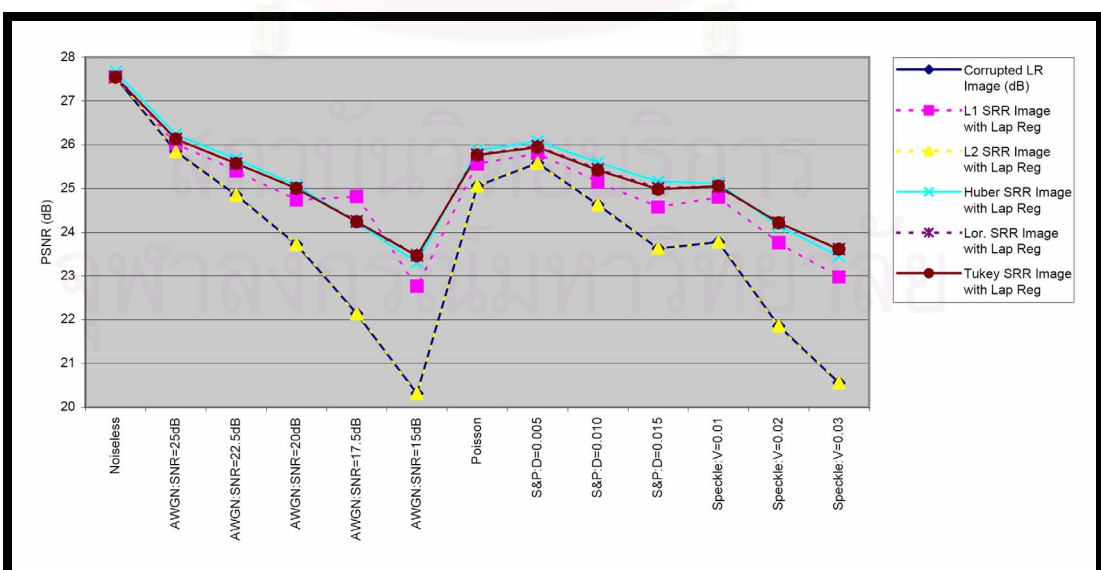


Figure 4.20 (b) : The experimental result of SRR algorithm using the proposed Registration (Foreman : The 110th Frame)

4.5 Experiments on SRR Algorithm using Robust Estimation Technique with Fast Affine Block-Based Registration [121-122]

The objective of this experiment is to demonstrate the performance of the proposed robust norm regarding to the SRR performance. The SRR algorithm is applied to the image sequence using the proposed registration (the fast affine block-based registration). This section presents the experiments and results obtained by the SRR algorithm using Huber, Lorentzian [122] and Tukey [121] norm with the classical registration. Later, the results of SRR algorithm using L1 and L2 are presented for performance comparison.

The experiment was implemented in MATLAB and the block size of LR images is fixed at 8x8 (or 16x16 for overlapping block), the search window is 9x9 for classical registration, the search window is 7x7 for proposed registration and 5 Frames for ML estimation process. The 38th- 42nd frame Susie sequence and the 108th- 112th frame Foreman sequence in QCIF format (176x144), are used in these experiments to generate to reconstruct the high resolution image of the 40th frame of Susie and 110th frame of Foreman respectively. Both sequences have complex-edge characteristic. Then, to simulate the effect of camera PSF, the images were convolved with a symmetric Gaussian low-pass filter with size of 3x3 and standard deviation of one. The blurred images were subsampled by the factor of two in each direction (88x72) and the blurred subsampled images were corrupted by Gaussian noise. The LR image sequence synthesis algorithm is shown in Figure 4.7.

The criterion for parameter selection in this experiment was to choose parameters which produce both most visually appealing results and highest PSNR. Therefore, to ensure fairness, each experiment was repeated several times with different parameters and the best result of each experiment was chosen [97-100].

4.5.1 Susie Sequence (The 40th Frame)

4.5.1.1 Noiseless

The original HR image is shown in Fig. 4.21(a-1) and one of corrupted LR images is shown in Fig. 4.21(a-2). Next, the result of implementing the SRR algorithm using L1 estimator, L2 estimator, Huber estimator, Lorentzian estimator and Tukey estimator are shown in Figs. 4.21(a-3) - 4.21(a-7), respectively. From the results, Huber estimator can

reconstruct the noiseless image slightly better than L1 and L2 estimator respectively.

4.5.1.2 AWGN (Additive White Gaussian Noise)

This experiment is a 5 AWGN cases at SNR=25, 22.5, 20, 17.5 and 15dB respectively and the original HR images are shown in Fig. 4.21(b-1) - Fig. 4.21(f-1) respectively. The corrupted images at SNR=25, 22.5, 20, 17.5 and 15dB are showed in Fig. 4.21(b-2) - Fig. 4.21(f-2) respectively.

At the high SNR (SNR=25 and 22.5dB) or low noise power, the Huber estimator result gives slightly higher PSNR than Lorentzian and Tukey estimator result. All three robust estimator results have higher PSNR than L1 and L2 estimator result. At SNR=25dB and 22.5dB, the result of implementing the SRR algorithm using L1 estimator, L2 estimator, Huber estimator, Lorentzian estimator and Tukey estimator are shown in Figs. 4.21(b-3) - 4.21(b-7) and Figs. 4.21(c-3) - 4.21(c-7) respectively.

At low SNR (SNR=20dB, 17.5dB and 15dB) or high noise power, the Tukey estimator result give the best performance than Huber and Lorentzian estimator result. Huber, Lorentzian and Tukey estimator result have higher PSNR than L1 and L2 estimator result. At SNR=20dB, SNR=17.5dB and SNR=15dB, the result of implementing the SRR algorithm using L1 estimator, L2 estimator, Huber estimator, Lorentzian estimator and Tukey estimator are shown in Fig. 4.21(d-3) - Fig. 4.21(d-7), Fig. 4.21(e-3) - Fig. 4.21(e-7) and Fig. 4.21(f-3) - Fig. 4.21(f-7) respectively.

From the result, all proposed robust estimators give the best result for SRR estimating than classical L1 and L2 estimator. The result demonstrates the higher resistant to the registration error of the proposed robust estimator.

4.5.1.3 Poisson Noise

The original HR image is shown in Fig. 4.21(g-1) and one of corrupted LR images is shown in Fig. 4.21(g-2). The Lorentzian estimator result gives the highest PSNR. Huber, Lorentzian and Tukey estimator result have higher PSNR than L1 and L2 estimator result. The result of implementing the SRR algorithm using L1 estimator, L2 estimator, Huber estimator, Lorentzian estimator and Tukey estimator are shown in Figs. 4.21(g-3) - 4.21(g-7) respectively.

From the result, all proposed robust estimators gives the better SRR result than L1 and L2 estimators because all proposed robust estimators are more resistant to the registration error.

4.5.1.4 Salt&Pepper Noise

This experiment is a 3 Salt&Pepper Noise cases at $D=0.005$, $D=0.010$ and $D=0.021$ respectively and the original HR images are shown in Fig. 4.21(h-1) – Fig. 4.21(j-1) respectively. The corrupted images at $D=0.005$, $D=0.010$ and $D=0.015$ are showed in Fig. 4.21(h-2), Fig. 4.21(i-2) and Fig. 4.21(j-2) respectively. The results of the Huber, Lorentzian and Tukey have higher PSNR than these of L1 and L2 estimators.

At $D=0.005$, $D=0.010$ and $D=0.015$, the result of implementing the SRR algorithm using L1 estimator, L2 estimator, Huber estimator, Lorentzian estimator and Tukey estimator are shown in Figs. 4.21(h-3) - 4.21(h-8), Fig. 4.21(i-3) - 4.21(i-8) and Fig. 4.21(j-4) - 4.21(j-8) respectively.

From the result, all proposed robust estimators give the better SRR results than L1 and L2 estimators because all proposed robust estimators are more resistant to the registration error.

4.5.1.5 Speckle Noise

The last experiment is a 3 Speckle Noise cases for 40th frame Susie sequence at $V=0.01$, $V=0.02$ and $V=0.03$ respectively and the original HR images are shown in Figs. 4.21(k-1) –4.21(m-1) respectively. The corrupted images at $V=0.01$, $V=0.02$ and $V=0.03$ are showed in Fig. 4.21(k-2), Fig. 4.21(l-2) and Fig. 4.21(m-2) respectively. The Huber, Lorentzian and Tukey give higher PSNR than L1 and L2 estimator results. At $V=0.01$, $V=0.02$ and $V=0.03$, the result of implementing the SRR algorithm using L1 estimator, L2 estimator, Huber estimator, Lorentzian estimator and Tukey estimator are shown in Figs. 4.21(k-3) - 4.21(k-8), Figs. 4.21(l-3) - 4.21(l-8) and Figs. 4.21(m-4) - 4.21(m-8) respectively.

From the result, all proposed robust estimators gives the better SRR results than L1 and L2 estimators because all proposed robust estimators are more resistant to the registration error. Moreover, L2 estimator can slightly enhancement the image in this case because the L2 norm is very sensitive to outliers (registration error) where the influence function increases linearly and without bound.



Figure 4.21 : The experimental result of the SRR algorithm using proposed robust estimation technique with proposed registration



Figure 4.21 : The experimental result of the SRR algorithm using proposed robust estimation technique with proposed registration (Susie Sequence : The 40th frame)) (Con.)



Figure 4.21 : The experimental result of the SRR algorithm using proposed robust estimation technique with proposed registration (Susie Sequence : The 40th frame)) (Con.)

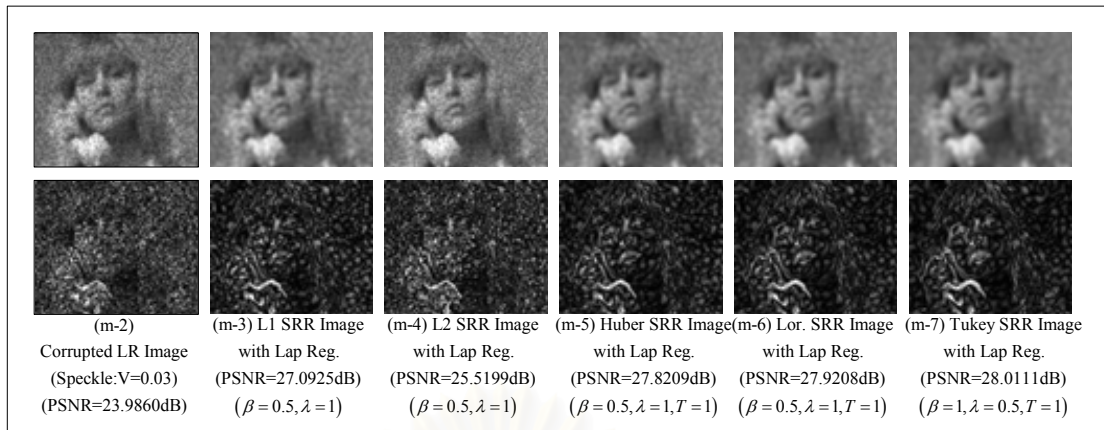


Figure 4.21 : The experimental result of the SRR algorithm using proposed robust estimation technique with proposed registration (Susie Sequence : The 40th frame)) (Con.)

4.5.2 Foreman Sequence (The 110th Frame)

4.5.2.1 Noiseless

The original HR image is shown in Fig. 4.22(a-1) and one of corrupted LR images is shown in Fig. 4.22(a-2). Next, the result of implementing the SRR algorithm using L1 estimator, L2 estimator, Huber estimator, Lorentzian estimator and Tukey estimator are shown in Figs. 4.22(a-3) - 4.22(a-7) respectively. From the results, Huber estimator reconstructs the noiseless image slightly better than L1 and L2 estimator respectively.

4.5.2.2 AWGN (Additive White Gaussian Noise)

This experiment is a 5 AWGN cases at SNR=25, 22.5, 20, 17.5 and 15dB respectively and the original HR images are shown in Figs. 4.22(b-1) - 4.22(f-1) respectively. The corrupted images at SNR=25, 22.5, 20, 17.5 and 15dB are showed in Figs. 4.22(b-2) - 4.22(f-2) respectively.

At the high SNR (SNR=25 and 22.5dB) or low noise power, the Huber estimator result gives slightly higher PSNR than Lorentzian and Tukey estimator result. Huber, Lorentzian and Tukey estimator result have higher PSNR than L1 and L2 estimator result. At SNR=25dB and SNR=22.5dB, the result of implementing the SRR algorithm using L1 estimator, L2 estimator, Huber estimator, Lorentzian estimator and Tukey

estimator are shown in Figs. 4.22(b-3) - 4.22(b-7) and Figs. 4.22(c-3) - 4.22(c-7) respectively.

At low SNR (SNR=20dB, SNR=17.5dB and SNR=15dB) or high noise power, the Tukey estimator result give the best performance than Huber and Lorentzian estimator result. Huber, Lorentzian and Tukey estimator result have higher PSNR than L1 and L2 estimator result. At SNR=20dB, SNR=17.5dB and SNR=15dB, the result of implementing the SRR algorithm using L1 estimator, L2 estimator, Huber estimator, Lorentzian estimator and Tukey estimator are shown in Figs. 4.22(d-3) - 4.22(d-7), Figs. 4.22(e-3) - 4.22(e-7) and Figs. 4.22(f-3) - 4.22(f-7) respectively.

From the result, all proposed robust estimators give the best result for SRR estimating than classical L1 and L2 estimator. The result demonstrates the higher resistant to the registration error of the proposed robust estimator.

4.5.2.3 Poisson Noise

The original HR image is shown in Fig. 4.22(g-1) and one of corrupted LR images is shown in Fig. 4.22(g-2). The Lorentzian estimator result gives the highest PSNR than Huber, Tukey, L1 and L2 estimator. However, Huber, Lorentzian and Tukey estimator result have higher PSNR than L1 and L2 estimator result. The result of implementing the SRR algorithm using L1 estimator, L2 estimator, Huber estimator, Lorentzian estimator and Tukey estimator are shown in Fig. 4.22(g-3) - Fig. 4.22(g-7) respectively.

From the result, all proposed robust estimators gives the better SRR result than the classical L1 and L2 estimators because all proposed robust estimators are more resistant to the registration error.

4.5.2.4 Salt&Pepper Noise

This experiment is a 3 Salt&Pepper Noise cases at $D=0.005$, $D=0.010$ and $D=0.015$ respectively and the original HR images are shown in Fig. 4.22(h-1) – Fig. 4.22(j-1) respectively. The corrupted images at $D=0.005$, $D=0.010$ and $D=0.015$ are showed in Fig. 4.22(h-2), Fig. 4.22(i-2) and Fig. 4.22(j-2) respectively. The Huber, Lorentzian and Tukey give higher PSNR than L1 and L2 estimator results.

At $D=0.005$, $D=0.010$ and $D=0.015$, the result of implementing the SRR algorithm using L1 estimator, L2 estimator, Huber estimator, Lorentzian estimator and Tukey estimator are shown in Figs.

4.22(h-3) - 4.22(h-8), Figs. 4.22(i-3) - 4.22(i-8) and Figs. 4.22(j-4) - 4.22(j-8) respectively.

From the result, all proposed robust estimators gives the better SRR result than the classical L1 and L2 estimators because all proposed robust estimators are more resistant to the registration error.

4.5.2.5 Speckle Noise

The last experiment is a 3 Speckle Noise cases for 40th frame Susie sequence at $V=0.01$, $V=0.02$ and $V=0.03$ respectively and the original HR images are shown in Fig. 4.22(k-1) – Fig. 4.22(m-1) respectively. The corrupted images at $V=0.01$, $V=0.02$ and $V=0.03$ are showed in Fig. 4.22(k-2), Fig. 4.22(l-2) and Fig. 4.22(m-2) respectively. The Huber, Lorentzian and Tukey give higher PSNR than L1 and L2 estimator results. At $V=0.01$, $V=0.02$ and $V=0.03$, the result of implementing the SRR algorithm using L1 estimator, L2 estimator, Huber estimator, Lorentzian estimator and Tukey estimator are shown in Figs. 4.22(k-3) - 4.22(k-8), Figs. 4.22(l-3) - 4.22(l-8) and Figs. 4.22(m-4) - 4.22(m-8) respectively.

From the result, all proposed robust estimators gives the better SRR result than L1 and L2 estimator because all proposed robust estimators can stand with the registration error. Moreover, L2 estimator can slightly enhancement the image in this case because the L2 norm is very sensitive to outliers (registration error) where the influence function increases linearly and without bound.



Figure 4.22 : The experimental result of the SRR algorithm using proposed robust estimation technique with proposed registration



Figure 4.22 : The experimental result of the SRR algorithm using proposed robust estimation technique with proposed registration (Foreman Sequence : The 110th frame) (Con.)

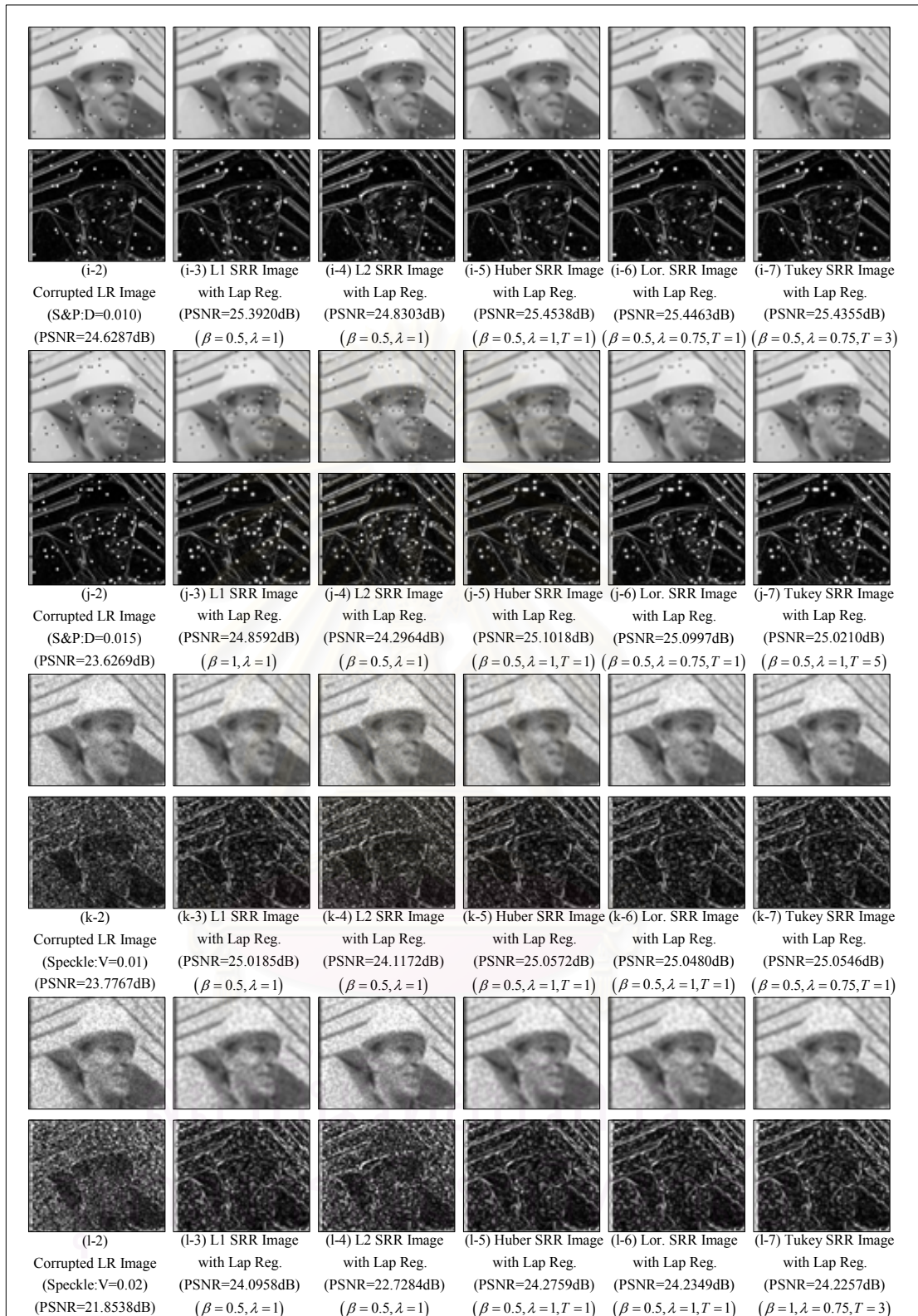


Figure 4.22 : The experimental result of the SRR algorithm using proposed robust estimation technique with proposed registration (Foreman Sequence : The 110th frame) (Con.)

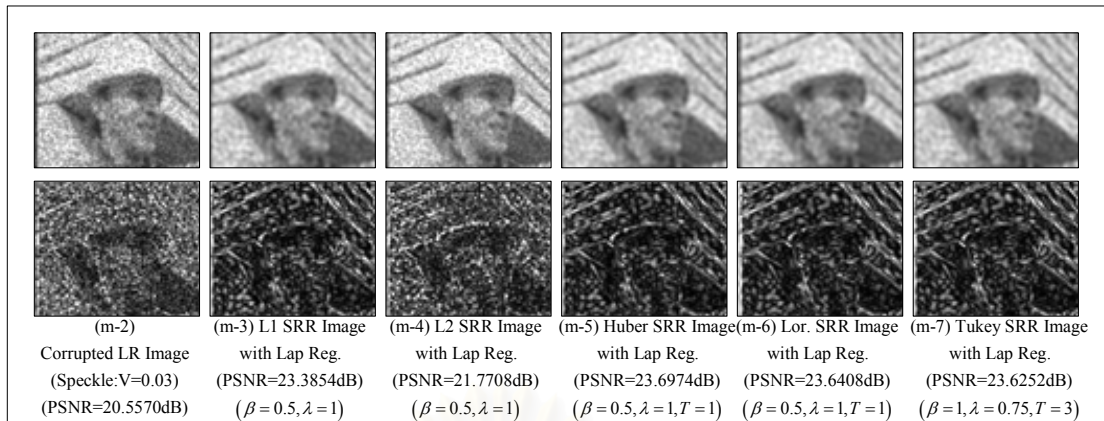


Figure 4.22 : The experimental result of the SRR algorithm using proposed robust estimation technique with proposed registration (Foreman Sequence : The 110th frame)) (Con.)

4.4.5 Experimental Conclusion on the SRR Algorithm using Robust Estimation Technique with Fast Affine Block-Based Registration

From all experimental results of both Susie Sequence (40th Frame) and Foreman Sequence (110th Frame) shown in Fig. 4.23 and Fig. 4.24 respectively, all comparatively experimental results are concluded as follow:

- The SRR algorithm using Huber, Lorentzian and Tukey norm with the proposed registration gives the highest PSNR because these robust estimators are designed to be robust and reject outliers (registration error). The norms are more forgiving on outliers; that is, they should increase less rapidly than L1 and L2.
- The SRR algorithm using L1 norm gives the higher PSNR than the SRR algorithm using L2 norm because L2 norm is more sensitive the outliers such as the registration error (and the L2 influence function increases linearly and without bound) than L1 norm.
- The SRR algorithm using L2 norm with the proposed registration gives the lowest PSNR because L2 norm is more sensitive the outliers such as the registration error.

PSNR (dB)	Noise Model												
	Noiseless	AWGN:SNR=25dB	AWGN:SNR=22.5dB	AWGN:SNR=20dB	AWGN:SNR=17.5dB	AWGN:SNR=15dB	Poisson	S&P:D=0.005	S&P:D=0.010	S&P:D=0.015	Speckle:V=0.01	Speckle:V=0.02	Speckle:V=0.03
Corrupted LR Image	32.169	30.149	29.057	27.574	25.777	23.739	27.989	29.351	27.321	25.521	27.53	25.272	23.986
L1 SRR Image with Lap Reg	32.169	30.662	30.019	29.13	28.019	26.688	29.311	30.087	28.73	27.519	29.156	27.719	27.093
L2 SRR Image with Lap Reg	32.169	30.235	29.432	28.375	27.004	25.271	28.851	29.528	27.898	26.278	28.394	26.663	25.52
Huber SRR Image with Lap Reg	32.169	30.767	30.209	29.581	28.761	27.732	29.734	30.255	29.439	28.75	29.459	28.408	27.821
Lor. SRR Image with Lap Reg	32.169	30.746	30.169	29.525	28.711	27.757	29.633	30.204	29.327	28.651	29.4	28.356	27.921
Tukey SRR Image with Lap Reg	32.169	30.718	30.122	29.475	28.628	27.702	29.551	30.201	29.266	28.486	29.38	28.349	28.011

Figure 4.23 (a) : The experimental result table of SRR algorithm using the proposed Registration (Susie : The 40th Frame)

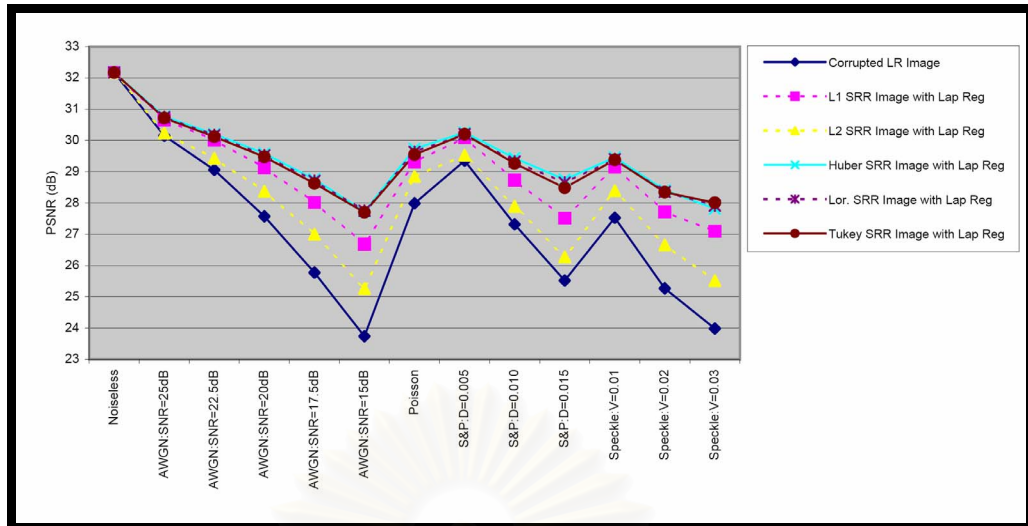


Figure 4.23 (b) : The experimental result of SRR algorithm using the proposed Registration (Susie : The 40th Frame)

PSNR (dB)	Noise Model												
	Noiseless	AWGN:SNR=25dB	AWGN:SNR=22.5dB	AWGN:SNR=20dB	AWGN:SNR=17.5dB	AWGN:SNR=15dB	Poisson	S&P:D=0.005	S&P:D=0.010	S&P:D=0.015	Speckle:V=0.01	Speckle:V=0.02	Speckle:V=0.03
Corrupted LR Image	27.545	25.847	24.851	23.721	22.14	20.312	25.058	25.582	24.629	23.627	23.777	21.854	20.557
L1 SRR Image with Lap Reg	27.545	26.147	25.583	24.961	24.089	23.115	25.792	25.974	25.392	24.859	25.019	24.096	23.385
L2 SRR Image with Lap Reg	27.545	25.847	24.851	24.039	22.828	21.189	25.104	25.582	24.83	24.296	24.117	22.728	21.771
Huber SRR Image with Lap Reg	27.545	26.126	25.582	25.036	24.316	23.511	25.783	25.963	25.454	25.102	25.057	24.276	23.697
Lor. SRR Image with Lap Reg	27.545	26.134	25.583	25.018	24.273	23.502	25.785	25.967	25.446	25.1	25.048	24.235	23.641
Tukey SRR Image with Lap Reg	27.545	26.133	25.578	25.005	24.254	23.475	25.782	25.967	25.436	25.021	25.055	24.226	23.625

Figure 4.24 (a) : The experimental result table of SRR algorithm using the proposed Registration (Foreman : The 110th Frame)

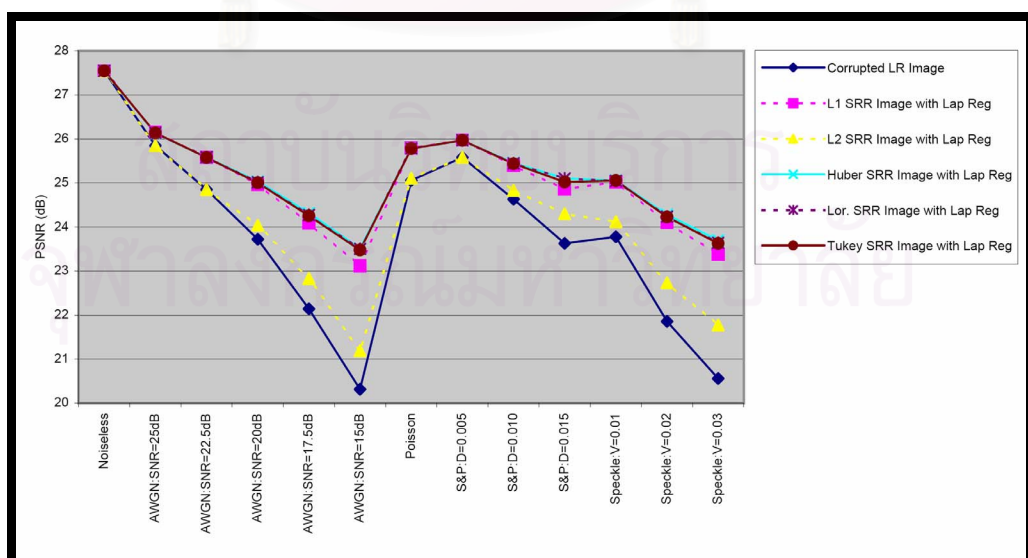


Figure 4.24 (b) : The experimental result of SRR algorithm using the proposed Registration (Foreman : The 110th Frame)

CHAPTER V

CONCLUSIONS

This dissertation presents the highly accurate sub-pixel images registration and three robust norm estimators for the SRR framework. Several images and noise models were tested for their effectiveness. The performance was analyzed both in terms of the PSNR and visually appealing results.

5.1 Conclusions of the Dissertation

In this dissertation, the highly accurate sub-pixel images registration and robust norm estimators are proposed and applied to SRR algorithms. First, this dissertation proposed a novel M3SS image registration for fast affine block-based registration. M3SS exploits the benefits of both the affine block-based motion estimation and 3SS. The experiment investigates the accuracy performance of the proposed registration (affine block-based) compared with the classical registration (translation block-based). This experiment intends to study the registration accuracy that is traditionally used in the SRR algorithm and the proposed registration accuracy. Three standard video sequences (Carphone, Foreman and Stefan) in QCIF format (176x144) were used as the test sequences that can be categorized by moving characteristic. First, Carphone sequence has only a moving foreground but the background is almost stationary. Second, Foreman sequence has both slightly moving foreground and background. Finally, Stefan sequence has both dramatically moving foreground and background. Although the proposed sub-pixel registration algorithm requires higher computation than the classical algorithm but the proposed algorithm has far better PSNR performance in our experiment. The affine block-based registration algorithm clearly gives a higher accuracy than the classical algorithm both objectively and subjectively. By using this proposed registration algorithm, the super-resolution algorithm, which is described later, can be applied on the general sequence that have complex motions such as Foreman and Susie sequence.

Second, both the proposed registration and the classical registration the SRR algorithm were examined in the SRR framework using L1 and L2 norms for evaluating the registration impact to SRR performance. For the same norm estimation technique, the SRR algorithm with the proposed registration gives the higher PSNR than the SRR algorithm with the classical registration. Next, The SRR algorithm using

L1 norm with the proposed registration gives the highest PSRN. The SRR algorithm using L1 norm gives the higher PSRN than the SRR algorithm using L2 norm because L2 norm is more sensitive the outliers such as the registration error (and the L2 influence function increases linearly and without bound) than L1 norm. Finally, the SRR algorithm using L2 norm with the classical registration can not enhance measured image because the registration error is high and L2 norm is more sensitive the outliers.

Third, this dissertation propose an novel approach using a novel robust estimation norm function (Huber, Lorentzian and Tukey norm function) for SRR and the proposed robust SRR can be effectively applied on the images that are corrupted by various noise models. Therefore, this experiment is examined how the estimation techniques impact to the SRR performance by ignoring the registration error. (All corrupted low resolution images are synthesized from the same original high resolution image.) From the experimental result, the SRR algorithm using Huber and Lorentzian norm with the proposed registration gives the highest PSRN especially for high power noise. For Salt&Pepper Noise cases, the Huber, Lorentzian and Tukey estimator give the far better reconstruction than L1 and L2 estimator because these robust estimators are designed to be robust and reject outliers. The norms are more forgiving on outliers; that is, they should increase less rapidly than L2. Next, The SRR algorithm using Tukey norm gives the lower PSRN than the Huber, Lorentzian and L2 norm because Tukey norm is excessively robust against the outliers (and the Tukey influence function equal zero) therefore some information losses. Finally, The SRR algorithm using L1 norm with the proposed registration gives the lowest PSRN because the L1 norm is excessively robust against the outliers.

Forth, this dissertation examines the performance of the SRR algorithm using proposed estimation norms (Huber, Lorentzian and Tukey norm function) when the SRR algorithm is used for the real image sequence. The 38th- 42nd frame Susie sequence and the 108th- 112th frame Foreman sequence are used in these experiments to generate the super-resolution image. Hence, the SRR algorithm for this experiment is used the classical registration process (translational block-based). From the experimental result, the SRR algorithm using Huber, Lorentzian and Tukey norm with the classical registration gives the highest PSRN because these robust estimators are designed to be robust and reject outliers (registration error). The norms are more forgiving on outliers; that is, they should increase less rapidly than L1 and L2. Next, The SRR algorithm using L1 norm gives the higher PSRN than the SRR algorithm

using L2 norm because L2 norm is more sensitive the outliers such as the registration error (and the L2 influence function increases linearly and without bound) than L1 norm. Finally, L2 estimator fails to enhance the image in the inaccurate registration because the L2 norm is very sensitive to outliers (registration error) where the influence function increases linearly and without bound.

Finally, this dissertation examines the performance of the SRR algorithm using proposed estimation norms (Huber, Lorentzian and Tukey norm function) and using the proposed registration (affine block-based) when the SRR algorithm is used for the real image sequence. . The 38th- 42nd frame Susie sequence and the 108th- 112th frame Foreman sequence are used in these experiments to generate the super-resolution image. From the experimental result, The SRR algorithm using Huber, Lorentzian and Tukey norm with the proposed registration gives the highest PSRN because these robust estimators are designed to be robust and reject outliers (registration error). The norms are more forgiving on outliers; that is, they should increase less rapidly than L1 and L2. Next, The SRR algorithm using L1 norm gives the higher PSRN than the SRR algorithm using L2 norm because L2 norm is more sensitive the outliers such as the registration error (and the L2 influence function increases linearly and without bound) than L1 norm. L2 estimator can slightly enhancement the image because the registration is more accurate than the result from the translation registration. The L2 norm is very sensitive to outliers (registration error) where the influence function increases linearly and without bound therefore the L1 estimator give the better result for SRR estimating than L2.

5.2 Contributions of the Dissertation

In this dissertation, we proposed a regularized ML framework for solving SRR problems. This framework helped us construct a well-defined description of several aspects of this problem from an estimation theoretic point of view, allowing us to make fundamental contributions to both the methodology and the science of image fusion, reconstruction, and enhancement.

5.2.1 A Comprehensive Survey of the Literature on the SRR

In Chapter (1), this dissertation reviews a comprehensive survey of the literature on the SRR (Super-Resolution Reconstruction) algorithms and related image restoration algorithms in the last two decades. This work is significant in that it covers virtually the entire literature and categorizes existing multiframe restoration methods according to their common characteristics in a systematic framework, drawing together research which utilizes a broad variety of approaches.

Moreover, this dissertation reviews traditional image registrations for SRR algorithm in the last two decades. Later, we described a general theory regarding SRR algorithm using regularized ML (L1 and L2 estimator) of a high-quality image from a set of low-resolution noisy and blurred images. Moreover, several classical SRR regularized functions, such as Laplacian, MRF and BTV, and its solutions are presented in Chapter 2.

5.2.2 The Highly Accurate Sub-Pixel Images Registration on the SRR

This dissertation propose a novel image registration (motion estimation) algorithm which describes the complex motion more efficiently and gives a very accurate result, affine block-based motion estimation described in Section 3.1.1. M3SS algorithm, that is designed to reduce a computational load in section 3.1.2, is proposed. Moreover, the range of affine parameter (motion vector) are proposed in Eq.(3.3) - Eq.(3.3) for the search window for the 7x7 displacement window (translational deformation) and $\pm 20^\circ$ degree (rotation, extraction or expansion deformation). From the experimental result, three standard video sequences (Carphone, Foreman and Stefan) in QCIF format (176x144) were used as the test sequences which can be categorized by

moving characteristic. The proposed registration has a higher accuracy than the classical registration in both subjective and objective measurement as described in Section 4.1.

Later, the proposed registration is incorporated to the SRR Regularized ML framework thus an observation model for SRR is improved under affine block-based motion. Consequently, the SRR using the proposed registration can be applied on real image sequences such as Susie and Foreman sequences. The performance of the SRR algorithms is higher than the SRR using the classical registration as shown in Section 4.2.

5.2.3 The Robust Estimations on the SRR

This dissertation proposes the robust norm estimation for SRR algorithm that can be applied on several noise models. The SRR algorithm using proposed robust norms (Huber and Lorentzian norm function) give higher PSNR than the SRR algorithm using L1 or L2 norms because these robust estimators are designed to be robust and reject outliers as shown in Section 4.3. From the experimental result, SRR algorithm using the Huber norm gives highest PSNR for the low noise power (or low power of outliers), SRR algorithm using the Lorentzian norm gives highest PSNR for the moderate noise power (or moderate power of outliers) and SRR algorithm using the Tukey norm gives highest PSNR for the high noise power (or high power of outliers).

Next, this dissertation proposes the iterative robust SRR algorithm (Huber, Lorentzian and Tukey norm function) using the classical registration for the real image sequence such as Susie and Foreman Sequence. Not only does the SRR algorithm can be applied on the several noise models but this SRR algorithm can be apply on the real sequences as well. The classical registration gives the registration error severely hence the SRR algorithm using L2 norm with the classical registration can not enhance measured image. However, the SRR algorithm using the proposed norm gives the highest PSNR because these robust estimators are designed to be robust and reject outliers (such as the registration noise) as shown in Section 4.4.

5.2.4 The Highly Accurate Sub-Pixel Images Registration and the Robust Estimations on the SRR

This dissertation proposed the iterative robust SRR algorithm using the affine block-based registration for the real image sequence such as Susie and Foreman Sequence. Therefore, this SRR algorithm can be applied on both any noise models and on the real image sequences. The proposed registration gives the registration error moderately thus the SRR algorithm using L2 norm with the proposed registration can enhance measured image. However, the SRR algorithm using the proposed norm gives the better PSNR because these robust estimators are designed to be robust and reject outliers (such as the registration noise) as shown in Section 4.5.

5.2.5 Program Development

Based on the material presented in this dissertation, we have developed a Matlab based software. The main objective of this software tool is the implementation and comparison of several registration techniques and SRR algorithms. In particular, the techniques described in this dissertation and several references therein are includes.

- Image Registration (Motion Estimation) Technique
- The user is able to specify the type of norm estimation such as L1, L2, Huber, Lorentzian or Tukey.
- The user is able to specify the type of regularized functions such are Laplacian, Huber-Laplacian, Lorentzian-Laplacian, Tukey- Laplacian, MRF (Markov Random Field), HMRF (Huber MRF) or BTV (Bi-Total Variance).
- The parameters of the imaging system may be specified by the user.
 - The size of image block
 - The PSF or point spread function
 - The noise model (such as AWGN, Poisson, Salt&Pepple or Speckle) and noise intensity

- The parameter of the SRR algorithm using the regularized ML approach may be specified by the user.
 - The size of image block
 - The Regularized Parameter
 - The step size in the direction of the gradient.
 - The norm constant parameters



สถาบันวิทยบริการ
จุฬาลงกรณ์มหาวิทยาลัย

5.3 Future Research on SRR algorithms

- Several parameters (such as Regularized Parameter, step size, norm constant parameter) are still manually specified. The optimal values are found by experiments for most visually appealing results with highest PSNR. Automatic parameter specification is necessary for the practical SRR algorithms in the future research.
- One important extension for our algorithms is the incorporation of blur identification algorithms in the SRR algorithm because many single-frame blind deconvolution algorithms have been suggested in the last two decades.
- Although the sub-pixel registrations are an essential part of SRR algorithms and several sub-pixel registrations [3, 6, 18, 78, 110] have been proposed in the last two decades, Only few simple sub-pixel registrations have been used in the SRR algorithm such as global translation [97-100], global affine [25], block-based translation. Therefore, more realistic and higher accurate registrations are still required for higher accurate result in the SRR algorithms.
- Few SRR algorithms have addressed resolution enhancement of compressed video sequences. Compression artifacts can dramatically decrease the performance of any SRR algorithms. Considering compression color artifacts in designing novel multiframe demosaicing algorithms is the part of our ongoing work.
- Computational resources are becoming progressively more powerful and cheaper therefore this makes it feasible to implement algorithms which were previously prohibitive in terms of their computational complexity. The likely result will be the development of more accurate motion estimation methods, more realistic observation and prior models and more powerful restoration frameworks leading ultimately to improvements in restored image quality.

REFERENCES

1. A. M. Thompson, J. C. Brown, J. W. Kay and D. M. Titterton, A Study of Methods of Choosing the Smoothing Parameter in Image Restoration by Regularization, IEEE Transactions on Pattern Analysis and Machine Intelligence 13, 4 (April 1991) : 326-339.
2. A. J. Patti and Y. Altunbasak, Artifact Reduction for Set Theoretic Super Resolution Image Reconstruction with Edge Constraints and Higher-Order Interpolation, IEEE Transactions on Image Processing 10, 1 (Jan. 2001) : 179-186.
3. A. W. Fitzgibbon, Stochastic Rigidity : Image Registration for Nowhere-Static Scenes, Researching Report, Robotics Research Group, Department of Engineering Science, University of Oxford, 2001 : 1-8.
4. B. Bascle, A. Blake and A. Zisserman, Motion Deblurring and Super-Resolution from an Image Sequence, Researching Report, Robotics Research Group, Department of Engineering Science, University of Oxford, 1996 : 1-10.
5. B. Anconelli, Method and Software for Deconvolution of Interferometric Images, Thesis Proposal of PhD Program in Computer Science, University of Genova, Dec. 2003 : pp. 1-25.
6. B. Zitova and J. Flusser, Image Registration Method: a Survey, Elsevier Image and Vision Computing 21, (June 2003) : 977-1000.
7. B. K. Gunturk, Y. Altunbasak and R. M. Mersereau, Color Plane Interpolation Using Alternating Projections, IEEE Transactions on Image Processing 11, 9 (Sep. 2002) : 997-1013
8. B. K. Gunturk, Y. Altunbasak and R. M. Mersereau, Super-Resolution Reconstruction of Compressed Video Using Transform-Domain Statistics, , IEEE Transactions on Image Processing 13, 1, (Jan. 2004) : 33-43
9. C. A. Segall, R. Molina and A. K. Katsaggelos, High-resolution Images from Low-Resolution Compressed Video, IEEE Signal Processing Magazine 20, 3 (May 2003) : 37-48.
10. C. Bouman and K. Sauer, A Generalized Gaussian Image Model for Edge-Preserving MAP Estimation, IEEE Transactions on Image Processing 2, 3 (July 1993) : 293-310.
11. C. Stiller and J. Konrad, Estimating Motion in Image Sequences, IEEE Signal Processing Magazine 15, 4 (July 1999) : 70-91.
12. D. B. Bradshaw and N. G. Kingsbury, Combined Affine and Translational Motion Compensation Scheme Using Triangular Tessellations, Proceeding of the 1997 IEEE International Conference on Acoustics, Speech and Signal Processing (ICASSP '97), 1997 : 2645-2648.

13. D. Capel and A. Zisserman, Super-Resolution from Multiple Views using Learnt Image Models, Researching Report, Robotics Research Group, Department of Engineering Science, University of Oxford, 2001 : 1-8.
14. D. Geman and C. Yang, Nonlinear Image Recovery with Half-Quadratic Regularization, IEEE Transactions on Image Processing 4, 7 (July 1995) : 932-946.
15. D. Kundur and D. Hatzinakos, Blind Image Deconvolution, IEEE Signal Processing Magazine 13, 5 (May 1996) : 43–64.
16. D. Kundur and D. Hatzinakos, Blind Image Deconvolution Revisited, IEEE Signal Processing Magazine 13, 11 (Nov. 1996) : 61– 63.
17. D. Kundur and D. Hatzinakos, A Novel Blind Deconvolution Scheme for Image Restoration Using Recursive Filtering, IEEE Transactions on Signal Processing 46, 2 (Feb. 1998) : 375–390.
18. D. Lim, Achieving Accurate Image Registration as the Basis for Super-Resolution, Master Thesis, School of Computer Science and Software Engineering, The University of Western Australia, 2002.
19. D. P. Capel, Image Mosaicing and Super-Resolution, Doctoral Dissertation, Robotics Research Group, Department of Engineering Science, University of Oxford, 2001.
20. D. Rajan, S. Chaudhuri and M. V. Joshi, Multi-Objective Super Resolution Concepts and Examples, IEEE Signal Processing Magazine 20, 3 (May 2003) : 49-61.
21. D. Rajan and S. Chaudhuri, Simultaneous Estimation of Super-Resolution Scene and Depth Map from Low Resolution Defocuses Observations, IEEE Transactions on Pattern Analysis and Machine Intelligence 25, 9 (Sep. 2003) : 1102-1117.
22. D. Schilling and P. C. Cosman, Preserving Step Edges in Low Bit Rate Progressive Image Compression, IEEE Transactions on image processing, 12 (Dec. 2003) : 1473-1484.
23. E. Shechtman, Y. Caspi and M. Irani, Space-Time Super-Resolution, IEEE Transactions on Pattern Analysis and Machine Intelligence 27, 4 (April 2005) : 531-545.
24. G. Demoment, Image Reconstruction and Restoration: Overview of Common Estimation Structures and Problems, IEEE Transactions on Acoustics, Speech and Signal Processing 37, 12 (Dec. 1989) : 2024-2036.
25. G. Rochefort, F. Champagnat, G. L. Besnerais and Jean-François Giovannelli, An Improved Observation Model for Super-Resolution Under Affine Motion, IEEE Transactions on Image Processing 15, 11 (Nov. 2006) : 3325-3337.

26. G. M. Callico, A. Nunez, R. P. Llopis and R. Sethuraman, Low-cost and real-time super-resolution over a video encoder IP, Proceedings of the Fourth International Symposium on Quality Electronic Design (ISQED'03), IEEE Computer Society, 2003.
27. H. Hasegawa, T. Ono, I. Yamada and K. Sakaniwa, An Iterative MPEG Super-Resolution with an Outer Approximation of Framewise Quantization Constraint, IEICE Trans. on Fundamentals E88-A, 9 (Sep. 2005).
28. Hua-Mei Chen, S. Lee, R. M. Rao, Mohamed-Adel Slamani and P. K. Varshney, Imaging for Concealed Weapon Detection : A tutorial overview of development in imaging sensors and processing, IEEE Signal Processing Magazine, 5 (Mar. 2005) : 16-24.
29. Hu He, L. P. Kondi, Resolution Enhancement of Video Sequences with Adaptively Weighted Low-Resolution Images and Simultaneous Estimation of the Regularization Parameter, Proceeding of IEEE International Conference on Acoustics, Speech and Signal Processing, Montreal, Canada, III (May 2004) : 213-216.
30. Hu He, L. P. Kondi, Resolution Enhancement of Video Sequences with Simultaneous Estimation of the Regularization Parameter, SPIE Journal of Electronic Imaging 13, 3 (July 2004) : 586-596.
31. Hu He, L. P. Kondi, A Regularization Framework for Joint Blur Estimation and Super-Resolution of Video Sequences, Proceeding of the 2005 International Conference on Image Processing (ICIP '05), Genova, Italy, Sep. 2005.
32. Hu He and Lisimachos P. Kondi, An Image Super-Resolution Algorithm for Different Error Levels Per Frame, IEEE Transactions Image Processing 15, 3 (March 2006) : 592-60.
33. H. Lanteri, M. Roche, O. Cuevas and C. Aime, A General Method to devise Maximum-Likelihood Signal Restoration Multiplicative Algorithms with Non-Negativity Constraints, Elsevier Science B.V., (Nov. 2000) : 945-974.
34. H. Nagahara, Y. Yaji and M. Yachida, Super-Resolution Modeling, IEEE Conference on Multisensor Fusion and Integration for Intelligent Systems 2003, 2003 : 215-221.
35. I. M. Elfadel and R. W. Picard, Miscibility Matrices Explain the Behavior of Grayscale Textures Generated by Gibbs Random Field, SPIE Intelligent Robots and Computer Vision IX, Boston, USA, (Nov. 1990) : 524-535.
36. I. M. Elfadel and R. W. Picard, Gibbs Random Fields, Cooccurrences, and Texture Modeling, Perceptual Computing Group Technical Report #204, Media Laboratory, MIT, USA, (Jan. 1993) : 1-34.

37. I. M. Elfadel and R. W. Picard, Gibbs Random Fields, Cooccurrences, and Texture Modeling, IEEE Transactions on Pattern Analysis and Machine Intelligence 16, 1 (Jan. 1994) : 24-37.
38. I. M. Elfadel and R. W. Picard, On the Structure of Aura and Co-occurrence Matrices for the Gibbs Texture Model, Perceptual Computing Group Technical Report #160, Media Laboratory, MIT, USA, (June 1994) : 1-24.
39. I. Patras and M. Worring, Regularized Patch Motion Estimation, Proceeding of the 16th International Conference on Pattern Recognition (ICPR'02), 2002.
40. J. Wegger, Estimation of Motion in Image Sequences, Master Thesis, Department of Electrical Engineering, Institution of Technology, Linkopings University, Sweden, 2000.
41. J. Sun, N. N. Zheng, H. Tao and H. Y. Shum, Image Hallucination with Primal Sketch Priors, Proceedings of the 2003 IEEE Computer Society Conferences on Computer Vision and Pattern Recognition (CVPR'03), 2003
42. J. Y. A. Wang and E. H. Adelson, Spatio-Temporal Segmentation of Video Data, Proceedings of the SPIE : Image and Video Processing II 2182, San Jose, USA, (Feb. 1994).
43. K. Popat and R. W. Picard, Gibbs Random Fields : Temperature and Parameter Analysis, IEEE International on International Conference on Acoustics, Speech and Signal Processing (ICASSP), Adelaide, Australia, (April 1994).
44. K. Popat and R. W. Picard, Cluster-Based Probability Model Applied to Image Restoration and Compression, IEEE International on International Conference on Acoustics, Speech and Signal Processing (ICASSP), Adelaide, Australia, (April 1994).
45. K. R. Namuduri, Motion Estimation Using Spatio-Temporal Contextual Information, IEEE Transactions on Circuits and Systems for Video Technology 14, 8 (Aug. 2004) : 1111-1115.
46. L. P. Kondi, D. A. Scribner, J. M. Schuler, A Comparison of Digital Image Resolution Enhancement Techniques, Proceeding on SPIE AeroSense Conference (Infrared and Passive Millimeter-wave Imaging Systems: Design, Analysis, Modeling, and Testing), Orlando, FL, (April 2002) : 220-229.
47. M. A. Robertson, Computationally-Efficient Post-Processing of Compressed Video Streams, Master Thesis, Electrical Engineering, The University of Notre Dame, Indiana, USA, March 1998.
48. M. Ben-Ezra and S. K. Nayar, Motion-Based Motion Deblurring, IEEE Transactions on Pattern Analysis and Machine Intelligence 26, 6 (June 2004) : 689-698.

49. M. Elad and A. Feuer, Restoration of a Single Superresolution Image from Several Blurred, Noisy and Undersampled Measured Images, IEEE Transactions on Image Processing 6, 12 (Dec. 1997) : 1646-1658.
50. M. Elad and A. Feuer, Superresolution Restoration of an Image Sequence: Adaptive Filtering Approach, IEEE Transactions on Image Processing 8, 3 (Match 1999) : 387-395.
51. M. Elad and A. Feuer, Super-Resolution Reconstruction of Image Sequences, IEEE Transactions on Pattern Analysis and Machine Intelligence 21, 9 (Sep. 1999) : 817-834.
52. M. Elad and Y. Hecov Hel-Or, A Fast Super-Resolution Reconstruction Algorithm for Pure Translational Motion and Common Space-Invariant Blur, IEEE Transactions on Image Processing 10, 8 (Aug. 2001) : 1187-1193.
53. M. Elad and A. Feuer, Super-Resolution Restoration of Continuous Image Sequence – Adaptive Filtering Approach, Technical Report, The Technion, The Electrical Engineering Faculty, Israel Institute of Technology, Haifa, 1-12
54. M. Elad, On the Original of the Bilateral Filter and Ways to Improve It, IEEE Transactions on Image Processing 11, 10 (Oct. 2002) : 1141-1151.
55. M. G. Kang and A. K. Katsaggelos, General Choice of the Regularization Functional in Regularized Image Restoration, IEEE Transactions on Image Processing 4, 5 (May 1995) : 594-602.
56. M. G. Kang and A. K. Katsaggelos, Simultaneous Multichannel Image Reconstruction and Estimation of the Regularization Parameter, IEEE Transactions on Image Processing 6, 5 (May 1997) : 774-778.
57. M. G. Kang and S. Chaudhuri, Super-Resolution Image Reconstruction, IEEE Signal Processing Magazine 20, 3 (May 2003) : 19 – 20.
58. M. J. Black, A. Rangarajan, On The Unification Of Line Processes, Outlier Rejection and Robust Statistics with Applications in Early Vision, International Journal of Computer Vision 19, 1 (July 1996) : 57-92.
59. M. J. Black, G. Sapiro, D. Marimont, D. Heeger, Robust Anisotropic Diffusion: Connections Between Robust Statistics, Line Processing and Anisotropic Diffusion, Scale-Space Theory in Computer Vision, Scale-Space'97, B. ter Haar Romeny, L. Florack, J. Koenderink, and M. Viergever (Eds.), Springer Verlag, LNCS 1252, Utrecht, the Netherlands, July 1997 : 323-326.

60. M. J. Black, G. Sapiro, D. H. Marimont and D. Herrger, Robust Anisotropic Diffusion, IEEE Transactions on Image Processing 7, 3 (March 1998).
61. M. J. Black and G. Sapiro, Edges as Outliers: Anisotropic Smoothing Using Local Image Statistics, Scale-Space Theories in Computer Vision, Second International Conference on Scale-Space '99, Corfu, Greece, LNCS 1682, Springer, (Sep. 1999) : 259-270.
62. M. K. Ng and N. K. Bose, Analysis of Displacement Error in High-Resolution Image Reconstruction With Multisensors, IEEE Transactions on Circuits and systems : Fundamental Theory and Application 49, 6 (June 2002) : 806-813.
63. M. K. Ng and Nirmal K. Bose, Mathematical analysis of super-resolution methodology, IEEE Signal Processing Magazine 20, 3 (May 2003) : 62 – 74.
64. M. R. Banham and A. K. Katsaggelos, Digital Image Restoration, IEEE Signal Processing Magazine 14, 2 (March 1997) : 24–41.
65. M. Trimeche, R. C. Bilcu and J. Yrjanainen, Adaptive Outlier Rejection in Image Super-Resolution, EURASIP Journal on Applied Signal Processing, Article ID 38052, Hindawi Publishing Corporation, 2006 : 1-12.
66. M. Victor, W. Zibetti and J. Mayer, Simultaneous Super-Resolution for Video Sequences, Proceeding of the 2005 International Conference on Image Processing (ICIP '05), Genova, Italy, Sep. 2005.
67. M. Vega, R. Molina and A. K. Katsaggelos, A Bayesian Super-Resolution Approach to Demosaicing of Blurred Image, EURASIP Journal on Applied Signal Processing, Article ID 25072, Hindawi Publishing Corporation, 2006 : 1-12.
68. N. C. Gallagher, JR. Gary L. Wise, A Theoretical Analysis of the Properties of Median Filters, IEEE Transactions on Acoustics, Speech and Signal Processing ASSP-29, 6 (Dec. 1981) : 1136-1141.
69. N. K. Bose, M. K. Ng and A. C. Yau, A Fast Algorithm for Image Super-Resolution from Blurred Observations, EURASIP Journal on Applied Signal Processing, Article ID 35726, Hindawi Publishing Corporation, 2006 : 1-14.
70. N. Nguyen, P. Milanfar and G. Golub, A Computationally Efficient Superresolution Image Reconstruction Algorithm, IEEE Transactions on Image Processing 10, 4 (Apr. 2001) : 573-583.
71. N. X. Nguyen, Numerical Algorithms for Image Superresolution, Doctoral Dissertation, Department of Scientific Computing and Computational Mathematics, Stanford University, 2000.

72. P. L. Combettes and M. R Civanlar, The Foundations of Set Theoretic Estimation, IEEE International Conference on Acoustics, Speech and Signal Processing (ICASSP 1991), 1991 : 1921-1924.
73. P. L. Combettes, The Foundations of Set Theoretic Estimation, Proceedings of the IEEE 81, 2 (Feb.1993) : 182-208.
74. P. Milanfar, A Model of the Effect of Image Motion in the Radon Transform Domain, IEEE Transactions on Image Processing 8, 9 (Sep. 1999) : 1276-1281.
75. P. Vandewalle, S. Susstrunk and M. Vetterli, Double Resolution from a Set of Aliased Images, Proceeding IS&T/SPIE Electronic Imaging 2004: Sensors and Camera Systems for Scientific, Industrial, and Digital Photography Applications V 5301, 1 (Jan. 2004) : 374-382.
76. P. Vandewalle, S. Susstrunk and M. Vetterli, A Frequency Domain Approach to Super-Resolution Imaging from Aliased Low Resolution Images, Technical Journal, Department of Electrical Engineering and Computer Science, UC Berkeley, USA, May, 2004 : 1-21.
77. P. Vandewalle, L. Sbaiz, M. Vetterli and S. Susstrunk, Super-Resolution from Highly Undersampled Images, Proceeding of the 2005 International Conference on Image Processing (ICIP '05), Genova, Italy, Sep. 2005.
78. P. Vandewalle, S. Susstrunk and M. Vetterli, A Frequency Domain Approach to Registration of Aliased Images with Application to Super Resolution, EURASIP Journal on Applied Signal Processing, Article ID 71459, Hindawi Publishing Corporation, 2006 : 1-14.
79. P. Marziliano and M. Vetterli, Reconstruction of Irregularly Sampled Discrete-Time Bandlimited Signals with Unknown Sampling Locations, IEEE Transactions on Signal Processing 48, 12 (Dec. 2000) : 3462-3471.
80. R. C. Gonzalez and R. E. Woods, Digital Image Processing, Addison-Wesley Publishing Company, 1992
81. R. Kimmel, Demosaicing: Image Reconstruction from Color CCD Samples, IEEE Transactions on Image Processing 8, 9 (Sep. 1999) : 1221-1228.
82. R. L. Stevenson, B. E. Schmitz and E. J. Delp, Discontinuity Persevering Regularization of Inverse Visual Problems, IEEE Transactions on Systems, Man and Cybernetics 24, 3 (March 1994).
83. R. Molina, J. Nunez, F. Cortijo and J. Mateos, Image Restoration in Astronomy : A Bayesian Perspective, Technical Report, Department of Computer Science, University of Granada, Espana.

84. R. Molina, On the Hierarchical Bayesian Approach to Image Restoration Applications to Astronomical Images, IEEE Transactions on Pattern Analysis and Machine Intelligence 16, 11 (Dec. 1995) : 1122-1128.
85. R. Molina, A. K. Katsaggelos and J. Mateos, Bayesian and Regularization Methods for Hyperparameter Estimation in Image Restoration, IEEE Transactions on Image Processing, 8, 2 (Feb. 1999) : 231-246.
86. R. Molina, M. Vega, J. Abad and A. K. Katsaggelos, Parameter Estimation in Bayesian High-Resolution Image Reconstruction With Multisensors, IEEE Transactions on Image Processing 12, 12 (Dec. 2003) : 1655-1667.
87. R. Pan and S. J. Reeves, Efficient Huber-Markov Edge-Preserving Image Restoration, IEEE Transactions on Image Processing 15, 12 (Dec. 2006) : 3728-3735.
88. R. R. Schultz and R. L. Stevenson, A Bayesian Approach to Image Expansion for Improved Definition, IEEE Transactions on Image Processing 3, 3 (May 1994) : 233-242.
89. R. R. Schultz and R. L. Stevenson, Extraction of High-Resolution Frames from Video Sequences, IEEE Transactions on Image Processing 5, 6 (June 1996) : 996-1011.
90. R. W. Picard, I. M. Elfadel and A. P. Pentland, Markov/Gibbs Texture Modeling : Aura Matrices and Temperature Effects, Proceeding of the IEEE Conference on Computer Vision and Pattern Recognition, Maui, June 1991 : 371-377.
91. R. W. Picard, Gibbs Random Fields : Temperature and Parameter Analysis, IEEE International on International Conference on Acoustics, Speech and Signal Processing (ICASSP), San Francisco, USA, March 1992 : 45-48.
92. S. Baker and T. Kanade, Limits on Super-Resolution and How to Break Them, IEEE Transactions on Pattern Analysis and Machine Intelligence 24, 9 (Sep. 2002) : 1167-1183.
93. S. Borman, Topics in Multiframe Superresolution Restoration, Doctoral Dissertation, Electrical Engineering, The University of Notre Dame, Indiana, USA, April 2004.
94. S. Chaudhuri and D. Rani Taur, High-Resolution Slow-Motion Sequencing, IEEE Signal Processing Magazine 20, 3 (Mar. 2005) : 16-24.
95. S. C. Park, M. K. Park and M. G. Kang, Super-Resolution Image Reconstruction : A Technical Overview, IEEE Signal Processing Magazine 20, 3 (May 2003) : 21 - 36.

96. S. C. Park, M. G. Kang, A. Segall and A. K. Katsaggelos, Spatially Adaptive High-Resolution Image Reconstruction of DCT-Based Compressed Images, IEEE Transactions on Image Processing 13, 4 (April 2004) : 573-585.
97. S. Farsiu, M. D. Robinson, M. Elad and P. Milanfar, Advances and Challenges in Super-Resolution, International Journal of Imaging Systems and Technology 14, 2 (2004) : 47–57.
98. S. Farsiu, M. D. Robinson, M. Elad and P. Milanfar, Fast and Robust Multiframe Super Resolution, IEEE Transactions on Image Processing 13, 10 (Oct 2004) : 1327-1344.
99. S. Farsiu, M. Elad and P. Milanfar, Multiframe Demosaicing and Super-Resolution of Color Images, IEEE Transactions on Image Processing 15, 1 (Jan. 2006) : 141-159.
100. S. Farsiu, M. Elad and P. Milanfar, Video-to-Video Dynamic Super-Resolution for Grayscale and Color Sequence, EURASIP Journal on Applied Signal Processing, Article ID 61859, Hindawi Publishing Corporation, 2006 : 1-12.
101. S. Haykin, Adaptive Filter Theory, Fourth Edition, Prentice Hall Information and System Science Series, 2002.
102. S. P. Kim, N. K. Bose, and H. M. Valenzuela, Recursive Reconstruction of High Resolution Image from Noisy Undersampled Multiframe, IEEE Transactions on Acoustic, Speech, Signal Processing 38 (1990) : 1013–1027.
103. S. P. Kim and Wen-Yu Su, Recursive High-Resolution Reconstruction of Blurred Multiframe Images, IEEE Transactions on Image Processing 2, 4 (Oct. 1993) : 534-539.
104. S. S. Beauchemin and J. L. Barron, The Computation of Optical Flow, ACM Computing Surveys 27, 3 (Sep. 1995) : 433-467.
105. S. V. Vaseghi, Advanced Signal Processing and Digital Noise Reduction, John Wiley & Sons Ltd., 1996.
106. S. Zhu and Kai-Kuang Ma, A New Diamond Search Algorithm for Fast Block-Matching Motion Estimation, IEEE Transactions on Image Processing 9, 2 (Feb. 2000) : 287-290.
107. T. S. Huang and R. Y. Tsan, Multiple frame image restoration and registration, Advances in Computer Vision and Image Processing 1, T. S. Huang, Ed. Greenwich, CT: JAI, 1984 : 317-339.
108. Viet-Nam Dang, Abdol-Reza Mansouri and Janusz Konrad, Motion Estimation For Region-Based Video Coding, Proceeding of the 1995 International Conference on Image Processing (ICIP '95), 1995 : 189-192.

109. V. Patanavijit and S. Jitapunkul, A Modified Three-Step Search Algorithm for Fast Affine Block Base Motion Estimation, International Workshop on Advanced Image Technology 2006 (IWAIT 2006), Okinawa, Japan, Jan. 2006 : 99-104.
110. V. Patanavijit and S. Jitapunkul, An Iterative Super-Resolution Reconstruction of Image Sequences using a Bayesian Approach with BTV Prior and Affine Block-Based Registration, IEEE Canadian Conference on Computer and Robot Vision 2006 (CRV 2006), Quebec City, Canada, June 2006.
111. V. Patanavijit and S. Jitapunkul, An Iterative Super-Resolution Reconstruction of Image Sequences using Affine Block-Based Registration, ACM International Symposium on Multimedia Over Wireless (IWCMC 2006), Vancouver, Canada, July 2006 : 51–56.
112. V. Patanavijit and S. Jitapunkul, An Iterative Super-Resolution Reconstruction of Image Sequences using a Bayesian Approach and Affine Block-Based Registration, 14th European Signal Processing Conference (EUSIPCO 2006), Florence, Italy, Sep. 2006.
113. V. Patanavijit and S. Jitapunkul, A Lorentzian Bayesian Approach for Robust Iterative Multiframe Super-Resolution Reconstruction with Lorentzian-Tikhonov Regularization (The Best Paper Award), IEEE International Symposium on Communications and Information Technologies 2006 (ISCIT 2006), Bangkok, Thailand, Oct. 2006 : 1–6 (F3A-4).
114. V. Patanavijit and S. Jitapunkul, A Robust Iterative Multiframe Super-Resolution Reconstruction using a Huber Statistical Estimation Technique, IEEE International Conference on Communications and Networking in China 2006 (CHINACOM 2006), Beijing, China, Oct. 2006.
115. V. Patanavijit and S. Jitapunkul, A Robust Iterative Multiframe Super-Resolution Reconstruction using a Bayesian Approach with Lorentzian Norm, Tenth IEEE International Conference on Communication Systems (ICCS 2006), Singapore, Oct. 2006.
116. V. Patanavijit and S. Jitapunkul, A Lorentzian Stochastic Estimation for an Robust and Iterative Multiframe Super-Resolution Reconstruction, The Annual International Technical Conference of IEEE Region 10 (IEEE TENCON 2006), Wan Chai, Hong Kong, Nov. 2006.
117. V. Patanavijit and S. Jitapunkul, A Robust Iterative Multiframe Super-Resolution Reconstruction using a Bayesian Approach with Tukey's Biweight, IEEE International Conference on Signal Processing 2006 (ICSP 2006), Guilin, China, Nov. 2006.

118. V. Patanavijit and S. Jitapunkul, An Iterative Super-Resolution Reconstruction of Image Sequences using Fast Affine Block-Based Registration with BTV Regularization, IEEE Asia Pacific Conference on Circuits and System (APCCAS 2006), Singapore, Dec. 2006 : 1746-1749.
119. V. Patanavijit and S. Jitapunkul, A Robust Iterative Multiframe Super-Resolution Reconstruction using a Huber Bayesian Approach with Huber-Tikhonov Regularization, IEEE International Symposium on Intelligent Signal Processing and Communication System (ISPACS 2006), Tottori, Japan, Dec. 2006.
120. V. Patanavijit and S. Jitapunkul, A Lorentzian Stochastic Estimation for A Robust Iterative Multiframe Super-Resolution Reconstruction with Lorentzian-Tikhonov Regularization, EURASIP Journal on Applied Signal Processing (EURASIP JASP) : Special Issue on Super-Resolution Enhancement of Digital Video, Hindawi Publishing Corporation, May 2007.
121. V. Patanavijit, P. Sermwuthisarn and S. Jitapunkul, A Robust Iterative Super-Resolution Reconstruction of Image Sequences using a Tukey's Biweight Bayesian Approach with Fast Affine Block-Based Registration, IEEE International Conference on Multimedia & Expo (ICME 2007), Beijing, China, July 2007.
122. V. Patanavijit, S. Tae-O-Sot and S. Jitapunkul, A Robust Iterative Super-Resolution Reconstruction of Image Sequences using a Lorentzian Bayesian Approach with Fast Affine Block-Based Registration, IEEE International Conference on Image Processing (ICIP 2007), San Antonio, Texas, USA, Sep. 2007.
123. V. Z. Mesarovic, N. P. Galatsanos and A. K. Katsaggelos, Regularized Constrained Total Least Squares Image Restoration, IEEE Transactions on Image Processing 4, 8 (Aug 1995) : 1096-1108.
124. X. Jing and Lap-Pui Chau, An Efficient Three-Step Search Algorithm for Block Motion Estimation, IEEE Transactions on Multimedia 6, 3 (June 2004) : 435-438.
125. Y. Wang, J. Osterman and Ya-Qin Zhang, Video Processing and Communication, Prentice Hall, Inc., 2001.
126. Y. Altunbasak, A. J. Patti and R. M. Mersereau, Super-Resolution Still and Video Reconstruction from MPEG-Coded Video, IEEE Transactions on Circuits and Systems for Video Technology 12, 4 (April 2002) : 217-226.

127. Z. Lin and Heung-Yeung Shum, Fundamental Limits of Reconstruction-Based Superresolution Algorithms under Local Translation, IEEE Transactions on Pattern Analysis and Machine Intelligence 26, 1 (Jan. 2004) : 83-97.
128. Z. Jiang, Tien-Tsin Wong and H. Bao, Practical Super-Resolution from Dynamic Video Sequences, Proceedings of the 2003 IEEE Computer Society Conference on Computer Vision and Pattern Recognition (CVPR'03), 2003



สถาบันวิทยบริการ
จุฬาลงกรณ์มหาวิทยาลัย

LISTS OF PUBLICATION

International Journal Paper

1. V. Patanavijit and S. Jitapunkul, A Lorentzian Stochastic Estimation for A Robust Iterative Multiframe Super-Resolution Reconstruction with Lorentzian-Tikhonov Regularization, EURASIP Journal on Applied Signal Processing (EURASIP JASP): Special Issue on Super-Resolution Enhancement of Digital Video, Article ID 34821, Hindawi Publishing Corporation, 2007 : 1-21. (ISI Impact Factor=0.463 according to 2006 Journal Citation Reports released by Thomson Scientific (ISI) in 2007)

International Conference Paper

1. V. Patanavijit and S. Jitapunkul, A Modified Three-Step Search Algorithm for Fast Affine Block Base Motion Estimation, International Workshop on Advanced Image Technology 2006 (IWAIT 2006), Okinawa, Japan, pp. 99-104, Jan. 2006.
2. V. Patanavijit and S. Jitapunkul, An Iterative Super-Resolution Reconstruction of Image Sequences using a Bayesian Approach with BTV Prior and Affine Block-Based Registration, IEEE Canadian Conference on Computer and Robot Vision 2006 (CRV 2006), Quebec City, Canada, June 2006.
3. V. Patanavijit and S. Jitapunkul, An Iterative Super-Resolution Reconstruction of Image Sequences using Affine Block-Based Registration, ACM International Symposium on Multimedia Over Wireless (IWCMC 2006), Vancouver, Canada, pp. 51–56, July 2006.
4. V. Patanavijit and S. Jitapunkul, An Iterative Super-Resolution Reconstruction of Image Sequences using a Bayesian Approach and Affine Block-Based Registration, 14th European Signal Processing Conference (EUSIPCO 2006), Florence, Italy, Sep. 2006.
5. V. Patanavijit and S. Jitapunkul, A Lorentzian Bayesian Approach for Robust Iterative Multiframe Super-Resolution Reconstruction with Lorentzian-Tikhonov Regularization (The Best Paper Award), IEEE International Symposium on Communications and Information Technologies 2006 (ISCIT 2006), Bangkok, Thailand, pp. 1–6 (F3A-4), Oct. 2006.

6. V. Patanavijit and S. Jitapunkul, A Robust Iterative Multiframe Super-Resolution Reconstruction using a Huber Statistical Estimation Technique, IEEE International Conference on Communications and Networking in China 2006 (CHINACOM 2006), Beijing, China, Oct. 2006.
7. V. Patanavijit and S. Jitapunkul, A Robust Iterative Multiframe Super-Resolution Reconstruction using a Bayesian Approach with Lorentzian Norm, Tenth IEEE International Conference on Communication Systems (ICCS 2006), Singapore, Oct. 2006.
8. V. Patanavijit and S. Jitapunkul, A Lorentzian Stochastic Estimation for an Robust and Iterative Multiframe Super-Resolution Reconstruction, The Annual International Technical Conference of IEEE Region 10 (IEEE TENCON 2006), Wan Chai, Hong Kong, Nov. 2006.
9. V. Patanavijit and S. Jitapunkul, A Robust Iterative Multiframe Super-Resolution Reconstruction using a Bayesian Approach with Tukey's Biweight, IEEE International Conference on Signal Processing 2006 (ICSP 2006), Guilin, China, Nov. 2006.
10. V. Patanavijit and S. Jitapunkul, An Iterative Super-Resolution Reconstruction of Image Sequences using Fast Affine Block-Based Registration with BTV Regularization, IEEE Asia Pacific Conference on Circuits and System (APCCAS 2006), Singapore, pp. 1746-1749, Dec. 2006.
11. V. Patanavijit and S. Jitapunkul, A Robust Iterative Multiframe Super-Resolution Reconstruction using a Huber Bayesian Approach with Huber-Tikhonov Regularization, IEEE International Symposium on Intelligent Signal Processing and Communication System (ISPACS 2006), Tottori, Japan, Dec. 2006.
12. V. Patanavijit, P. Sermwuthisarn and S. Jitapunkul, A Robust Iterative Super-Resolution Reconstruction of Image Sequences using a Tukey's Biweight Bayesian Approach with Fast Affine Block-Based Registration, IEEE International Conference on Multimedia & Expo (ICME 2007), Beijing, China, July 2007.

- 13.V. Patanavijit, S. Tae-O-Sot and S. Jitapunkul, A Robust Iterative Super-Resolution Reconstruction of Image Sequences using a Lorentzian Bayesian Approach with Fast Affine Block-Based Registration, IEEE International Conference on Image Processing (ICIP 2007), San Antonio, Texas, USA, Sep. 2007.



สถาบันวิทยบริการ
จุฬาลงกรณ์มหาวิทยาลัย

VITAE

Vorapoj Patanavijit was born in Bangkok, Thailand in 1973. He received the B.Eng. and M.Eng. degrees from the Department of Electrical Engineering at the Chulalongkorn University, Bangkok, Thailand, in 1994 and 1997 respectively. In 1998, He joined Faculty of Engineering, Assumption University as a full-time lecturer until now. He is currently pursuing the Doctoral degree in electrical engineering at Chulalongkorn University, Bangkok, Thailand. He works in the field of signal processing and multidimensional signal processing, specializing, in particular, on SRR (Super-Resolution Reconstruction), Image/Video Reconstruction, Enhancement, Fusion, Denoising, Inverse Problems, Motion Estimation and Registration.



สถาบันวิทยบริการ
จุฬาลงกรณ์มหาวิทยาลัย